2016

Laser waterjet heat treatment on super-hard materials

Jingnan Zhao
Iowa State University

Laser waterjet heat treatment on super-hard materials

by

Jingnan Zhao

A dissertation submitted to the graduate faculty

in partial fulfillment of the requirements for the degree of

DOCTOR OF PHILOSOPHY

Major: Mechanical Engineering

Program of Study Committee:
Pranav Shrotriya, Major Professor
Reza Montazami
Ganesh Balasubramanian
Scott Chumbley
Jarad Niemi

Iowa State University

Ames, Iowa

2016

TABLE OF CONTENTS

ACKNOWLEDGMENTS

I would like to express my gratitude to everyone was involved in any of the projects that make this dissertation. I would like to thank my major professor, Dr. Pranav Shrotriya, for the opportunity to work with him. He has offered his support through his knowledge, expertise, and time. The success of my projects would not have been possible without his professional experience, patient guidance, and valuable inputs.

I also would like to thank all my committee members: Dr. Scott Chumbley for teaching me in the courses I took with them that prepared me with the needed knowledge for my work in these projects; Dr. Ganesh Balasubramanian and Dr. Reza Montazami for their comments and valuable suggestions on these projects; Dr. Jarad Niemi for his help on my experiment design and statistic data analysis.

Special thanks to all my collaborators for their support and contributions to this work. I greatly treasure the experience of working with Dr. Pal Molian. Also, I would like to thank all the fellow students I worked with or shared thoughts with: Ammar Melaibary, Zhuoru Wu, Wong Kwang Shiong, Zhichen Zhu, Agnivo Gosai, and Abdullah Alshehri.

In addition, I would like to send special thanks to my family: my parents, my wife, and my kid. They have provided the love and support I needed to pass through my difficult times. This dissertation is proof of their support.

Finally, I would like to thank Diamond Innovations, Inc, and Dr. Volodymyr Bushlya for the boron nitride samples.

ABSTRACT

The use of the hybrid laser waterjet heat (LWH) treatment process to develop super-hard materials is a new field of research that has the potential to develop materials with hardness characteristics that compare with or exceed that of diamond. The research presented in this dissertation investigated the hardness improvement mechanism of boron nitride (BN) materials by investigating the optimization of LWH process parameters and studying the microstructural refinement of BN materials. The study of the LWH system parameters investigated the relationship between LWH system parameters and the BN materials' hardness change ratio. Upon the study, the optimal LWH system parameters (laser fluence, laser beam overlap percentage, boron nitride composition, laser pass number, and laser intensity) were identified in order to maximize BN material hardness. For the BN material microstructure refinement study, scanning electron microscopy (SEM), Raman spectroscopy, and finite element methods (FEM) were used to investigate the microstructure of pre- and post-LWH-treated BN materials. Analytical and experimental approaches were conducted throughout all of the studies, and a variety of analysis techniques were applied. Results indicate that LWH treatment is a feasible approach to improve the hardness of select materials while providing a potential method to develop new super-hard materials for the tooling industry.

CHAPTER I

INTRODUCTION

1.1 Introduction to super-hard materials

Diamond is considered to be the hardest material on the earth with a hardness varying between 70 and 100 GPa depending on the quality and purity of its crystal structure. Diamond is a member of the super-hard materials which are classified as having hardness values greater than 40 GPa (Stan Veprek & Argon, 2002). Diamond ($H_k \approx 70 - 100$ GPa) and cubic boron nitride (cBN) ($H_k \approx 40 - 50$ GPa) are well-known super-hard materials used in many applications, such as mechanical cutting, abrasives, polishing materials, and wear-resistant and protective coatings (Brazhkin, Lyapin, & Hemley, 2002; A. A. Melaibari et al., 2016).

Although diamond is the hardest material, it has limitations in the tooling industry. Diamond is not an ideal tool for cutting ferrous materials because its chemical instabilities trigger a reaction with ferrous materials and produce iron carbide. Also, diamond is not effective at high temperatures because of its thermal instability. The second hardest material on the earth, cBN (Dubrovinskaia et al., 2007), has a microstructure similar to that of diamond and can be used to cut ferrous metals and perform in high temperature environments. Although cBN has good mechanical properties, chemical inertness and thermal stability, it cannot replace diamond as its hardness is well below that of diamond. Thus, the search for new superhard materials is not only of great scientific interest, but also of great practical value.

In order to find the most effective super-hard materials for the tooling industry, the scientific reasons for a material's hardness must be understood. Diamond has a short bond length made of carbon atoms linked together in a face-centered cubic (FCC) lattice structure

to form a three-dimensional high symmetry network. The bond length is short because carbon is a light element. Each carbon atom is linked with four other carbon atoms in regular tetrahedrons, creating a cubic lattice with tremendous strength in all directions that forms an incredibly solid crystal structure (Jonathan B. Levine, Tolbert, & Kaner, 2009). Thus, when identifying potential super-hard materials, light elements, such as boron, carbon, and nitrogen are considered. These elements are capable of forming three-dimensional rigid lattices with shortened covalent bonds. Also, elements with very high densities of valence electrons should also be considered in order to guarantee the material resistant to squeezing. With these understandings, the search for new super-hard materials can be focused on the range of synthesized materials composed of light elements (Irifune, Kurio, Sakamoto, Inoue, & Sumiya, 2003; Meng et al., 2004).

According to the ideas discussed above, candidate hard materials that can be used as super-hard materials including cBN, wurtzite boron nitride (wBN) (A. A. Melaibari et al., 2016), boron carbide (B_4C) (Thévenot, 1990)(Jiménez et al., 1998), and osmium diboride (O_SB_2) (Basu, Raju, & Suri, 2006). Figure 1.1 shows the Vickers hardness of these named hard materials (John, Polwart, Troupe, & Wilson, 2002). Polycrystalline diamond (PCD) has the highest hardness but lowest oxidation temperature. Thus, PCD is unable to cut materials under high speeds since the heat created by cutting could oxide the PCD to carbon. CBN and WBN have high chemical inertness and oxidation temperatures that allow for high-speed manufacturing in various environments. Some researchers are working to increase the hardness of ceramic materials such as B_4C, Titanium diboride (TiB_2), and O_SB_2 in order to come close to or achieve diamond hardness. Thévenot achieved a hardness of 30 GPa for B_4C at room temperature (Thévenot, 1990). Gou and his group studied O_SB_2 and measured its hardness to

be 37 GPa (Gou, Wang, Zhang, Yan, & Gao, 2009). Thus, OsB_2 and B_4C Have not met the hardness qualifications to be considered as potential super-hard materials.

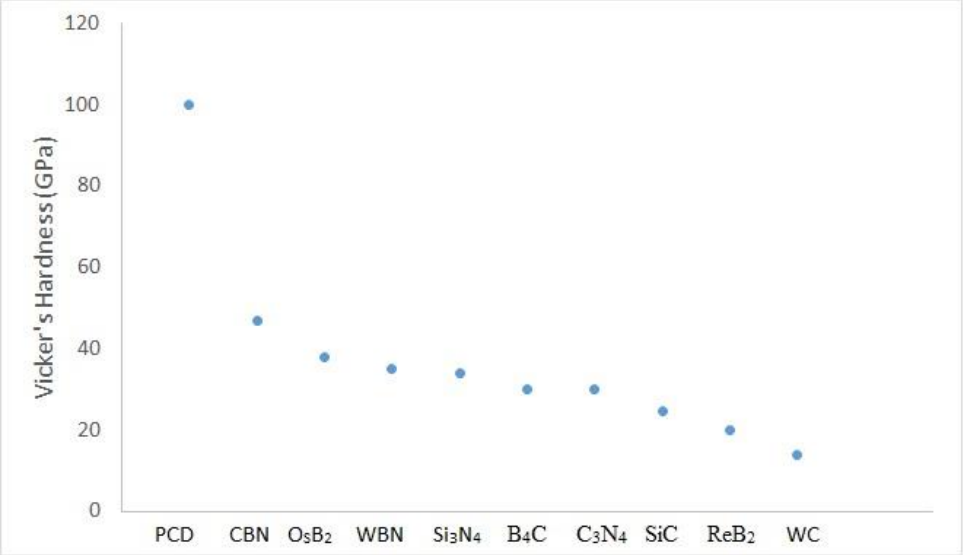

Figure 1.1 *Vicker's hardness of some superhard materials. It should be noted that, the hardness values of materials may depend on the sample quality. For example, the hardness of diamond depends on the quality and purity of the crystal*

Despite most previous works' efforts to create super-hard materials by synthesizing super-hard materials, many opportunities still remain unexplored. For example, the combination of Hall-Petch and quantum confinement effects has been used to design thermally stable and chemically inert nanoscale grain-size cBN/wBN composites with increased hardness. In order to achieve this kind of super-hard material, a novel laser/waterjet heat treatment (LWH) approach was performed on cBN/wBN composites. A preliminary study concluded that the hardness of the cBN/wBN was comparable to the hardness of diamond (Hansen, 2004; Li, Sun, & Chen, 1996; A. Melaibari, Molian, & Shrotriya, 2012).

1.2 Hardness measurements

Hardness is a characteristic of a material, not a fundamental physical property. The hardness is defined as a material's resistance to plastic deformation caused by certain pressures such as indentation. Hardness can be quantitated by the ratio of the applied load to the fully plastically-deformed area (S. Veprek, Argon, & Zhang, 2010). For this study, hardness measurements were performed on target materials with a given indenter using a fixed load. The indentation hardness value was obtained by measuring the area of the indentation (plastic deformation made by indentation). It can be noted that smaller measured indentation areas are indicative of harder materials.

In this study, two methods were used to measure hardness: Vickers and Knoop. Robert L. Smith and George E. developed the Vickers hardness test in 1921. It was developed as an alternative to the Brinell hardness test used especially to measure extremely hard materials (Smith, 1922). During the Vickers test, the target material surface is subjected to a standard load (1Kgf in this study) for a standard length of time (30 seconds in this study) by means of a pyramid-shaped diamond indenter. The 136 degree face angle of the diamond indenter results in an indentation strain that is equivalent to that of a spherical indenter (Fischer-Cripps, 2011). Since the shape of the indenter is a square, the resulting plastic deformation on the target material after a test is also square-shaped. Following the indentation, the diagonal length of the plastic deformation is measured with a calibrated microscope (400X in this study). The Vickers hardness (HV) is calculated using the following formula:

$$HV = 1.854F/d^2 \tag{1.1}$$

where, F is the applied load in kilograms force and d is the length of square diagonal in millimeters (Taniguchi, Akaishi, & Yamaoka, 1996).

The Knoop hardness test utilizes a rhombohedral-shaped diamond indenter with a longitudinal angle of 172° and a transverse angle of 130° (Knoop, Peters, & Emerson, 1939). Since the size of the plastic deformation made by the Knoop indenter is not uniform on longitudinal and horizontal directions, the Knoop hardness calculation is only based on the measurement of the long diagonal of the impression. As with the Vickers hardness tests the target material surface is subjected to a standard load (0.5Kgf in this study) for a standard length of time (30 seconds in this study). The Knoop hardness (HK) is calculated using the following formula:

$$HK = F/(C_p L^2) \tag{1.2}$$

where, F is the applied load in kilograms force, C_p is the correction factor related to the shape of the indenter, ideally 0.070279, and d is the length of the indentation along its longer axis in millimeters (Knoop et al., 1939).

1.3 Hybrid laser waterjet heat (LWH) treatment technique

A novel process which combines continuous wave CO_2 laser and water-jet heat treatment (LWH) was developed by our group to improve the hardness of boron nitride materials (A. A. Melaibari et al., 2016; A. Melaibari et al., 2012). The LWH treatment system (shown in Figure 1.2) consists of low-power (160W – 400W) laser heating followed by low-pressure waterjet quenching, which altogether creates compressive stresses along the laser path which are believed to induce changes in the microstructure of the target material.

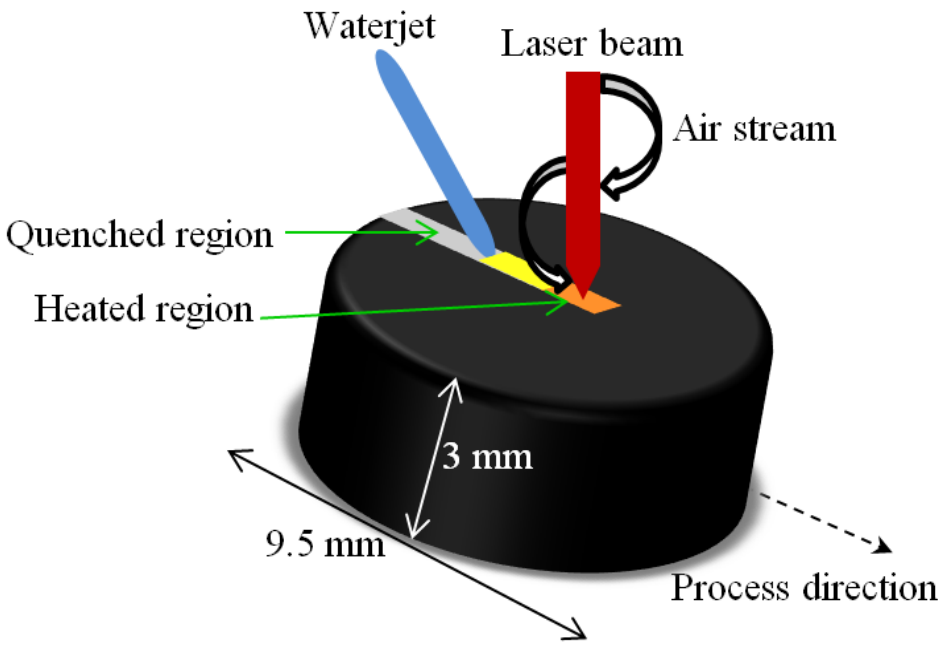

Figure 1.2. *Schematic of LWH machining system*

Figure 1.3 shows a model diagram of the LWH treatment head. The laser head was designed in order to be mounted on the existing laser-focusing hardware. The laser beam and assist gas are directed to the target material's surface through the central hole while the water is pumped from the inlet port to the exit port through an adjacent passage as shown in Figure 1.2 . The distance between the laser beam spot and the water-jet spot on the target material surface can be varied by changing the orifice angle. The head design allows the gas-assisted laser beam to be focused and permits water-jet flow and its commutation. The reflected water is removed through the high-pressure assistant gas so that water does not enter the laser heat and contaminate the focusing lens.

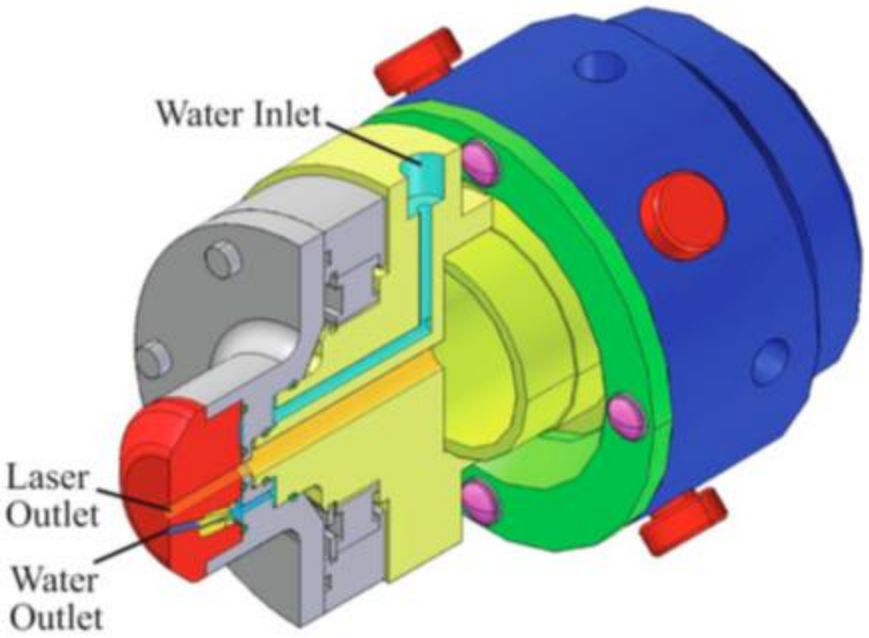

Figure 1.3. *Solid model of the Laser/Waterjet cutting head (Zhuoru Wu, 2015)*

The experimental setup of the LWH treatment system is shown in Figure 1.4. A continuous wave CO2 Laser (Laser Spectra Physics 820) with a 10.6 μm wavelength and 1 kW rated power was used in the LWH treatment system. The laser head was modified to accommodate the low-pressure waterjet (< 1000psi or < 8MPa) to realize the LWH treatment. A CNC table with freedom in the horizontal plane was implemented to control the movement of the sample mounted on it. The beam from the laser was sent through a focusing lens (127 mm focal length) and irradiated on the sample surface. The laser beam has a focal spot diameter of 0.2 mm when passed through the focusing lens. A defocused laser beam spot size with a diameter larger than 0.2 mm could be achieved when the distance between the laser head and target sample surface was changed. The distance between the waterjet and laser beam could also be changed by varying the location of the water spray hole on the laser nozzles. There are 3 nozzles with spacing of 2 mm, 4mm and 6mm between water and laser was manufactured.

In order to guarantee waterjet quench sample surface immediately after the laser beam, the 6 mm nozzle was employed by this study. A stream of compressed air with a designed pressure was employed around the laser beam in order to prevent direct interaction of the laser beam and water jet.

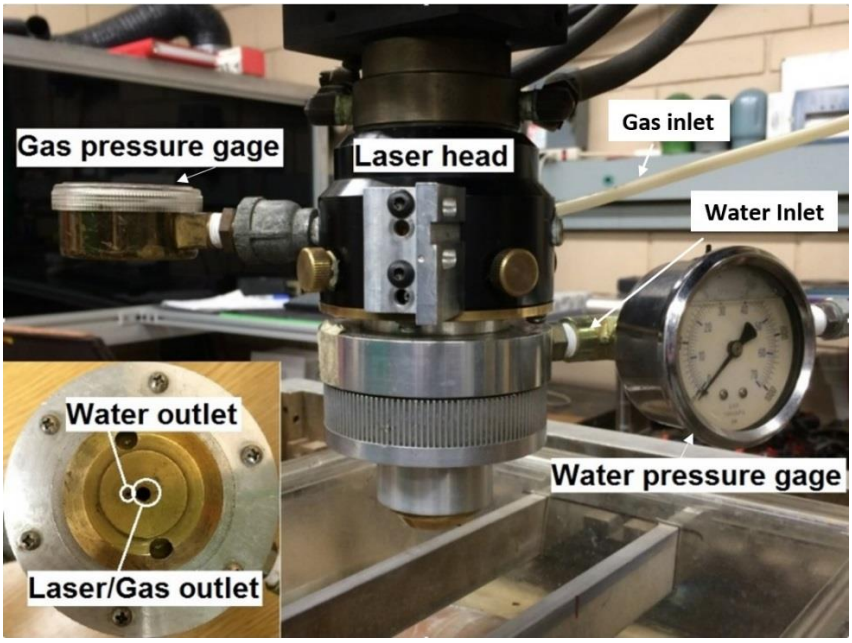

Figure 1.4. *Experimental setup of CO2-LWJ machining system*

1.4 Hardness change mechanism

It is well known that the hardening effect of grain boundaries can be described by the Hall-Petch equation, which shows that the material hardness (H) is dependent on grain size (d). Furthermore, the Hall-Petch equation reveals that a decrease in grain size leads to an increase in hardness as shown:

$$H = H_0 + \frac{K}{\sqrt{d}} \tag{1.3}$$

where, K is the strengthening coefficient (a constant specific to each material), and H_0 is the constant.

However, the Hall-Petch equation is limited in its ability to describe the hardening effect since material hardness cannot increase infinitely with infinitesimal grain size. Experimental results have shown the hardness of cubic boron nitride to be reduced to 25 GPa when the grain size decreases to a few nanometers (Dubrovinskaia et al., 2007). This kind of grain size softening is attributed to intergranular deformation by grain boundary sliding, which is the inverse of the Hall-Petch effect. Thus, the Hall-Petch equation is only valid for cases when the grain size is within tens of nanometers or higher. Since this study only investigated the hardening effect for materials with grain sizes on scales of hundreds of nanometers and micrometers, the inverse Hall-Petch effect was utilized.

In order for deformation to occur on a material, a dislocation movement must be developed. As resistance, grain boundaries impeding the dislocation propagation. Since the lattice structure of adjacent grains differs in orientation, more energy is required for a dislocation to change directions and transfer from one grain to other grains (Callister & Rethwisch, 2007). Hindering the movement of a dislocation will impede the development of plastic deformation and result in an increase in material hardness.

When a load is applied, the dislocations will move through the crystalline lattice until encountering a grain boundary, where the repulsive stress developed between grains will act as an impeding force to oppose continued dislocation motion. As more dislocations are created and clustered on the grain boundary, the ability of the dislocations to move past the boundary is eliminated. As dislocations generate repulsive stress fields, each successive dislocation will apply a repulsive force to neighboring dislocations in contact with the grain boundary. The repulsive forces act as a driving force to reduce the energetic barrier and allow the diffusion of dislocations across the grain boundary which leads to further deformation in the material.

When the grain size is decreased, the clustering of dislocations at the grain boundary is reduced and the amount of applied load required to move a dislocation across a grain boundary is increased. The higher the applied load required to create plastic deformation, the higher the material hardness. This is the relationship between grain size and material hardness as described by the Hall–Petch equation.

1.5 Dissertation Organization

Chapter 1 provides the motivation and background for the study and development of super-hard materials. This chapter reviews the hardness measurement mechanisms that have been reported in literature and used extensively for material hardness improvement research. Chapter 1 also gives a detailed summary of the design and principles of the laser waterjet heat (LWH) treatment system and the material hardness change mechanism for boron nitride (BN) which is the material of interest for this research study.

Chapter 2 addresses two topics in the field of LWH treatment which are the hardness improvement mechanism for LWH-treated BN and the effect of laser fluence on the hardness change of dual-phase BN. Chapter 3 is composed of an experimental investigation of the effect of laser beam overlap percentage on dual-phase BN material hardness improvement.

Chapters 4 and 5 include the works conducted to identify the relationship between LWH treated BN material hardness change ratio and LWH treatment parameters. Chapter 4 is the paper study on 55%cBN/45%TiN and 82%cBN/18%AlN commercial materials, which are cutting tool materials using in industry currently. Chapter 5 is the study on 5 different cBN compositions of un-commercial cBN/wBN composites, which were made under high-pressure high-temperature (HPHT) environment in Lund University.

Chapter 6 presents general conclusions observed in all of these studies and describes future research ideas to move forward with these projects.

1.6 References

Angseryd, J., Elfwing, M., Olsson, E., & Andrén, H. O. (2009). Detailed microstructure of a cBN based cutting tool material. *International Journal of Refractory Metals and Hard Materials*, *27*(2), 249–255.

Anstis, G. ., Chantikul, P., Lawn, B. ., & Marshall, D. . (1981). A critical evaluation of indentation techniques for measuring fracture toughness: I Direct crack measurements. *Journal of the American Ceramic Society*, *46*(September), 533–538.

Aouici, H., Yallese, M. A., Chaoui, K., Mabrouki, T., & Rigal, J. F. (2012). Analysis of surface roughness and cutting force components in hard turning with CBN tool: Prediction model and cutting conditions optimization. *Measurement: Journal of the International Measurement Confederation*, *45*(3), 344–353.

Basu, B., Raju, G. B., & Suri, A. K. (2006). Processing and properties of monolithic TiB 2 based materials. *International Materials Reviews*, *51*(6), 352–374.

Brazhkin, V. V., Lyapin, A. G., & Hemley, R. J. (2002). Harder than diamond: Dreams and reality. *Philosophical Magazine A*, *82*(2), 231–253.

Callister, W., & Rethwisch, D. (2007). *Materials science and engineering: an introduction*. *Materials Science and Engineering* (Vol. 94).

Demazeau, G., Biardeau, G., & Vel, L. (1990). Synthesis of cubic boron nitride using magnesium or magnesium-based fluoronitrides. *Materials Letters*, *10*(3), 139–144.

Dubrovinskaia, N., Solozhenko, V. L., Miyajima, N., Dmitriev, V., Kurakevych, O. O., & Dubrovinsky, L. (2007). Superhard nanocomposite of dense polymorphs of boron nitride: Noncarbon material has reached diamond hardness. *Applied Physics Letters*, *90*(10).

Fischer-Cripps, A. C. (2011). *Nanoindentation*. *Springer*.

Gou, H., Wang, Z., Zhang, J., Yan, S., & Gao, F. (2009). Structural stability and elastic and electronic properties of rhenium borides: first principle investigations. *Inorganic Chemistry*, *48*(2), 581–7.

Haines, J., L, J. M., & Bocquillon, G. (2001). M Aterials. *Recherche*, *1955*(1), 1–23.

Hansen, N. (2004). Hall-petch relation and boundary strengthening. *Scripta Materialia*, *51*(8 SPEC. ISS.), 801–806.

He, W., Bhole, S. D., & Chen, D. (2008). Modeling the dependence of strength on grain sizes in nanocrystalline materials. *Science and Technology of Advanced Materials*, *9*(1), 1–7.

Hou, X. D., Bushby, a J., & Jennett, N. M. (2008). Study of the interaction between the indentation size effect and Hall–Petch effect with spherical indenters on annealed polycrystalline copper. *Journal of Physics D: Applied Physics*, *41*(7), 074006.

Huang, Q., Yu, D., Xu, B., Hu, W., Ma, Y., Wang, Y., … Tian, Y. (2014). Nanotwinned diamond with unprecedented hardness and stability. *Nature*, *510*(7504), 250–3.

Irifune, T., Kurio, A., Sakamoto, S., Inoue, T., & Sumiya, H. (2003). Materials: Ultrahard polycrystalline diamond from graphite. *Nature*, *421*(6923), 599–600.

Jiménez, I., Sutherland, D., van Buuren, T., Carlisle, J., Terminello, L., & Himpsel, F. (1998). Photoemission and x-ray-absorption study of boron carbide and its surface thermal stability. *Physical Review B*, *57*(20), 13167–13174.

John, P., Polwart, N., Troupe, C. E., & Wilson, J. I. B. (2002). The oxidation of \lattplane{100} textured diamond. *Diamond and Related Materials*, *11*, 861–866.

Knoop, F., Peters, C. G., & Emerson, W. B. (1939). A sensitive pyramidal-diamond tool for indentation measurements. *Journal of Research of the National Bureau of Standards*, *23*(1), 39.

Levine, J. B., Betts, J. B., Garrett, J. D., Guo, S. Q., Eng, J. T., Migliori, A., & Kaner, R. B. (2010). Full elastic tensor of a crystal of the superhard compound ReB2. *Acta Materialia*, *58*(5), 1530–1535.

Levine, J. B., Tolbert, S. H., & Kaner, R. B. (2009). Advancements in the search for superhard ultra-incompressible metal borides. *Advanced Functional Materials*, *19*(22), 3519–3533.

Li, B., Sun, H., & Chen, C. (1996). Large indentation strain stiffening in nanotwinned cubic boron nitride. *Nature Communications*, *94*(May), 90.

Li, B., Sun, H., & Chen, C. (2014). Large indentation strain-stiffening in nanotwinned cubic boron nitride. *Nature Communications*, *5*(May), 4965.

Liu, K., & Li, X. P. (2001). Ductile cutting of tungsten carbide. *Journal of Materials Processing Technology*, *113*(1-3), 348–354.

Melaibari, A. A., Zhao, J., Molian, P., Bushlya, V., Zhou, J., Ståhl, J.-E., … Shrotriya, P. (2016). Ultrahard boron nitride material through a hybrid laser/waterjet based surface treatment. *Acta Materialia*, *102*, 315–322.

Melaibari, A., Molian, P., & Shrotriya, P. (2012). Laser/waterjet heat treatment of polycrystalline cubic/wurtzite boron nitride composite for reaching hardness of polycrystalline diamond. *Materials Letters*, *89*, 123–125.

Meng, Y., Mao, H., Eng, P., Trainor, T., Newville, M., Hu, M., … Hemley, R. (2004). The formation of sp3 bonding in compressed BN. *Nature Materials*, *3*(2), 111–114.

Dinesh Kalyanasundaram. (2009). Mechanics guided design of hybrid laser / waterjet system for machining hard and brittle materials. A dissertation of DOCTOR OF PHILOSOPHY in Iowa State Univerisity, Ames, Iowa.

Riedel, R. (1994). Novel Ultrahard Materials. *Advanced Materials*, *6*(7-8), 549–560.

Roy, T. K. (2015). Assessing hardness and fracture toughness in sintered zinc oxide ceramics through indentation technique. *Materials Science and Engineering: A*, *640*, 267–274.

Zhuoru Wu. (2015). The mechanism governing cutting of hard materials with hybrid Laser / Waterjet system through controlled fracture. A dissertation of DOCTOR OF PHILOSOPHY in Iowa State Univerisity, Ames , Iowa.

Smith, R. L. et al. (1922). an Accurate Method of Determining the Hardness of Metals, With Particular Refernce To Those of a High Degree of Hardness. *proc.Inst.Mech.Eng.*, *1*(May), 623–641.

Solozhenko, V. L., Kurakevych, O. O., & Le Godec, Y. (2012). Creation of nanostuctures by extreme conditions: High-pressure synthesis of ultrahard nanocrystalline cubic boron nitride. *Advanced Materials*, *24*(12), 1540–1544.

Superhard, U. (2007). Comment on " Synthesis of, *318*(December), 1–2.

Taniguchi, T., Akaishi, M., & Yamaoka, S. (1996). Mechanical Properties of Polycrystalline Translucent Cubic Boron Nitride as Characterized by the Vickers Indentation Method. *Journal of the American Ceramic Society*.

Thévenot, F. (1990). Boron carbide—A comprehensive review. *Journal of the European Ceramic Society*, *6*(4), 205–225.

Tyne, U. (1965). METAL BORIDES By N. *Quarterly Reviews*.

Ulrich, S., Ehrhardt, H., Schwan, J., Samlenski, R., & Brenn, R. (1998). Subplantation effect in magnetron sputtered superhard boron carbide thin films. *Diamond and Related Materials*, *7*, 835–838.

Vepřek, S. (1997). Conventional and new approaches towards the design of novel superhard materials. *Surface and Coatings Technology*, *97*(1-3), 15–22.

Vepřek, S. (1999). The search for novel, superhard materials. *Journal of Vacuum Science & Technology A: Vacuum, Surfaces, and Films*, *17*(5), 2401.

Veprek, S., & Argon, A. S. (2002). Towards the understanding of mechanical properties of super- and ultrahard nanocomposites. *Journal of Vacuum Science & Technology B: Microelectronics and Nanometer Structures*, *20*(2), 650.

Veprek, S., Argon, A. S., & Zhang, R. F. (2010). Design of ultrahard materials: Go nano! *Philosophical Magazine*, *90*(31-32), 4101–4115.

Wentorf, R. H. (1961). Synthesis of the Cubic Form of Boron Nitride. *The Journal of Chemical Physics*, *34*(3), 809.

Yin, L., Vancoille, E. Y. J., Lee, L. C., Huang, H., Ramesh, K., & Liu, X. D. (2004). High-quality grinding of polycrystalline silicon carbide spherical surfaces. *Wear*, *256*(1-2), 197–207.

CHAPTER II

ULTRAHARD BORON NITRIDE MATERIAL THROUGH A HYBRID LASER/WATERJET BASED SURFACE TREATMENT

A paper submitted for publication in the journal of Acta Materialia, (2016)

Ammar A. Melaibaria, Jingnan Zhaoa, Pal Moliana, Volodymyr Bushlyad, Jinming Zhou, Jan-Eric Ståhl, Igor Petrusha and Pranav Shrotriya

Abstract

We report a dual phase boron nitride (BN) material composed of 50% cubic and 50% wurtzite phases that has the same level of hardness as polycrystalline diamond. The dual phase BN material was initially synthesized from high pressure and high temperature consolidation of powder materials and subsequently, a laser/waterjet heat treatment (LWH) was applied to the material surface. The LWH process consisted of heating the sample surface using a continuous wave CO2 laser beam followed by tandem waterjet quenching of the laser irradiated material. The indentation hardness of the as-synthesized material was measured to be nominally 37 GPa. After the heat treatment the indentation hardness increased to nominal values of 75 GPa reaching the hardness of polycrystalline diamond 65-80 GPa. Dispersive Raman spectroscopy, high-resolution scanning electron microscope (HRSEM) and surface grazing XRD were used to characterize the BN phase signatures, grain size changes and phase transitions in both as-synthesized and heat treated material. Comparison of the as-synthesized and heat treated material microstructure revealed that heat treatment resulted in microstructure that consists of large grains; surrounded with regions of nano-grains between larger grains and; formation of solid interlayer along the grain boundaries. The increase in hardness was observed

for LWH processing at laser fluence below 35 J/mm², and LWH processing above this value resulted in spallation of BN material from the surface. Raman spectrums of the material processed below the laser fluence of 35 J/mm² indicated that there are minimal phase transitions in the material; however, above that fluence, BN transformed into hexagonal phase resulting in surface damage through spallation. A combination of amorphous phase formation at the grain boundaries and grain size refinement are suggested as the mechanisms responsible for the LWH processing induced hardness increase.

KEYWORDS: Ultrahard material; Boron Nitide; Laser Heat treatment; Microstructure; Composite wBN/cBN.

2.1 Introduction

Ultra-hard materials that are chemically inert and thermally stable at high temperatures are desirable for enhancing machining and wear performance in demanding chemical and thermal environments. Single and polycrystalline diamonds are the hardest materials (Vickers hardness -75-100 GPa); however, at high temperatures, diamond loses its chemical inertness and thermal stability. In contrast, cubic boron nitride (cBN) has exceptional chemical and thermal stability but has much lower hardness (35-45 GPa). Despite diamond's superior edge over cBN in hardness, the chemical inertness and thermal stability of cBN at high temperatures made it highly preferable particularly for machining hard alloys (Bhaumik, Divakar, & Singh, 1995; Fujisaki et al., 2009; Z. G. Wang, Rahman, & Wong, 2005; Zhang et al., 2008). Increasing the hardness of BN to the level of diamond is expected to result in chemically and

thermally inert ultrahard material that is suitable for range of demanding wear and machining applications.

A number of recent studies have investigated the formation, structure, and properties of cBN and have shown that it is possible to increase the hardness of dual phase boron nitride (Cubic and Wurtzite (cBN/wBN)) materials to that of diamond through nanotwinned grains (Tian et al., 2013) and selection of appropriate microstructure (Dubrovinskaia et al., 2007). Using first-principle calculations, Pan et al (Pan, Sun, Zhang, & Chen, 2009) showed that the large normal compressive stresses under indentation conditions can force wBN to reach a hardness of 114 GPa through a volume-conserving/bond-flipping structural phase transformation. They proposed a two-stage shear deformation mechanism responsible for this unexpected result.

Dubrovinskaia et al (Dubrovinskaia et al., 2007) measured a maximum load-invariant hardness of 85 GPa and a high fracture toughness of 15 MPa√m in cBN composites having nanoscale grain sizes (14 nm) coupled with the formation of dense hexagonal and cubic BN phases structures within the grains. The size effect of BN nanocomposites at 14 nm is at the transition between the strengthening due to stifled dislocation activity inside grains through the Hall–Petch effect and leveling off of plastic resistance due to increasing grain boundary shear (Melaibari, Molian, & Shrotriya, 2012; Veprek, Argon, & Zhang, 2010).

We report a dual phase boron nitride (BN) material composed of 50% cubic and 50% wurtzite phases that has the same level of hardness as polycrysalline diamond. The dual phase BN material was initially synthesized from high pressure and high temperature consolidation of powder materials and subsequently, a laser/waterjet heat treatment (LWH) was applied to the material surface. The LWH process consisted of heating the sample surface using a

continuous wave CO2 laser beam followed by tandem waterjet quenching of the laser irradiated material. The microstructure and phase composition of the material are analyzed to identify the mechanism contributing to the hardness improvement. The influence of laser fluence on the LWH treatment is investigated to identify the thermomechanical conditions necessary for hardness improvement.

2.2 Experimental Approach

2.2.1 Sintering of dual-phase materials

The samples used in this study were produced by high pressure-high temperature (HP-HT) sintering of wBN powders obtained via detonation synthesis of hexagonal boron nitride (hBN) at presence of water. It is known (Britun, Kurdyumov, & Petrusha, 1999) that wBN forms as a results of martensitic transformation of hBN, where the latice of the initial hBN transforms into a diamond-like latice of wBN with the following orintation relation (0 0 0 1)w || (0 0 0 1)h, [$\bar{1}$ 1 0 0]w || [$\bar{1}$ 1 0 0]h. The wBN particles have flake-like morphology which is related to the inheritance of the morphological shape of hBN phase during martensitic transformation. The size of the wBN particles in the basal plane normally reaches 1-3 μm, while the particle thickness is 0.1-0.3 μm. The particles, as a rule, possess the fragmented structure with azimuthal disorientation of the sub-structural elements (Britun et al., 1999).

Sintering was done on the Toroid type high pressure apparatus (Hubert et al., 1998) at pressure of 7.7±0.3 GPa and temperature of 1750±50 °C, i.e. in the region of thermodynamic stability of cubic boron nitride (cBN). Duration of the HP-HT treatment was 45 sec. The sintering of wBN under conditions of high pressure in the given temperature range leads to the formation of binderless dual phase microstructure as a result of incomplete wBN→cBN solid

phase transformation (Sachdev, 2003). The pressure-temperature conditions were selected such that the sintered material has 50±5% content of cBN phase which corresponds to a tool material known under trade name Hexanit-R. The material was sintered in the shape of round blanks and ground to the diameter of 9.52 and thickness of 3.18 mm which corresponds to standard tooling inserts RNGN09030T. The flat surfaces of the inserts were given the mirror finish using fine diamond grinding prior to Laser/Waterjet Heat (LWH) treatment experiments.

2.2.2 Laser waterjet heat (LWH) treatment experiment

The LWH process involves laser heating and water-jet quenching in tandem (Figure 2.1) using the (LWJ) system that has been previously design and used for machining brittle ceramics (Kalyanasundaram, Shehata, Neumann, Shrotriya, & Molian, 2008; Kalyanasundaram, Shrotriya, & Molian, 2009, 2010; Kalyanasundaram, 2009). The heat treatment was performed using a continuous wave CO_2 laser with power of 200 W and a process speed of 68 mm/s. The laser beam was immediately followed by waterjet stream of 400 kPa. Also, the laser beam was surrounded by a stream of air to prevent the laser-water interaction. To heat treat all the sample surface, the specimen surface was rastered with 50% overlap between adjacent passes. The laser heat treatment was performed with two different spot sizes (diameter of 1 mm and 0.8 mm) in order to achieve two different fluence levels: 35 J/mm² (low fluence) and 55 J/ mm² (high fluence)

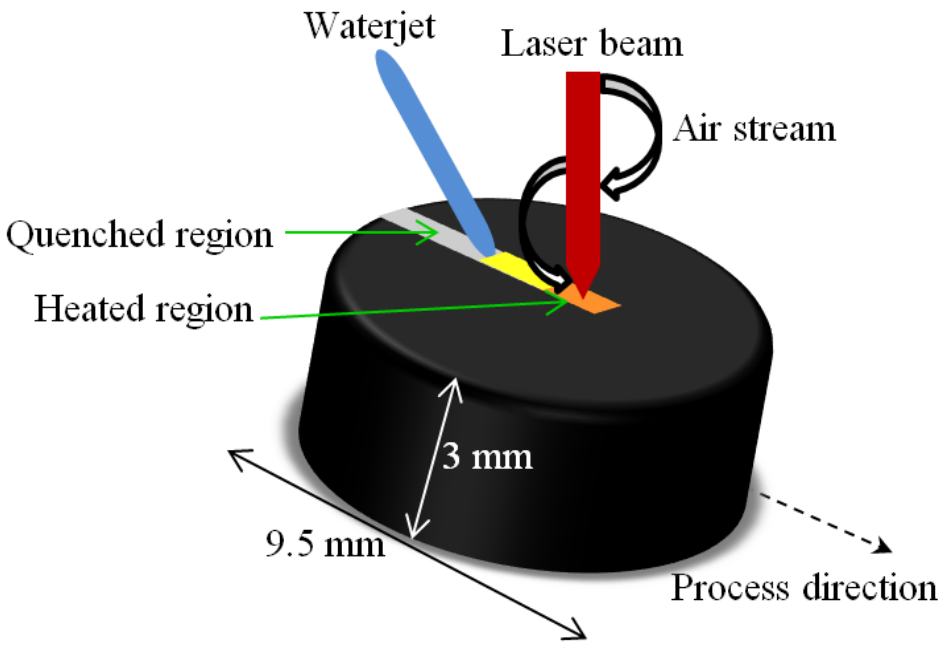

Figure 2.1. *Schematic of LWH process.*

2.2.3 Measurement of micro-hardness

The hardness measurements were conducted following the procedures that ensure reliable measurements for material s with hardness close to diamond (A.C. Fischer-Cripps, Bull, & Schwarzer, 2012; Anthony C. Fischer-Cripps, 2011). The indentation hardness tests were performed using a Tukon microhardness tester with a Vicker's diamond pyramid indenters (cube-corner indenter with α=45º and 70º center-face angle). Measurements were made on the length of the diagonals and compared with the measurements of the depth of the indentations using a high resolution (± 1 µm) optical microscope and optical profilometer to ensure the accuracy of the data. A number of hardness measurements (20) were made to ensure the reliability and repeatability of the test data.

2.2.4 Microstructure and phase composition characterization

The microstructure of the as-sintered and heat treated materials were characterized using high resolution SEM (HRSEM). General microstructure analysis of initial (untreated)

sample was done on HRSEM LEO/Zeiss 1560 in high current mode which resolves most of the problems with sample charging but affects the resolution. Detailed analysis of both untreated and LWJ treated samples was done on HRSEM FEI Nova NanoLab 600.

The phase compositions of the as-sintered and treated samples were characterized using grazing angle x-ray diffraction (XRD) and Raman spectroscopy. Quantitative XRD analysis was used for determination of the cBN and wBN content. The technique used is based on the measurement of intensities of closely located lines 200c and 102w for cubic and wurtzitic phases respectively (Levitas & Shvedov, 2002). The calculation of the volumetric content of cBN (αc) is done with the help of regression equation αc = 1,71x −1,17x2 + 0,46x3, where parameter $x = I^c_{200}/\left(I^c_{200} + I^w_{102}\right)$ changes from zero to 1.

Dispersive Raman spectroscopy analysis (Renishaw-inVia Raman Microscopy) was performed to identify the phases before and after the heat treatment process using Ar-ion laser with a 20 μm entrance slit width, 50 mW laser power, and 488 nm operating wavelength. XRD measurements in grazing angle setups were performed using a STOE Darmstadt Bragg-Brentano diffractometer operated at 40 kV and 40 mA using Cu Kα source.

2.3 Experimental Results

2.3.1 As-sintered material

Scanning electron micrograph of the as-sintered PCBN samples are plotted in Figure 2. The microstructure consists of two types of structures with different size and morphology. It also contained many structural defects in the form of dislocations, stacking faults and point defects (Sun et al., 2004; Veprek et al., 2010). The first type is lamellas that are 0.5-2 μm in length and 0.15-0.2 μm in thickness. Majority of lamellas exhibit form changes of bending and

fragmentation with displacement. Two features can be distinguished: regular band contrast across the thickness and interfaces at which the fragmentation can take place. The second type of structure is the independent grains with polyhedral faceting. Such polyhedral grains have the particle size of 0.2-0.3 μm. Their most common location is at the fragmentation sites and interfaces inside lamellas. Lamella/polyhedron and polyhedron/polyhedron interfaces have both straight-line boundaries which result in formation of pores. The lamellas are originally the wurtzite BN grains that were fragmented during cold compaction prior to HP-HT (high pressure-high temperature) processing. Smaller polyhedral grains originate mainly during fragmentation of lamellas under HP-HT conditions and evolve during recrystallization process. Such fragmentation takes place due to both kink band nucleation and formation of interfaces via slip along prismatic and basal planes. Phase composition of the initial material is wurtzite BN, cubic BN and multilayer polytypes. Confirmation of the existence of these polytypes is the micro-band sub-structure of lamellas which comprises of thin wBN and cBN layers as a result of layerwise wBN → cBN transformation as shown in the transmission electron micrograph and associated selected area electron diffraction map in Figure 2.2.

Quantitative X-ray diffraction analysis indicated that volume content of cBN phase in the as-synthesized samples equaled 44%, which is close to the value targeted when selecting HP-HT conditions. The content was calculated from the above $\alpha c = f(x)$ dependence which however did not consider the influence of material texturing (Levitas & Shvedov, 2002).

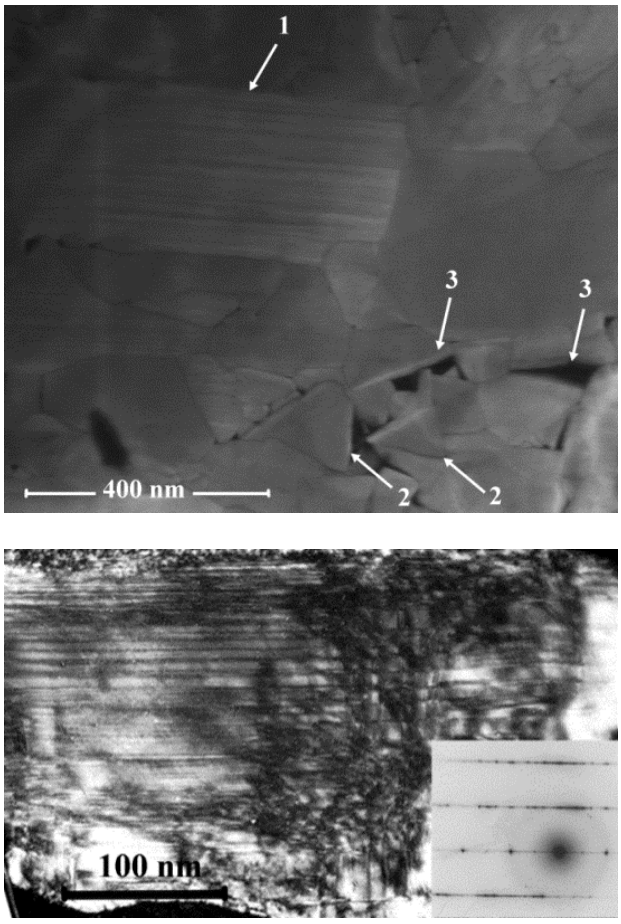

Figure 2.2 *(top) Detailed microstructure of untreated wBN/cBN composite: (1) Micro-band sub-structure of the lamellas; (2) Polyhedral grains at the fragmentation interfaces; (3) Pores due to polyhedral faceting. (bottom) Dark field (in 002 wBN - 111 cBN joint reflection) TEM of micro-band sub-structure and corresponding SAED.*

2.3.2 LWH processing of BN material

Visual examination of laser heat treated samples with low fluence revealed a color change from light-absorbing black/gray to transparent white. Such an effect is ascribed to a change in crystal morphology following Sachdev's classification of the crystalline morphology of cBN according to color, size and transparency (Sachdev, 2003). A transparent cBN of white to amber implies tetrahedral crystal morphology (as opposed to octahedral) with small grain

size and loss of boron. It may be noted that the color may also be caused by inclusions, dopants or defects. The formation of transparent white of cBN provides some clues on the possible phase, stoichiometry and grain size changes in laser heat treatment.

In the high fluence treated sample, the LWH treatment resulted in surface damage through spallation of materials along the centerline of the laser beam path. In the damaged regions, the laser irradiated top surface was removed exposing the underlying material layers. Using an optical microscope (Leica M205 A stereo microscope), the depth of the spallation region was measured to vary between 1 to 3 microns. The undamaged surface surrounding the spallation area showed a similar color change from black/grey to transparent white as observed on the low fluence treated sample.

Representative SEM images of the LWH processed surface are shown in Figs 2.3 and 2.4. The microstructure consists of the same two grain types- lamellas and polyhedrons- as the untreated samples. Similar sub-structure as the untreated sample is also observed. The main differences as compared to the untreated microstructure are highlighted in the SEM images. As shown in the highlighted region 1 of Figs 2.3 and 2.4, the large lamella have sub-divided to form smaller lamellar grains of size 100-200 nm with smooth facets as opposed to straight-line faceting in untreated state. In addition, a distinct interlayer is observed at the boundary of some of the grains. Cavities/pores at the interfaces of all such particles have smoothened shape as well. As shown in the highlighted region 2 of Figs 2.3 and 2.4, microstructure in the as-received samples has been refined to form clusters of nanosized grains (sizes between 20-30 nm) that are sandwiched between larger grains.

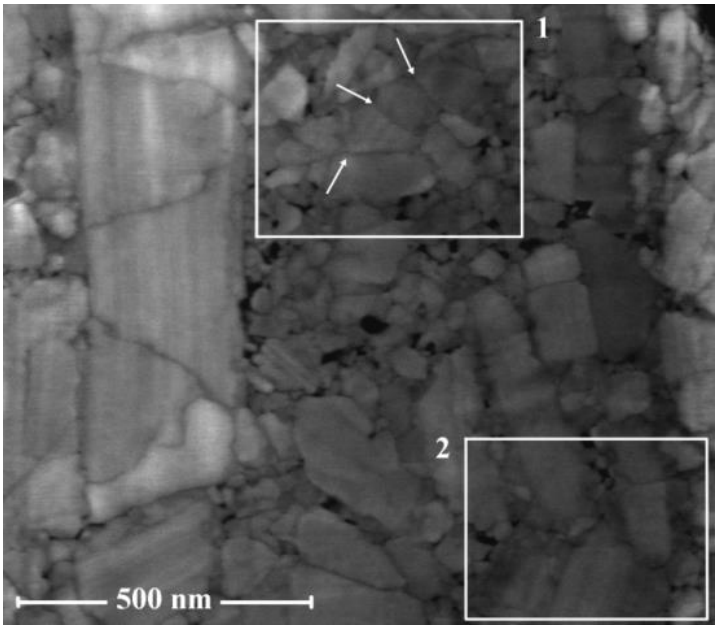

Fig 2.3 *HRSEM of the LWJ treated microstructure showing the lamellas with the smoothened faceting and: (1) Region of polyhedral grains without pores with solid interlayer at the grain boundary; (2) Regions of nano-sized grains of rounded shape between larger grains.*

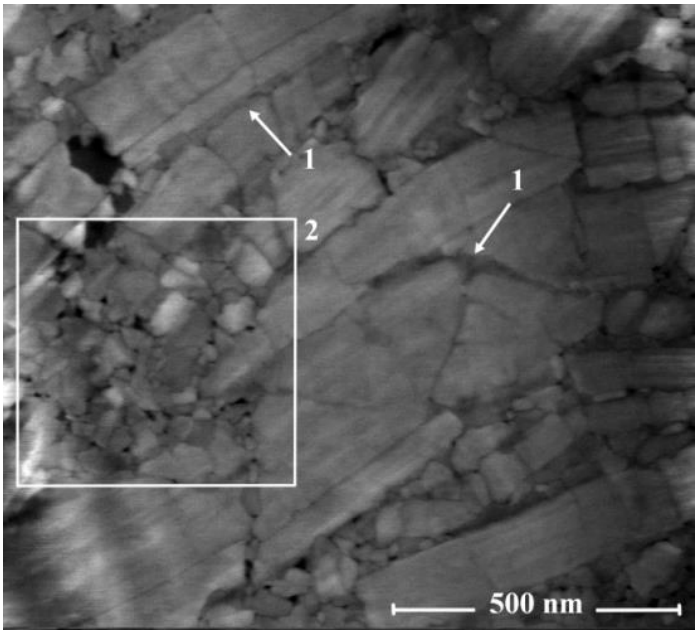

Fig 2.4 *HRSEM of the LWJ treated microstructure showing the smaller lamella grains with: (1) Interlayer at grain boundaries; (2) agglomeration of nano-sized grains of rounded shape.*

2.3.3 Hardness measurements

Results of the hardness experiments on the untreated, low fluence treated and high fluence treated samples are plotted in Fig 2.5. On the high fluence treated samples the hardness measurements were conducted at the bottom of the spalled area as well as on the undamaged surface. As shown in Figure 2.5, the hardness of the as-synthesized surface was found to be 37 ± 5 GPa, while the hardness of the laser treated surface was found to be 72 ± 10 and 75 ± 16 GPa for the low fluence and undamaged high fluence treated surfaces, respectively. The LWJ has almost doubled the hardness in the low energy fluence treatment and the undamaged surface on the high energy fluence treated samples. In the damaged regions on the high fluence treated sample, the hardness was found to be 32 ± 11 GPa which is similar but slightly lower than the hardness of the as-synthesized material. Another indicator of the increased hardness of the LWH treated samples was the damage to indenters used for hardness measurements. In the initial tests, two diamond indenters with $\alpha = 45^{o}$ center-face angle were broken performing these hardness tests. Hence, an indenter with center-face angle $\alpha = 70^{o}$ was used for the hardness measurement in order to reduce the chance of breaking another diamond indenter. The nominal hardness values measured with both indenters were found to be consistent but the scatter in hardness values was found to be greater with lower face angle indenter. The nominal value as well as the total range and dispersion of the measured values are plotted in Fig.6 to show the LWH treatment results in a statistically significant difference of the measured hardness values.

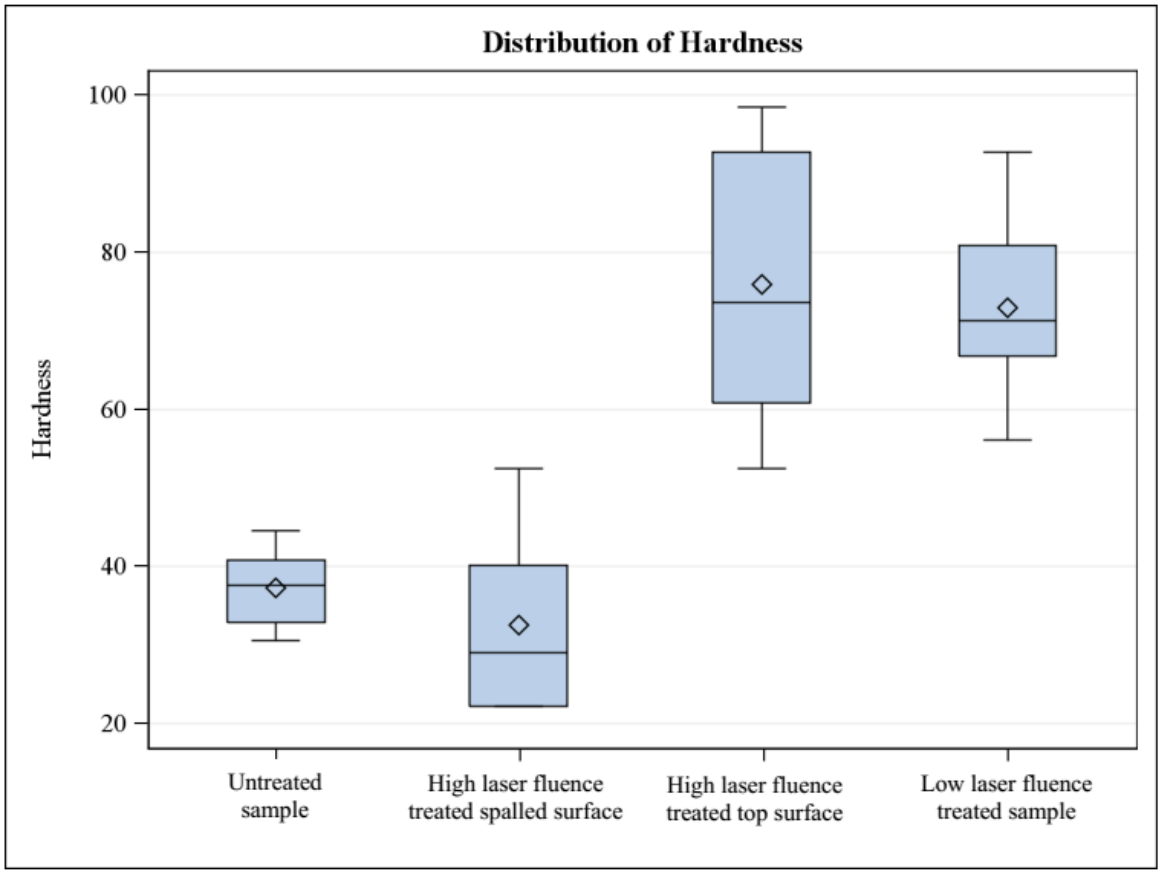

Fig 2.5 *Vicker's indentation hardness test data of dual phase wBN/cBN using high and low energy fluence.*

2.4 Raman Spectroscopy and X-ray diffraction characterization

2.4.1 Surface grazing angle XRD analysis

The XRD analysis did not show any major differences before and after the treatment on the surfaces that have shown increase in hardness. XRD analysis was not performed on the damaged surfaces. In the traditional X-Ray analysis, the low attenuation coefficient of boron nitride leads to large penetration depth (up to 2-3 mm into the bulk thickness). In this case the relative surface contribution can become negligible. Hence, surface grazing angle XRD analysis was used because of its shallower penetration depth and surface sensitivity. The

diffraction patterns obtained for different grazing angles are plotted in Figure 2.6 to characterize the differences between untreated and treated samples. As shown in Fig 2.6, the wBN peaks are either almost the same for treated and untreated sample at all the different grazing angles. However, the cBN peak at 2θ = 50.5 deg for different grazing angles is always higher for LWH treated samples implying a small increase in cBN.

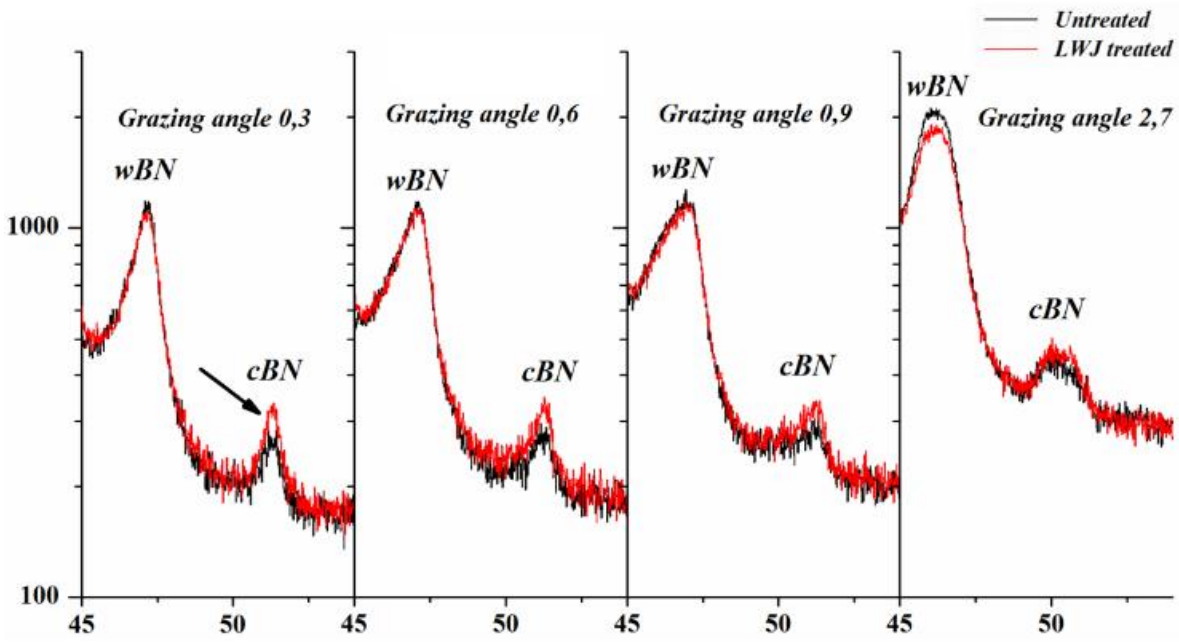

Figure 2.6 *Grazing angle XRD indicating minor increase in cBN content on the heat treated surface.*

2.4.2 Raman analysis

The Raman spectrums obtained for untreated surface, damage free treated surface and damaged surface exposed due to spalling damage are plotted in Figure 2.7. The Raman spectrum of untreated sample exhibits the two distinct peaks of cBN at 1307 cm^{-1} and 1058 cm^{-1} associated with the longitudinal (LO) and transverse (TO) optical phonon modes respectively (Bergman & Nemanich, 1996). The cBN peaks at 1058 cm-1 overlaps with one

of the wBN peaks. The Raman analysis of the untreated sample also revealed the 962 and 1040 cm^{-1} peak for wBN. It is generally difficult to identify the Raman peaks for wBN because of its small size (submicron) and shock-wave method of production (Taniguchi, Akaishi, & Yamaoka, 1996). Many characteristic peaks at 950, 1015, 1053, 1075, 1246, 1280 and 1295 cm^{-1} have been reported based on theoretical and experimental observations (Karch, Bechstedt, Pavone, & Strauch, 1996; Ohba, Miwa, Nagasako, & Fukumoto, 2001; Ohba et al., 2001) but usually not all of these peaks are detectable. The Raman spectra of treated and undamaged samples also show the peaks of cBN (1302 and 1052 cm^{-1}) and wBN (962 and 1040 cm^{-1}). However, the ratio of cBN to wBN peak in the overlapped region appear to be increased after LWJ treatment. Such an increase may be attributed to partial transformation of wBN→cBN (Sachdev, 2003). In addition, an unidentified hump-like peak around 1205 cm^{-1} is also observed. This hump-like peak can be assigned to amorphous boron (B12) or a rich boron phase of BN (Kuhlmann, Werheit, Lundström, & Robers, 1994; Z. Wang, Zhao, Lazor, Annersten, & Saxena, 2005) which may correspond to the solid interlayers observed at the grain boundaries in the HRSEM images. Due to the high reactivity of amorphous boron to oxygen, we expect that boron-rich phase of BN are more likely to be present along the boundaries of BN particles.

In the surfaces exposed due to spallation of the laser treated material, the characteristic peaks from cBN and wBN are observed. However, the ratio of the wBN peaks to cBN peaks is even smaller than that observed in damage-free surfaces, suggesting an increased transformation of wBN to cBN under high fluence treated surfaces. In addition, the hexagonal boron nitride (hBN) peak at 1362 cm^{-1} peak indicates a transformation of cBN→hBN where hBN typically has a 1366 cm^{-1} peak (Meng et al., 2004). The volumetric increase associated

with cBN→hBN may have resulted in spallation of surface layer off the surface since hBN volume is larger than cBN.

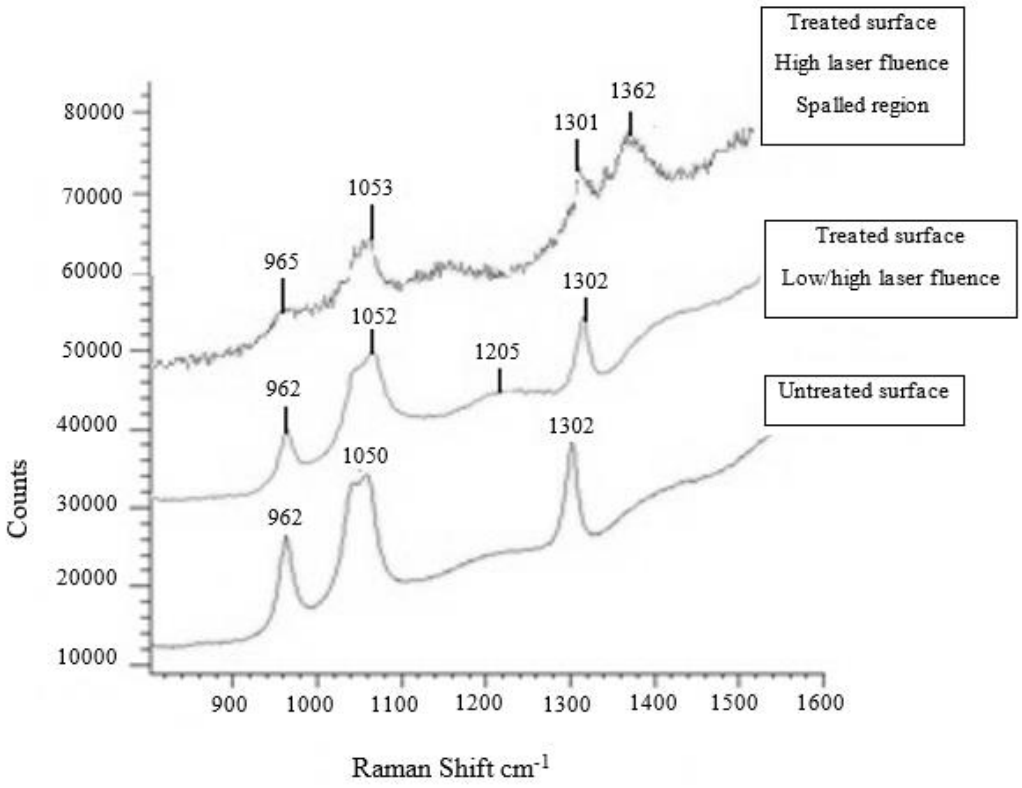

Figure 2.7 *Raman spectra of untreated sample (bottom spectrum), low laser fluence treated sample (middle spectrum), and peeled off region in the high laser fluence treated sample (top spectrum).*

2.5 Discussion

The average hardness of the untreated samples is almost doubled with the LWJ treatment with low energy fluence and on the undamaged surfaces of the samples treated with high energy fluence. Finite element analysis was applied to estimate the thermomechanical loads applied to the sample during the LWH processing. An axisymmetric finite element model

was used to model the localized heating due to incidence of laser beam followed by the quenching of the heated material surface due to the water-jet. Water quenching leads to rapid decrease of temperature in the circular zone heated by low-power laser therefore the heating and subsequent cooling associated with LWH processing can be modeled as an axis symmetric problem. The Gaussian profile of the laser beam is approximated as a surface heat source whose intensity at distance r from center is given as:

$$I_h(r) = a_s I_o e^{\left(\frac{-2r^2}{w^2}\right)} \tag{2.1}$$

where as represents the absorption coefficient, I_0 represents laser intensity at center of beam, w represents the diameter of the laser beam. The absorption coefficient was chosen to be 0.75 (Melaibari et al., 2012). The laser intensity at the center of the beam was calculated based on the laser fluence used in the laser heat treatment experiment. The duration of laser spot interaction with sample surface was calculated to equal the duration that a laser beam is incident at a material point during experiments. Thermal quenching due to the waterjet was modeled using convective heat transfer coefficient of 10,000 W/ m^2 K such that the sample surface is rapidly cooled down to water temperature on the action of waterjet. Finite element analysis package ABAQUS was utilized to compute the temperature and stress fields for both low and high laser fluence experiments. The finite element mesh was refined till the computed temperature and stress field became independent of the element size.

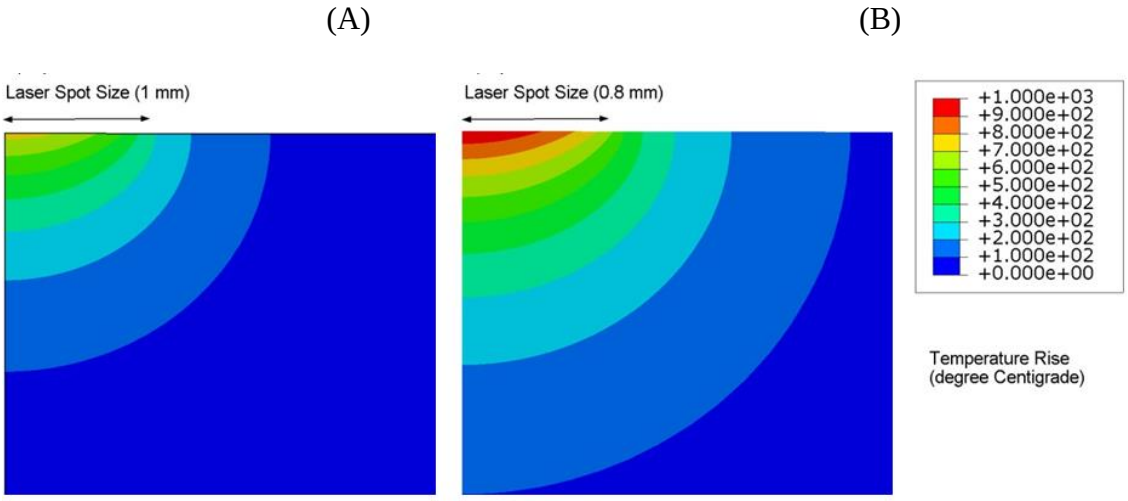

Figure 2.8 *Temerature distribution at the end of laser irradiation during LWH processing: (A) sample treated at low laser fluence (35 J/mm2); and (B) sample treated at high laser fluence (55 J/mm2)*

During LWH surface treatment, the temperature of the surface increased rapidly during laser heating and attained a maximum value at the end of the laser irradiation. After the laser heating, the sample surface was rapidly cooled due to the waterjet quenching. The computed temperature field in the samples at the end of laser irradiation is plotted in Figs 2.8(a) and (b), for low fluence and high fluence laser processing experiments, respectively. The localized heating of the sample surface also led to development of large compressive stresses in the laser heated area. The radial stress field in the sample at the end of laser irradiation is plotted in Figs 2.9(a) and (b), for low fluence and high fluence laser processing experiments, respectively. The stress field in the sample dissipated as the sample is rapidly cooled down with the waterjet. The numerical results show that during LWH treatment at low fluence conditions, the treated surface is heated to approximately 900-1000 K (700 – 800 °C) and subjected to maximum biaxial compressive stress of 1 GPa. While the sample processed at high fluence conditions are subjected to maximum temperatures of 1200 –1300 K (900 – 1000

°C) and maximum biaxial compressive stress of 1.5 GPa. The numerical results indicate the microstructural changes in the material are caused by heating the sample surface above 900 K under a biaxial compressive stress of 1 GPa. The rapid cooling of the sample surface may result in quenching the surface and thus refining the microstructure. In addition to microstructure refinement, the laser heating may also result in transformation of cBN (sp^3 phase) to hBN (sp^2 phase) and the volumetric expansion associated with the phase transformation results in surface damage. The average hardness of damaged surface was found to be lower than the hardness of the original material (untreated). The hBN phase has a relative smaller hardness than cBN and wBN (Meng et al., 2004). Therefore, the observed reduction of hardness in the damaged region can be result of the presence of hBN phase. Numerical results on the high fluence LWJ treatment indicate that phase transformation occurs only when the surface layers are heated above 1200 K. In order to achieve high hardness over the whole surface, the LWJ treatment should heat the sample surface between 900 -1200 K as heating above the higher temperature results in surface damage.

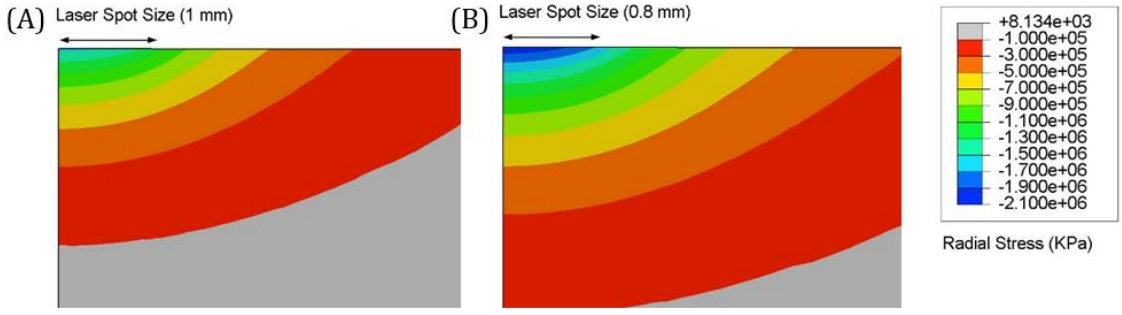

Figure 2.9 *Maximum radial stress LWH treatment: (A) Stress distribution in sample treated at low laser fluence (35 J/mm2); and (B) Stress distribution in sample treated at high laser fluence (55 J/mm2)*

Several mechanisms can be attributed to the observed increase in hardness. First one is the formation of amorphous phase at the grain boundaries as noted by presence of the

interfacial layer at grain boundaries (Figs 2.4 and 2.5, and the supplemental material). Such phase is expected to introduce the grain-boundary strengthening mechanism via inhibiting ease of dislocation movement across the boundary (He, Bhole, & Chen, 2008). Second one is the microstructure refinement that results in formation of zones with nano-sized grains that are expected to increase the energy needed to initiate and propagate deformation. The subdivision of the lamella grain has also reduces the effective grain size of the composite. The formation of the nano-sized grains between the larger lamellar grains results in a refined microstructure with fewer pores "defects" as compared to as-received materials.

The hardness of wBN samples may be increased through transformation of wBN to finely dispersed cBN. But this mechanism is expected to have a minimal influence in the observed increase in surface hardness because the phase composition of the LWH treated material does not change as shown on Figs 2.6 and 2.7. Additionally, the thermo-mechanical conditions during LWH processing are not conducive for transformation from wurtzite to cubic phase material. Such a transformation (wBN -> cBN) requires temperature around 1200-1500o C and high pressures of 6-8 GPa (Britun et al., 1999). The presence of water, impurities, and inclusions could reduce the pressure needed for such transformation as transformation of amorphous BN to cBN in the presence of water is reported to occur at 5.5 GPa (Taniguchi, Kimoto, Tansho, Horiuchi, & Yamaoka, 2003) but transformation is not expected at the temperature and stress magnitudes applied during the LWJ processing.

Therefore, it can be concluded that grain-boundary strengthening due to formation of interlayer amorphous phase, and significant reduction in grain-size of the material are the dominant mechanisms underlying the observed hardness increase.

2.6 Conclusion

Laser-waterjet treatment composed of tandem laser heating and waterjet quenching is utilized to increase the hardness of dual phase boron nitride based material such that treated surface matches the hardness of polycrystalline diamond. Microstructural and phase characterization reveal that combination of amorphous phase formation at the grain boundaries and nano-sized grain formation may be the mechanisms responsible for the increased hardness. The LWJ treatment is able to achieve the microstructure refinement associated with hardness increase for laser fluence over a narrow range 35-55 J/mm2. LWH treatment with laser fluence above this range results in spallation damage due to formation of hexagonal boron nitride through phase transformation. Numerical analysis of the LWH treatment shows that the microstructure refinement is associated with heating the surface above 900 K and rapidly quenching the surface.

2.7 Reference

Bergman, L., & Nemanich, R. J. (1996). Raman Spectroscopy for Characterization of Hard, Wide-Bandgap Semiconductors: Diamond, GaN, GaAlN, AlN, BN. Annual Review of Materials Science, 26(1), 551–579.

Bhaumik, S. K., Divakar, C., & Singh, A. K. (1995). Machining Ti6Al4V alloy with a wBN-cBN composite tool. Materials and Design, 16(4), 221–226.

Britun, V. F., Kurdyumov, A. V., & Petrusha, I. A. (1999). Wurtzitic boron nitride thermal stability and transformation into the rhombohedral boron nitride modification when heated. Materials Letters, 41(2), 83–88.

Dubrovinskaia, N., Solozhenko, V. L., Miyajima, N., Dmitriev, V., Kurakevych, O. O., & Dubrovinsky, L. (2007). Superhard nanocomposite of dense polymorphs of boron

nitride: Noncarbon material has reached diamond hardness. Applied Physics Letters, 90(10).

Fischer-Cripps, A. C. (2011). Nanoindentation. Springer. http://doi.org/10.1007/978-1-4419-9872-9

Fischer-Cripps, A. C., Bull, S. J., & Schwarzer, N. (2012). Critical review of claims for ultra-hardness in nanocomposite coatings. Philosophical Magazine, 92(13), 1601–1630.

Fujisaki, K., Yokota, H., Furushiro, N., Yamagata, Y., Taniguchi, T., Himeno, R., … Higuchi, T. (2009). Development of ultra-fine-grain binderless cBN tool for precision cutting of ferrous materials. Journal of Materials Processing Technology, 209(15-16), 5646–5652.

He, W., Bhole, S. D., & Chen, D. (2008). Modeling the dependence of strength on grain sizes in nanocrystalline materials. Science and Technology of Advanced Materials, 9(1), 1–7.

Hubert, H., Garvie, L. a J., Devouard, B., Buseck, P. R., Petuskey, W. T., & McMillan, P. F. (1998). High-Pressure, High-Temperature Synthesis and Characterization of Boron Suboxide (B 6 O). Chemistry of Materials, 10(6), 1530–1537.

Kalyanasundaram, D., Shehata, G., Neumann, C., Shrotriya, P., & Molian, P. (2008). Design and validation of a hybrid laser/water-jet machining system for brittle materials. Journal of Laser Applications, 20(2), 127.

Kalyanasundaram, D., Shrotriya, P., & Molian, P. (2009). Obtaining a Relationship Between Process Parameters and Fracture Characteristics for Hybrid CO[sub 2] Laser⁄Waterjet Machining of Ceramics. Journal of Engineering Materials and Technology, 131(January), 011005.

Kalyanasundaram, D., Shrotriya, P., & Molian, P. (2010). Fracture mechanics-based analysis for hybrid laser/waterjet (LWJ) machining of yttria-partially stabilized zirconia (Y-PSZ). International Journal of Machine Tools and Manufacture, 50(1), 97–105.

Karch, K., Bechstedt, F., Pavone, P., & Strauch, D. (1996). Lattice dynamics of BN and AlN. Physica B, 220, 445–447.

Kuhlmann, U., Werheit, H., Lundström, T., & Robers, W. (1994). Optical properties of amorphous boron. Journal of Physics and Chemistry of Solids, 55(7), 579–587.

Levitas, V., & Shvedov, L. (2002). Low-pressure phase transformation from rhombohedral to cubic BN: Experiment and theory. Physical Review B, 65(10), 104109.

Melaibari, A., Molian, P., & Shrotriya, P. (2012). Laser/waterjet heat treatment of polycrystalline cubic/wurtzite boron nitride composite for reaching hardness of polycrystalline diamond. Materials Letters, 89, 123–125.

Meng, Y., Mao, H., Eng, P., Trainor, T., Newville, M., Hu, M., … Hemley, R. (2004). The formation of sp3 bonding in compressed BN. Nature Materials, 3(2), 111–114.

Ohba, N., Miwa, K., Nagasako, N., & Fukumoto, A. (2001). First-principles study on structural, dielectric, and dynamical properties for three BN polytypes. Physical Review B, 63(11), 115207.

Pan, Z., Sun, H., Zhang, Y., & Chen, C. (2009). Harder than diamond: Superior indentation strength of wurtzite BN and lonsdaleite. Physical Review Letters, 102(5), 1–4.

Dinesh Kalyanasundaram. (2009). Mechanics guided design of hybrid laser / waterjet system for machining hard and brittle materials. A dissertation of DOCTOR OF PHILOSOPHY in Iowa State Univerisity, Ames , Iowa.

Sachdev, H. (2003). Influence of impurities on the morphology and Raman spectra of cubic boron nitride. Diamond and Related Materials, 12(8), 1275–1286.

Sun, J., Ling, H., Pan, W. J., Xu, N., Ying, Z. F., Shen, W. D., & Wu, J. D. (2004). Chemical Structure and Micro-Mechanical Properties of Ultra-Thin Films of Boron Carbide Prepared by Pulsed-Laser Deposition. Tribology Letters, 17(1), 99–104.

Taniguchi, T., Akaishi, M., & Yamaoka, S. (1996). Mechanical Properties of Polycrystalline Translucent Cubic Boron Nitride as Characterized by the Vickers Indentation Method. Journal of the American Ceramic Society.

Taniguchi, T., Kimoto, K., Tansho, M., Horiuchi, S., & Yamaoka, S. (2003). Phase transformation of amorphous boron nitride under high pressure. Chemistry of Materials, 15(14), 2744–2751.

Tian, Y., Xu, B., Yu, D., Ma, Y., Wang, Y., Jiang, Y., … Liu, Z. (2013). Ultrahard nanotwinned cubic boron nitride. Nature, 493(7432), 385–8.

Veprek, S., Argon, A. S., & Zhang, R. F. (2010). Design of ultrahard materials: Go nano! Philosophical Magazine, 90(31-32), 4101–4115.

Wang, Z. G., Rahman, M., & Wong, Y. S. (2005). Tool wear characteristics of binderless CBN tools used in high-speed milling of titanium alloys. Wear, 258(5-6), 752–758.

Wang, Z., Zhao, Y., Lazor, P., Annersten, H., & Saxena, S. K. (2005). In situ pressure Raman spectroscopy and mechanical stability of superhard boron suboxide. Applied Physics Letters, 86(4), 10–13.

Zhang, J. Y., Yu, Q. X., Pang, S. Q., Meng, S. S., Wang, T. S., & Hu, J. T. (2008). Development & application of polycrystal cubic boron nitride cutting tool material. Advances in Machining and Manufacturing Technology Ix, 375-376, 168–171 741.

CHAPTER III

ULTRAHARD POLYCRYSTALLINE CUBIC/WURTZITE BORON NITRIDE COMPOSITE THROUGH HYBRID LASER/WATERJET HEAT (LWH) TREATMENT

A paper published in the conference proceedings of the 44th NAMRI/SME conference

Jingnan Zhao, Pranav Shrotriya

Abstract

Ultra-hard materials that are chemically inert and thermally stable at high temperatures are desirable for enhancing machining and wear performance in demanding chemical and thermal environments. Single and polycrystalline diamonds are the hardest tool materials; however, at high temperatures, diamond reacts with ferrous alloys, losing its chemical inertness and thermal stability. In contrast, cubic boron nitride (cBN) has exceptional chemical and thermal stability but has much lower hardness (35-45 GPa). Increasing the hardness of BN is expected to fill the property gap in state-of-the-art tool materials as shown and to generate huge industrial interest for meeting the stringent design requirements such as machining optical surfaces and reducing the cost and time for machining ferrous materials. A novel laser/waterjet heat treatment (LWH) process is investigated to enhance the surface hardness of a dual phase boron nitride (BN) material composed of 50% cubic and 50% wurtzite phases. Results indicate that experimentally measured hardness increase is dependent on the processing parameter such as laser fluence and overlap between heat treatment passes. Statistical analysis is carried out to identify the processing parameter that result in maximum hardness increase.

KEYWORDS: Binderless cBN, Composite wBN/cBN, Laser Heat Treatment, Hardness.

3.1 Introduction

Despite most previous works' efforts to create superhard materials by synthesizing superhard materials, many opportunities still remain unexplored. For example, there is a design of the thermally stable and chemically inert nanoscale grain size cBN/wBN composite with increased hardness through microstructure refinement and nanotwinned grains (Huang et al., 2014; Li et al., 1996; Li, Sun, & Chen, 2014). However, the synthesis of specialized microstructures is challenging and involved. The Hall-Petch relation states that the material hardness has a negative relationship with its grain size which gives us an opportunity to enhance the material hardness. Nanograined diamond has been successfully synthesized from pure graphite at 2300 to 2500℃ and 12 to 25 GPa. It's grain sized controlled in 10 to 30 nm with a high Koop hardness of 110 to 140 GPa (Irifune et al., 2003). However, the oxidation temperature of the nanograined diamond still very low (about 680℃ in air) (Solozhenko, Kurakevych, & Le Godec, 2012). Demazeau (Demazeau, Biardeau, & Vel, 1990) used magnesium fluoronitrides as flux-precursor to convert hBN into cBN under high temperature and high pressure (HTHP). However, the synthesized cBN has flux as chemical impurity that reduced the physical properties of it. Many physical as well as chemical processes have been explored in order to synthesize cBN films or cBN/wBN composites. Nevertheless, these different processes is often very difficult to reproduce. Therefore, surface treatment based approaches that can be used to enhance the hardness of commercially produced boron nitride tools are highly desired as they can be easily integrated into conventional manufacturing processes.

In order to find the most effective superhard materials, we should know what makes materials hard. In diamond, tetrahedral bonded sp3 carbon atoms form a three dimensional

high symmetry network (S. Veprek et al., 2010). In addition, the bond length is short as carbon is a light element. Thus, when we look for the superhard materials, light elements, such as boron, carbon, and nitrogen are considered (Brazhkin et al., 2002). These elements are capable of forming three-dimensional rigid lattices with short covalent bonds. Moreover, in order to guarantee the materials resistance to compressive loads, elements with very high densities of valence electrons are considered. With these ideas, the search of new superhard materials has focused on the synthesis of range of materials composed of light elements and some of these superhard materials are plotted with respect to their measured Vicker's hardness in Figure 3.1.

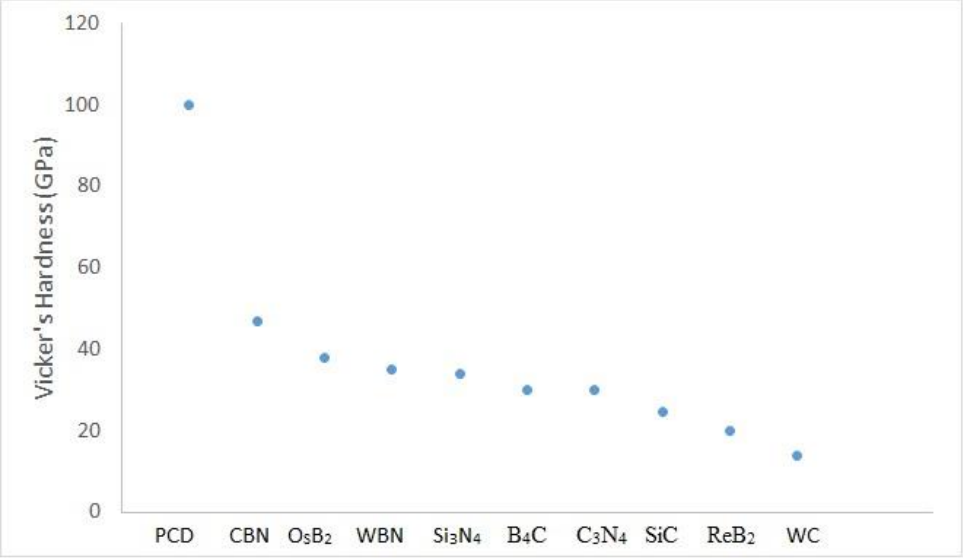

Figure 3.1 *Vicker's hardness of some superhard materials. It should be noted that, the hardness values of materials may depend on the sample quality. For example, the hardness of diamond depends on the quality and purity of the crystal* (Vepřek, 1999).

Carbon nitride (C_3N_4) is theoretically predicted to have hardness approaching that of diamond (He, Bhole, & Chen, 2008). However, after three decades of research studies, there is no synthetic sample of C_3N_4 that has validated this hardness prediction (Haines, L, & Bocquillon, 2001). Boron carbide (B_4C) is a superhard technical ceramic with an extreme

Vicker's hardness of 30 GPa (Ulrich, Ehrhardt, Schwan, Samlenski, & Brenn, 1998). B_4C was thought to be one of the potential superhard materials that could replace diamond in the future, but its hardness decreased from 30 GPa at room temperature to around 20 GPa at 1000 degrees Celsius (Thévenot, 1990). Thus, B_4C could not be considered as a new candidate superhard material to replace diamond (Thévenot, 1990). Metal borides are a binary compounds with elements from each of the main groups of the periodic table (Tyne, 1965). Unlike carbon-based materials; metal borides can be created in large synthetic quantities under ambient conditions (Jonathan B. Levine et al., 2009). Osmium diboride (OsB_2), an example of metal boride, has a high bulk modulus (395 GPa) and therefore is considered as a potential superhard material. However, its maximum Vicker's hardness has been measured to be only 37 GPa (Gou et al., 2009). Rhenium diboride (ReB_2), another example of metal borides, was also considered as a potential superhard material because of its high calculated values of bulk modulus and shear modulus (J.B. Levine et al., 2010). However, Dubrovinskaia, Dubrovinsky and other researchers have measured and reported the Vicker's hardness of ReB_2 to be only 19 to17 GPa at a range of load from 3 N to 49 N (Dubrovinskaia, Dubrovinsky, and Solozhenko 2007). Thus, OsB_2 and ReB_2 could not be considered as potential super-hard materials to reach diamond hardness. Ceramic and cermet machining tool materials, such as tungsten carbide (WC), silicon nitride (Si3N4), and silicon carbide (SiC), as hard materials has been widely used in tooling industry. They all have high wear-resistant but their Vickers hardness are 14 GPa (Liu & Li, 2001), 34GPa, and 24.6GPa (Yin et al., 2004)for WC, Si3N4, and SiC respectively. Thus, they could not be the potential super-hard materials to replace diamond tools.

Despite most previous works' efforts to create super-hard materials by synthesizing super-hard materials, many opportunities still remain unexplored. For example, there is a design of the thermally stable and chemically inert nanoscale grain size cBN/wBN composite with increased hardness through microstructure refinement and nano-twinned grains (Huang et al., 2014; Li et al., 1996, 2014). However, the synthesis of specialized microstructures is challenging and involved. The Hall-Petch relation states that the material hardness has a negative relationship with its grain size which gives us an opportunity to enhance the material hardness. Nano-grained diamond has been successfully synthesized from pure graphite at 2300 to 2500℃ and 12 to 25 GPa. It's grain sized controlled in 10 to 30 nm with a high Koop hardness of 110 to 140 GPa (Irifune et al., 2003). However, the oxidation temperature of the nano-grained diamond still very low (about 680℃ in air) (Solozhenko et al., 2012). Demazeau (Demazeau et al., 1990) used magnesium fluoronitrides as flux-precursor to convert hBN into cBN under high temperature and high pressure (HTHP). However, the synthesized cBN has flux as chemical impurity that reduced the physical properties of it. Many physical as well as chemical processes have been explored in order to synthesize cBN films or cBN/wBN composites. Nevertheless, these different processes is often very difficult to reproduce. Therefore, surface treatment based approaches that can be used to enhance the hardness of commercially produced boron nitride tools are highly desired as they can be easily integrated into conventional manufacturing processes.

In order to achieve enhanced hardness in commercially produced cubic boron nitride materials, a novel laser/waterjet heat treatment (LWH) was performed on cBN/wBN composite, and a preliminary study was conducted to find that the hardness of the cBN/wBN composite could reach the hardness of diamond (A. A. Melaibari et al., 2016; A. Melaibari et al., 2012).

The new discovery of cBN/wBN composite whose hardness matches the hardness of diamond can have vast implications in the tooling industry. Hence, in this paper, a series of experiments on LWH treatment of dual phase cBN/wBN tools was designed in order to identify the optimum processing parameters that result in maximum enhancement of surface hardness.

In previous studies Melaibari et al. (A. A. Melaibari et al., 2016) have designed a laser/waterjet heat treatment (LWH) and applied to enhance the surface hardness of dual phase 50% cubic boron nitride (cBN) and 50% wurtzite boron nitride (wBN) tool materials to match that of polycrystalline diamond tool materials. In the LWH process, a shaped laser beam was scanned across the sample to heat the surface material below the melting point and a tandem waterjet followed the laser beam to quench the heated material. Fig 3.2 shows a schematic of continuous wave CO_2 laser/waterjet nozzle system where the beam is separated from waterjet for a distance of 2 to 6 mm. The LWH processing consisted of surface heating the cBN samples using a low power continuous wave CO_2 laser beam followed by tandem waterjet quenching of the laser beam path to cause stress-induced microstructural changes. The low laser fluence prevented melting, scribing, or cutting of boron nitride. During LWH processing, maximum surface temperatures after laser irradiation for a duration of 0.02 s were estimated to be around 1000-1300 K indicating that the material surface is heated at approximately 50,000 K/s and rapidly quenched back to room temperature (A. A. Melaibari et al., 2016). Localized heating of the surface leads to development of large compressive stresses (~2 GPa) in the laser-heated area. Hence, the key characteristics of LWH are the thermomechanical loading associated with rapid heating and cooling that generates non-equilibrium microstructures in the treated samples. Experimental results showed that surface treatment over a narrow range of laser fluence (35 to 55 J/m^2) results in enhanced hardness of dual-phase materials. LWH treatment

of boron nitride tools with laser fluence greater than 55 J/m^2 results in spallation damage on sample surface due to phase transformation of cBN to hexagonal boron nitride. While no change in cBN surfaces was observed for surface treatment below laser fluence of 35 J/m^2.

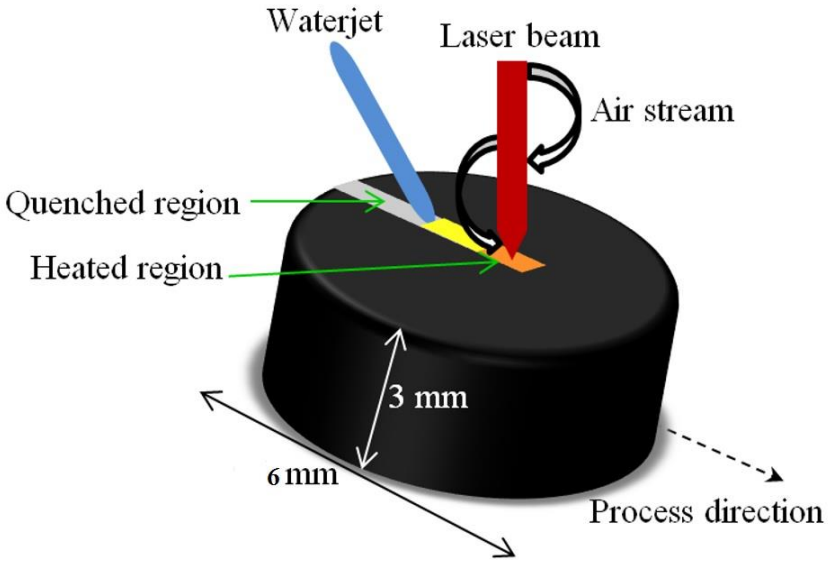

Figure 3.2 *Schematic of LWJ heat treatment process*

Given this narrow range of the laser fluence associated with damage free hardness enhancement, experiments were conducted to the study on the influence of repeated LWH treatment on hardness enhancement in dual phase boron nitride materials. The laser beam was scanned in a raster pattern to treat the sample surface. The overlap between adjacent scan lines in the raster pattern was varied to investigate the influence of repeated LWH treatment on the hardness enhancement and to identify the processing parameters associated with maximum enhancement in surface hardness.

3.2 Method

A continuous wave CO2 laser (Laser Spectra Physics 820) was employed to conduct the LWH experiments with a laser power of 180 W, a spot size of 1 mm, and with a laser fluence of 33 J/mm2. The sample was LWH treated by scanning the sample surface in a raster pattern with different overlaps between adjacent scans to study the influence of repeated laser heating and cooling. The overlap percentages of 0%, 20%, 50%, 70% and 100% were investigated.

The materials used in this study were binderless dual phase cBN/wBN with iron oxide as the impurity. The samples were synthesized to obtain a cBN content between 45% to 55% with wBN phase being the remainder. In order to identify the change of the sample's hardness, Vicker's micro-hardness tests were taken before and after heat treatment and the influence of overlap percentage on the hardness enhancement was investigated using a statistical regression analysis.

Based on previous study (A. A. Melaibari et al., 2016), low laser power fluence (1 mm spot size) was used on following experiments to prevent melting, scribing or cutting of boron nitride. In order to find the relationship between laser beam overlap and hardness improvement, the experimental study was designed by using randomized complete block design (RCB). RCB based experimental design procedure are able to determine a relationship between independent input process parameters and output data (process response) (Aouici, Yallese, Chaoui, Mabrouki, & Rigal, 2012). In this paper, laser beam overlap percentage is identified as the factor that affects the response— cBN/wBN composite hardness change ratio. Five levels of overlap percentages were used as the factor and the range of the factor was

selected based on preliminary research and experiment condition. The factor and its levels are presented in table 3.1.

Table 3.1 *Factor and levels*

Factor	Level				
	1	2	3	4	5
Overlap percentage between adjacent LWH treatment passes	0%	20%	50%	70%	100%

Note: 0% overlap indicates the 2nd laser beam is 1 mm (laser beam spot size is 1 mm) away from the 1st laser beam. And 20% overlap indicates the 2nd laser beam is 0.8 mm away from the 1st laser beam and so on.

Two pieces of binderless dual phase 50%wBN/50%cBN composites were used as work materials. The average hardness of each piece of cBN/wBN composite was 38 GPa and 39 GPa respectively. Ten areas for surface heat treatment were demarcated on two work pieces, where work piece 1 has two areas and work piece 2 has eight areas, and numbered from 1 to 10 (see Figure 3). Finally each of these 10 areas was LWH treated with a randomly assigned overlap percentage as shown in Table 3.2.

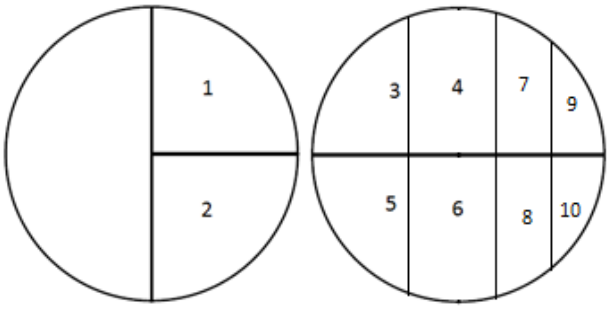

Figure 3.3 *Layout of heat treatment areas*

Table 3.2 *Experiment design*

Experiment design	Overlap percentage				
	0%	20%	50%	70%	100%
Area	8 and 10	3 and 6	2 and 4	1 and 5	7 and 9

Indentation hardness tests were performed using a Tukon microhardness tester with a Vicker's diamond pyramid indenter. The load was set at 1 kgf (9.8N), and the test duration was set at 30 seconds. Length measurements were made along the diagonal of the indentations using a high resolution (± 1 μm) optical microscope and optical profilometer to ensure that no fracture had occurred in the indentation zone. Vicker's hardness was then calculated using the relationship:

$$HV = \frac{1.8544L}{d^2} \tag{3.1}$$

where L is the load (kgf), and d is the average length of the two diagonals of the indentation.

Ten hardness tests were obtained at each area before and after LWH treatment. All indentation hardness can be considered reliable because no visible plastic deformation or damage of indenter diamond tip were observed after the measurements of hardness (Figure 3.4). In order to maintain precision while measuring the length of indentations, the indentation optical images were taken by optical microscope. The length of indentations were measured on optical images by a Java-based image processing program known as ImageJ.

A B

Figure 3.4 *The 100 X magnification images of square pyramid diamond tip before (A) and after (B) hardness measurements*

3.3 Result

Visual examination of LWH treated surfaces with 0%, 20%, and 50% overlap revealed only a color change from light-absorbing black/gray to transparent white in areas along the laser scan lines. Such an effect is ascribed to a change in crystal morphology following Sachdev's classification of the crystalline morphology of cBN according to color, size and transparency (Vepřek, 1997). A transparent cBN of white to amber color implies tetrahedral crystal morphology (as opposed to octahedral) with small grain size and loss of boron. It may be noted that the color may also be caused by inclusions, dopants or defects. The formation of transparent white color of the cBN has previously been associated with enhancement of surface hardness (A. Melaibari et al., 2012).

Visual examination of LWH treated surfaces with 70%, and 100% overlap revealed areas of spallation induced damage (about 200 to 400 micron wide) along the laser scan lines while the undamaged surface showed a color change similar to the LWH treated areas with

lower overlap percentage. A SEM image of the spallation induced surface damage is shown in Figure 3.5 and shows these damages were narrower than laser beam radius and were oriented along the laser scan directions.

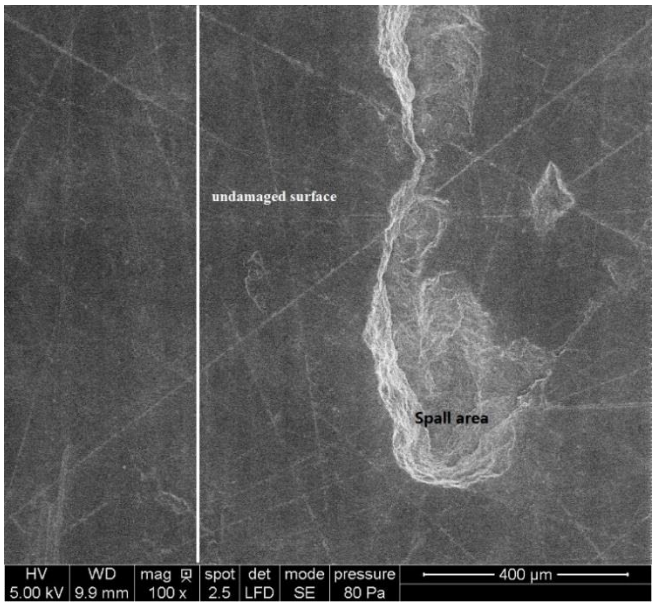

Figure 3.5 *The spalled region on 70% overlap LWH treated sample*

Measured Vickers hardness before and after LWH treatment for surface treated with different laser beam overlap percentage are plotted in Figure 3.6. The bars around each point show the standard deviations of the 15 different measurements performed for each data point. As shown in Figure 6, the hardness of the untreated sample was found to be 40 ± 4 GPa, 42 ± 9 GPa, 37 ±4 GPa, 38 ± 4 GPa, 36 ± 4 GPa, 36± 5 GPa, and 40 ± 4 GPa for 0% on sample 2, 20% on sample 2, 50% on sample 2, 50% on sample 1, 70% on sample 1, 70% on sample 2, and 100% on sample 2, respectively. After LWH treatment, the surface hardness on LWH with 0% on sample 2, 20% on sample 2, 50% on sample 2, 50% on sample 1, 70% on sample 1, 70% on sample 2, and 100% on sample 2 are found to be 51 ± 6 GPa, 54 ± 10 GPa, 61 ± 11 GPa, 65 ± 14 GPa, 66 ± 11 GPa, 53 ± 12 GPa, and 54 ± 4 GPa, respectively. The LWH

treatment resulted in maximum increase of 169% of the initial hardness in area treated with LWH with 50% overlap on sample 1. Another indicator of the increased hardness of the LWH treated sample was the hardness distribution on the laser beam track. Because the laser beam created by Laser Spectra Physics 820 is a Gaussian beam, the power density is not uniform along the entire beam path. Therefore, the laser beam energy irradiated on the cBN/wBN composite was not uniform along the width of the laser beam. On 0%, 20%, and 50% overlap LWH treated sample, hardness tests on the center of each laser track were slightly higher than those on the edge of the laser track. This hardness variation in the scan width resulted in the observed larger standard deviation in the LWH treated surfaces (Fig 3.6).

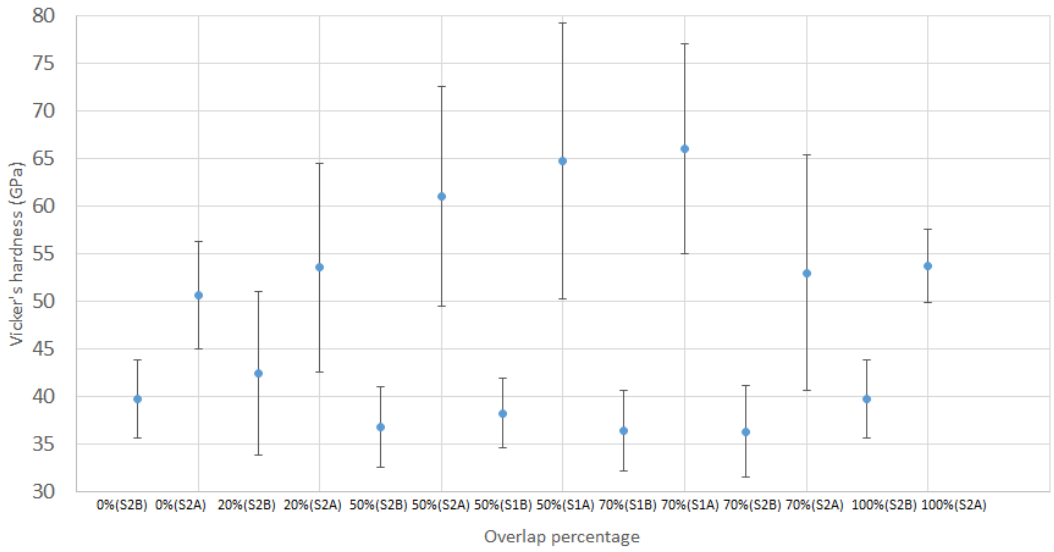

Figure 3.6 *Vicker's indentation hardness tests data of binderless cBN/wBN composite: 0%(S2B) means 0% overlap on sample 2 before LWH.*

The maximum hardness change ratio was observed on 50% overlap area that is 160% over than the untreated area. The minimum hardness change ratio was observed on 0% overlap area that is only 30% over the untreated area. In spite of 155% (very close to 50% overlap area) over the untreated area hardness in our data, the 70% overlap could not be considered the good

laser parameter for future studies. The hardness measurements on 70% overlap areas were taken only on undamaged surface where similar with 50% overlap treated area. According to our previous studies (A. A. Melaibari et al., 2016), the hardness on spall region might decrease compare with untreated material.

3.4 Discussion

In order to find the relationship between laser beam overlap and hardness improvement, a statistic model using randomized complete block design (RCB) was developed. A variance analysis of the hardness change ratio was made with the objective of analyzing the influence of laser beam overlap (OL) and sample property (initial hardness) difference (S) on the result. Table 3.3 shows the result of ANOVA for hardness change ratio. This analysis was conducted for a 10% significance level, i.e., for a 90% confidence level. This ANOVA table shows that laser beam overlap has a significant effect on the hardness change ratio. But the sample property difference has an insignificant effect on the hardness change ratio. Therefore, in the further studies, we will focus only on the effects of laser beam overlap.

Table 3.3 *ANOVA result for hardness change ratio*

Analysis of Variance			
Source	F Value	Pr > F	Remarks
OL	2.5174	0.0084	Significant
S	1.086	0.0245	Insignificant

Table 3.4 shows the statistical comparison results of Vicker's hardness tests of binderless 50%cBN/50%wBN as a function only of the laser beam overlap percentage. The highest hardness change was observed for 50% overlap that is 160% of the original hardness, and the lowest hardness change ratio was observed on 0% overlap that resulted in enhanced

hardness of only 130 % of the original hardness. Compare with 50% overlap, 70% and 100% overlap hardness change ratio are relatively smaller. The smaller enhancement in surface hardness may be due to the spalling surface damage (shown in Figure 5). Raman characterization of the LWH treated surface has shown that there is minimal changes in the phase composition in undamaged LWH treated areas but the spallation damage surface shows a phase transformation of cBN to the hexagonal boron nitride (hBN) (A. A. Melaibari et al., 2016). The hBN phase has a larger lattice volume and is significantly lower in hardness as compared to cBN and wBN phases. The volumetric expansion associated with cBN to hBN transformation may have resulted in the surface damage and observation of lower hardness enhancement at 70% and 100% overlap. In order to identify the overlap percentage associated with maximum enhancement, the hardness change ratio was fitted to statistical regression model of the overlap percentages as shown in Figure 3.7.

Table 3.4 *Experiment results for laser beam overlap*

Run No.	LWH parameter		OL (%)	Response factors		
	Moving Speed (inch/min)	Laser Power (W)		Average hardness before LWH (GPa)	Average hardness after LWH (GPa)	Hardness change ratio (%)
1	160	180	0	39	51	130
2	160	180	20	41	55	134
3	160	180	50	40	64	160
4	160	180	70	38	59	155
5	160	180	100	39	52	133

The relationship between the factors and the performance measures were modeled by secondary linear regression. The regression equation obtained was as follow. The cBN/wBN composites hardness change ratio before and after LWH treatment model is given below in Eq. (3.2). Its coefficient of determination (R2) is 93.5%.

$$Ratio = 1.307 + 0.485OL - 0.871(OL - 0.48)^2 - 1.653(OL - 0.48)^3 \quad (3.2)$$

where OL is the overlap percentage value.

The predicted values of ratio are compared with the corresponding experiment values that was depicted in Figure 3.7.

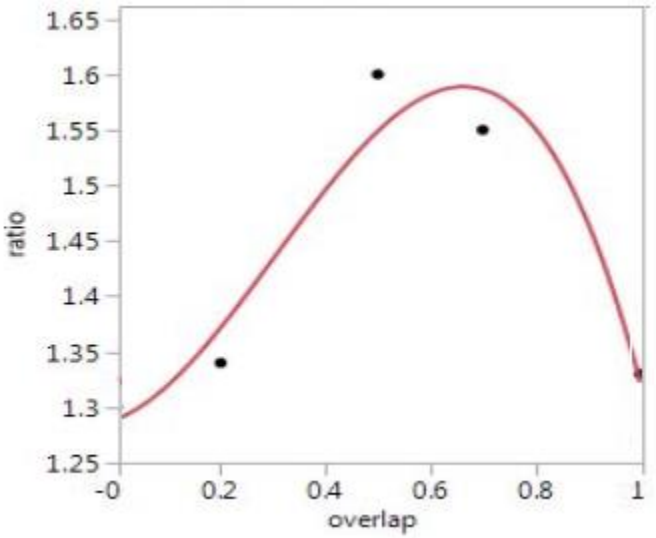

Figure 3.7 *cBN/wBN Vicker's hardness change ratio*

According to the statistical linear regression model, the OL value of 65-66% may result in maximum enhancement of surface hardness due to LWH treatment. In the current paper, the study of laser beam overlap effect on the hardness change ratio of cBN/wBN composite has led to a statistical model based on the experiment results. LWH experiments showed that the hardness of 50%cBN/50%wBN composite increase up to 160% of the original hardness value however this increase is not as dramatic as 200% of the original hardness reported in our previous investigations (A. A. Melaibari et al., 2016). The difference in hardness enhancement may be due to the differences in phase compositions and presence of microstructural defects in the samples. The samples used in the current study had an relative lower initial hardness of 39-40 GPa as compared to the initial hardness of 48 GPa for samples used in the earlier study

(A. A. Melaibari et al., 2016) . The difference in lower hardness may be due different phase composition cBN/wBN content and more microstructural defects. These results indicate that influence of sample composition on LWH induced hardness enhancement needs to be investigated. We are currently conducting experimental investigations to identify the influence of different wBN phase content on hardness enhancement and these results will be reported in a forthcoming article.

A finite element analysis was applied to estimate the thermal fields induced in the sample during the LWH processing. An axisymmetric finite element model was used to model the localized heating due to the incidence of laser beam followed by the quenching of the heated material surface due to the water-jet. Water quenching leads to rapid decrease of temperature in the circular zone heated by low-power laser therefore the heating and subsequent cooling associated with LWH processing can be modeled as an axis symmetric problem. The Gaussian profile of the laser beam is approximated as a surface heat source whose intensity at radial distance r from center is given in Eq. (3.3):

$$\mathrm{I(z)} = a_s I_0 \exp\left(\frac{-2r^2}{w^2}\right) \tag{3.3}$$

where I_0 is the intensity at the center of the beam, a_s is the absorption coefficient, and w is the diameter of the laser beam spot.

The absorption coefficient was chosen to be 0.75 (A. Melaibari et al., 2012). The laser intensity at the center of the beam was calculated based on the laser fluence used in the laser heat treatment experiment. The duration of laser spot interaction with sample surface was calculated to equal the duration that a laser beam is incident at a material point during experiments. Thermal quenching due to the waterjet was modeled using convective heat transfer coefficient of 10,000 W/ m^2 K such that the sample surface is rapidly cooled down to

room temperature on the action of waterjet (A. Melaibari et al., 2012). Finite element analysis package ABAQUS was utilized to compute the temperature and stress fields associated with LWH experiments. The boundary conditions and geometry of the FEM model are shown in Figure 3.8. The thermal and mechanical properties used to model pCBN response are listed in Table 3.5. The finite element mesh was refined till the computed temperature and stress field became independent of the element size.

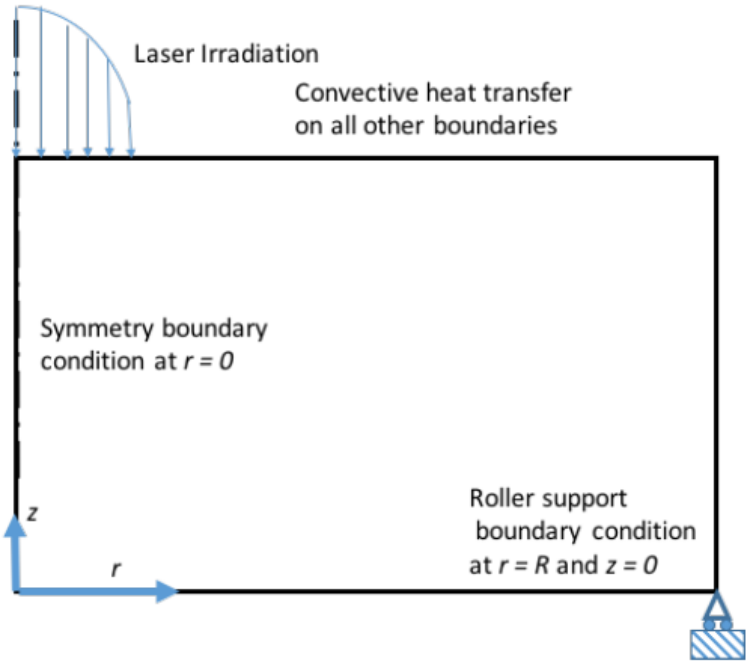

Figure 3.8 *Axissymetric finite element model with boundary conditions*

Table 3.5 *Thermal and mechanical properties of PCBN*

Density	Thermal Conductivity	Specific Heat Capacity	Poisson's Ratio	Young's Modulus	Thermal Expansion Coefficient
S	200 W/mK	920 J/Kgk	0.15	710 GPa	5.6×10^{-6}

During LWH surface treatment, the temperature of the surface increased rapidly during laser heating and attained a maximum value at the end of the laser irradiation. After the laser

heating, the sample surface was rapidly cooled due to the waterjet quenching. The computed temperature and stress field in the samples at the end of laser irradiation is plotted in Figs 3.9(a) and (b), respectively. The contour plots show that material near the irradiated surface is heated while the rest of the material remains at room temperature. The localized heating of the sample surface also led to development of large compressive stresses in the laser-heated area. The stress field in the sample dissipated as the sample is rapidly cooled down with the waterjet.

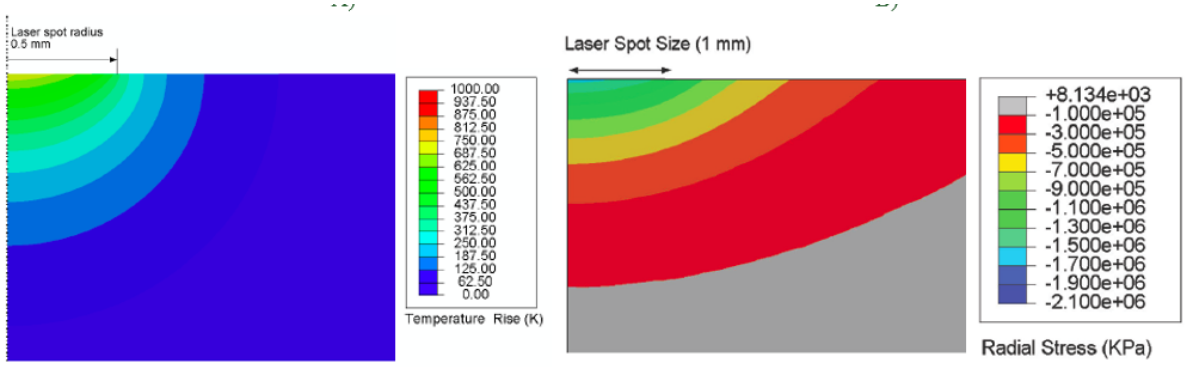

a) *b)*

Figure 3.9 *Contour plots of A) temperature and B) radial stress fields at the instant of maximum temperature during LWJ treatment.*

The temperature and stress calculation indicate that material under laser irradiation is subjected to a temperature rise of 700 K and compressive stresses of 1 GPa during laser heating and the heated material is rapidly quenched to room temperature under the waterjet action. The combined action of high temperatures and high compressive stresses may lead to microstructure refinement that results in hardness enhancement observed in the current experiments. The maximum increase in temperature on the sample surface are plotted in Figure 3.10 as a function of distance from laser beam center. This shows that for 0% the sample points are heated to maximum temperature when they lie under the laser beam scan but as the beam moves away the sample is only subjected to rise of 400 K in subsequent passes. The

magnitude of rise in subsequent passes increases monotonically as the overlap percentage is increased from 0% to 100%. At 70% overlap, points along the sample surface are subjected to as much as three laser irradiation during the raster pattern scan. During each of these scans the laser irradiated surface is subjected to temperature rise above 650 K and this repeated heating of the sample surface may have resulted in spallation surface damage.

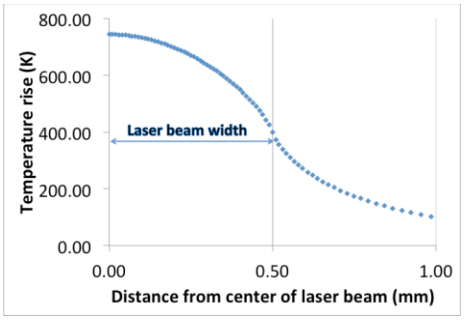

Figure 3.10 *Maximum temperature rise along the surface under laser beam during LWH treatment.*

3.5 Conclusion

Laser-waterjet treatment composed of tandem laser heating and waterjet quenching is utilized to increase the hardness of dual phase boron nitride based material such that hardness of treated surface is increased to 160% of the initial hardness. The LWJ treatment is able to achieve the maximum hardness increase for treatment with 33 J/mm2 with 50% overlap between adjacent passed during raster pattern laser scans. LWH treatment with same laser fluence but overlap percentage greater than 70% results in spallation damage. Numerical analysis of the LWH treatment shows that the microstructure refinement is associated with heating the surface above 900 K and rapidly quenching the surface. A statistical regression model was developed to find the optimal laser beam overlap percentage associate with maximum hardness change during LWH treatment.

3.6 References

Angseryd, J., Elfwing, M., Olsson, E., & Andrén, H. O. (2009). Detailed microstructure of a cBN based cutting tool material. *International Journal of Refractory Metals and Hard Materials*, *27*(2), 249–255.

Anstis, G. ., Chantikul, P., Lawn, B. ., & Marshall, D. . (1981). A critical evaluation of indentation techniques for measuring fracture toughness: I Direct crack measurements. *Journal of the American Ceramic Society*, *46*(September), 533–538.

Aouici, H., Yallese, M. A., Chaoui, K., Mabrouki, T., & Rigal, J. F. (2012). Analysis of surface roughness and cutting force components in hard turning with CBN tool: Prediction model and cutting conditions optimization. *Measurement: Journal of the International Measurement Confederation*, *45*(3), 344–353.

Basu, B., Raju, G. B., & Suri, A. K. (2006). Processing and properties of monolithic TiB 2 based materials. *International Materials Reviews*, *51*(6), 352–374.

Brazhkin, V. V., Lyapin, A. G., & Hemley, R. J. (2002). Harder than diamond: Dreams and reality. *Philosophical Magazine A*, *82*(2), 231–253.

Callister, W., & Rethwisch, D. (2007). *Materials science and engineering: an introduction*. *Materials Science and Engineering* (Vol. 94).

Demazeau, G., Biardeau, G., & Vel, L. (1990). Synthesis of cubic boron nitride using magnesium or magnesium-based fluoronitrides. *Materials Letters*, *10*(3), 139–144.

Dubrovinskaia, N., Solozhenko, V. L., Miyajima, N., Dmitriev, V., Kurakevych, O. O., & Dubrovinsky, L. (2007). Superhard nanocomposite of dense polymorphs of boron nitride: Noncarbon material has reached diamond hardness. *Applied Physics Letters*,

Fischer-Cripps, A. C. (2011). *Nanoindentation*. *Springer*.

Gou, H., Wang, Z., Zhang, J., Yan, S., & Gao, F. (2009). Structural stability and elastic and electronic properties of rhenium borides: first principle investigations. *Inorganic Chemistry*, *48*(2), 581–7.

Haines, J., L, J. M., & Bocquillon, G. (2001). M Aterials. *Recherche*, *1955*(1), 1–23.

Hansen, N. (2004). Hall-petch relation and boundary strengthening. *Scripta Materialia*, *51*(8 SPEC. ISS.), 801–806.

He, W., Bhole, S. D., & Chen, D. (2008). Modeling the dependence of strength on grain sizes in nanocrystalline materials. *Science and Technology of Advanced Materials*, *9*(1), 1–7.

Hou, X. D., Bushby, a J., & Jennett, N. M. (2008). Study of the interaction between the indentation size effect and Hall–Petch effect with spherical indenters on annealed polycrystalline copper. *Journal of Physics D: Applied Physics*, *41*(7), 074006.

Huang, Q., Yu, D., Xu, B., Hu, W., Ma, Y., Wang, Y., … Tian, Y. (2014). Nanotwinned diamond with unprecedented hardness and stability. *Nature*, *510*(7504), 250–3.

Irifune, T., Kurio, A., Sakamoto, S., Inoue, T., & Sumiya, H. (2003). Materials: Ultrahard polycrystalline diamond from graphite. *Nature*, *421*(6923), 599–600.

Jiménez, I., Sutherland, D., van Buuren, T., Carlisle, J., Terminello, L., & Himpsel, F. (1998). Photoemission and x-ray-absorption study of boron carbide and its surface thermal stability. *Physical Review B*, *57*(20), 13167–13174.

John, P., Polwart, N., Troupe, C. E., & Wilson, J. I. B. (2002). The oxidation of \lattplane{100} textured diamond. *Diamond and Related Materials*, *11*, 861–866.

Knoop, F., Peters, C. G., & Emerson, W. B. (1939). A sensitive pyramidal-diamond tool for indentation measurements. *Journal of Research of the National Bureau of Standards*, *23*(1), 39.

Levine, J. B., Betts, J. B., Garrett, J. D., Guo, S. Q., Eng, J. T., Migliori, A., & Kaner, R. B. (2010). Full elastic tensor of a crystal of the superhard compound ReB2. *Acta Materialia*, *58*(5), 1530–1535.

Levine, J. B., Tolbert, S. H., & Kaner, R. B. (2009). Advancements in the search for superhard ultra-incompressible metal borides. *Advanced Functional Materials*, *19*(22),

Li, B., Sun, H., & Chen, C. (1996). Large indentation strain stiffening in nanotwinned cubic boron nitride. *Nature Communications*, *94*(May), 90.

Li, B., Sun, H., & Chen, C. (2014). Large indentation strain-stiffening in nanotwinned cubic boron nitride. *Nature Communications*, *5*(May), 4965.

Liu, K., & Li, X. P. (2001). Ductile cutting of tungsten carbide. *Journal of Materials Processing Technology*, *113*(1-3), 348–354.

Melaibari, A. A., Zhao, J., Molian, P., Bushlya, V., Zhou, J., Ståhl, J.-E., … Shrotriya, P. (2016). Ultrahard boron nitride material through a hybrid laser/waterjet based surface treatment. *Acta Materialia*, *102*, 315–322.

Melaibari, A., Molian, P., & Shrotriya, P. (2012). Laser/waterjet heat treatment of polycrystalline cubic/wurtzite boron nitride composite for reaching hardness of polycrystalline diamond. *Materials Letters*, *89*, 123–125.

Meng, Y., Mao, H., Eng, P., Trainor, T., Newville, M., Hu, M., … Hemley, R. (2004). The formation of sp3 bonding in compressed BN. *Nature Materials*, *3*(2), 111–114.

Dinesh Kalyanasundaram. (2009). Mechanics guided design of hybrid laser / waterjet system for machining hard and brittle materials. A dissertation of DOCTOR OF PHILOSOPHY in Iowa State Univerisity, Ames , Iowa.

Riedel, R. (1994). Novel Ultrahard Materials. *Advanced Materials*, *6*(7-8), 549–560.

Roy, T. K. (2015). Assessing hardness and fracture toughness in sintered zinc oxide ceramics through indentation technique. *Materials Science and Engineering: A*, *640*, 267–274.

Zhuoru Wu. (2015). The mechanism governing cutting of hard materials with hybrid Laser / Waterjet system through controlled fracture. A dissertation of DOCTOR OF PHILOSOPHY in Iowa State Univerisity, Ames , Iowa.

Smith, R. L. et al. (1922). an Accurate Method of Determining the Hardness of Metals, With Particular Refernce To Those of a High Degree of Hardness. *proc.Inst.Mech.Eng.*, *1*(May), 623–641.

Solozhenko, V. L., Kurakevych, O. O., & Le Godec, Y. (2012). Creation of nanostuctures by extreme conditions: High-pressure synthesis of ultrahard nanocrystalline cubic boron nitride. *Advanced Materials*, *24*(12), 1540–1544.

Superhard, U. (2007). Comment on " Synthesis of, *318*(December), 1–2.

Taniguchi, T., Akaishi, M., & Yamaoka, S. (1996). Mechanical Properties of Polycrystalline Translucent Cubic Boron Nitride as Characterized by the Vickers Indentation Method. *Journal of the American Ceramic Society*.

Thévenot, F. (1990). Boron carbide—A comprehensive review. *Journal of the European Ceramic Society*, *6*(4), 205–225.

Tyne, U. (1965). METAL BORIDES By N. *Quarterly Reviews*.

Ulrich, S., Ehrhardt, H., Schwan, J., Samlenski, R., & Brenn, R. (1998). Subplantation effect in magnetron sputtered superhard boron carbide thin films. *Diamond and Related Materials*, *7*, 835–838.

Vepřek, S. (1997). Conventional and new approaches towards the design of novel superhard materials. *Surface and Coatings Technology*, *97*(1-3), 15–22.

Vepřek, S. (1999). The search for novel, superhard materials. *Journal of Vacuum Science & Technology A: Vacuum, Surfaces, and Films*, *17*(5), 2401.

Veprek, S., & Argon, A. S. (2002). Towards the understanding of mechanical properties of super- and ultrahard nanocomposites. *Journal of Vacuum Science & Technology B: Microelectronics and Nanometer Structures*, *20*(2), 650.

Veprek, S., Argon, A. S., & Zhang, R. F. (2010). Design of ultrahard materials: Go nano! *Philosophical Magazine*, *90*(31-32), 4101–4115.

Wentorf, R. H. (1961). Synthesis of the Cubic Form of Boron Nitride. *The Journal of Chemical Physics*, *34*(3), 809.

Yin, L., Vancoille, E. Y. J., Lee, L. C., Huang, H., Ramesh, K., & Liu, X. D. (2004). High-quality grinding of polycrystalline silicon carbide spherical surfaces. *Wear*, *256*(1-2), 197–207.

CHAPTER IV

HYBRID CO2 LASER WATERJET HEAT (LWH) TREATMENT OF BINDER BORON NITRIDE COMPOSITES WITH HARDNESS IMPROVEMENT

Jingnan Zhao, Pranav Shrrotriya

Abstract

Boron nitride (BN) material is chemically and thermally stable which makes it desirable for high speed machining in demanding chemical and thermal environments. Although the hardness of BN material is lower than that of single polycrystalline diamond, a laser waterjet heat (LWH) treatment process provides a new approach to achieve hardness values that are comparable to diamond hardness. This study investigates the hardness change of LWH-treated commercial cBN/TiN and cBN/AlN materials. Results indicate that measured hardness increases is dependent on the laser beam pass and the distance from the beam center.

KEYWORDS: Binder Boron Nitride, Laser Heat Treatment, Hardness, Fracture Toughness, Microstructure.

4.1 Introduction

The hardness is defined as a material's resistance of a material to a certain pressure which given by the ratio of the applied load to the fully developed plastically area (S. Veprek et al., 2010). Diamond is considered to be the hardest material on the earth whose hardness varies between 70 and 100 GPa depending on the quality and purity of the crystal. According to diamond's hardness, super-hard materials are classified as having hardness values greater than 40 GPa (Stan Veprek & Argon, 2002). Diamond ($H_k \approx 70 - 100\ GPa$) and cubic boron nitride (cBN with $H_k \approx 40 - 50\ GPa$), are well-known super-hard material that used in many

applications, such as mechanical cutting, abrasives, polishing materials, and wear-resistant and protective coatings.

Although diamond is the hardest material, it also has limitations in tooling industry. Diamond is not an ideal tool for cutting ferrous materials because its chemical instabilities cause diamond to react with ferrous materials to produce iron carbide. Also, diamond is not effective at high temperatures because of its thermal instability. Cubic boron nitride (cBN), the second hardest material on the earth (Dubrovinskaia et al., 2007), has a similar microstructure as diamond. It can be used to cut ferrous metals and perform in high temperature environments. Although cBN has good mechanical properties, chemical inertness and thermal stability, it cannot replace diamond as its hardness is well below that of diamond. Thus, searching for new superhard materials is not only of great scientific interest, but also of great practical value.

In order to find the most effective superhard materials for tooling industry, we should know what are the reasons make certain materials hard. Diamond has a short bond length made of carbon atoms linked together in a face-centered cubic (FCC) lattice structure to form a three dimensional high symmetry network. Each carbon atom is linked with four other carbon atoms in regular tetrahedrons, creating a cubic lattice with tremendous strength in all directions that forms an incredibly solid crystal structure (Jonathan B. Levine et al., 2009). In addition, the bond length is short as carbon is the light element. Thus, when we look for the super-hard materials, light elements, such as boron, carbon, and nitrogen are considered. These elements are capable of forming three-dimensional rigid lattices with shortened covalent bonds. Moreover, in order to guarantee the materials resistance to squeezing, the elements with very high densities of valence electrons should also be considered. With these ideas, the search of

new super-hard materials can be focused on the range of synthesized materials composed of light elements.

According to the ideas discussed above, some hard materials can be selected as potential super hard materials including cubic boron nitride, wurtzite boron nitride (wBN) (A. A. Melaibari et al., 2016), boron carbide (B_4C) (Thévenot, 1990, Jiménez et al., 1998), Titanium Diboride (TiB_2) (Riedel, 1994, Basu et al., 2006), etc. Table 4.1 shows the Knoop hardness, thermal stability, and chemical stability of those hard materials (John, Polwart, Troupe, & Wilson, 2002). Polycrystalline diamond (PCD) has the highest hardness but lowest oxidation temperature. Thus, PCD is unable to cut materials under high speed since the heat created by cutting could oxide the PCD to carbon. CBN and WBN have high chemical inertness and high oxidation temperature that allow for high speed manufacturing in various environments. Some researchers are working to improve the hardness of ceramic materials, such as Boron carbide (B_4C), Tianium diboride (TiB_2), Osmium diboride (OsB_2), and etc., to reach or close to diamond hardness. Thévenot made the B4C with hardness of 30 GPa at room temperature (Thévenot, 1990). Gou and his group studied on OsB_2 and measured its hardness to be only 37 GPa (Gou et al., 2009). Thus, OsB_2 and B_4C could not be considered as potential superhard materials to reach diamond hardness.

Table 4.1 *Properties of selected hard materials*

Synthetic materials	Formula	Hardness (Knoop GPa)	Oxidation temperature in air (°C)	Chemical stability
Polycrystalline Diamond	PCD	70-100	700	Reactive with ferrous materials
Cubic boron nitride	CBN	40-50	1300	High chemical inertness
Tianium diboride	TiB_2	30	1100	High chemical inertness
Boron carbide	B_4C	30	1400	High chemical inertness
wurtzite boron nitride	WBN	30	1200	High chemical inertness
Titanium nitride	TiN	21	800-900	High chemical inertness

Despite most previous works' efforts to create super-hard materials by synthesizing super-hard materials, many opportunities still remain unexplored. For example, the combination of Hall-Petch and quatum confinement effects have been used to design thermally stable and chemically inert nanoscale grain-size cBN/wBN composites with increased hardness. In order to achieve this kind of super-hard material, a novel laser/waterjet heat treatment (LWH) approach was performed on cBN/wBN composites. A preliminary study concluded that the hardness of the cBN/wBN was comparable to the hardness of diamond (A. Melaibari et al., 2012).

The hybrid LWH process allows elements of laser and water-jet treatment to be synergistically combined in a way so that material processing is accomplished by thermal shock-assisted fracturing of particles into microstructure refinement rather than the melting and solidification of surface material. The LWH process consists of a low-power laser (160 W – 400 W) for precise heating of a small processing zone (1 mm width) on the work-piece. The laser heating will create a temperature gradient in the treated zone, and rapid waterjet

quenching of the zone will develop thermal stresses that fracture the large particles which break into smaller particles within the treated zone (Dinesh Kalyanasundaram, 2009)

The new discovery of rapidly quenched cBN/wBN composites with hardness values approaching those of diamond can have vast implications in the tooling industry. Hence, in this paper, a series experiments on laser heat treated dual phase cBN/wBN tools was designed in order to identify the fundamental phase transition and microstructure refinement features that contribute to the hardness improvements.

In previous studies (A. A. Melaibari et al., 2016; A. Melaibari et al., 2012), the relationship between laser fluence, laser beam overlap percentage and hardness improvement was evaluated. The test results show that low laser fluence is a better choice which could improve the hardness of cBN/wBN composites without damaging the sample, and a laser beam overlap of around 50% will create the highest hardness improvement. However, the hardness improvement mechanism is still not clear since the hardness change ratio is not uniform throughout the laser beam track. Thus, a new experiment was designed for the study of laser/waterjet heat treated cBN/wBN composites in order to find the effect of the number of laser beam passes and laser power distribution on resulting hardness values.

4.2 Method

A continuous wave CO2 (Laser Spectra Physics 820) was employed to conduct the experiments with the laser parameters shown in Table 4.2. Three factors were studied in this paper. The first factor was the laser pass number. In previous studies, experiments were designed to find the relationship between material hardness change and the laser beam overlap. With different laser beam overlaps, the boron nitride (BN) material hardness change ratio

varied. Therefore, multiple laser beam hits in the same location of the BN material may enhance surface hardness. The following six levels of laser beam passes were used in this study: 1 pass, 2 passes, 4 passes, 8 passes, 16 passes, and 30 passes. The second factor was the distance of the laser beam track from the center of the beam. Five levels of the distance from the laser beam center were designed in this paper; 50 micron, 150 micron, 250 micron, 350 micron, and 450 micron. The laser beam used in this study was a Gaussian beam so the power density was not uniform along the entire beam path. Therefore, the laser beam energy irradiated on the cBN/wBN composite was not uniform along the width of the laser beam. The Gaussian profile of the laser beam was approximated as a surface heat source whose intensity at radial distance r from center is given in Eq. (4.1):

$$\mathrm{I(z)} = a_s I_0 \exp\left(\frac{-2r^2}{w^2}\right) \tag{4.1}$$

where I_0 is the intensity at the center of the beam, a_s is the absorption coefficient, and w is the diameter of the laser beam spot. The absorption coefficient was chosen to be 0.75 (A. A. Melaibari et al., 2016). The third factor is the boron nitride material's composition. Two kinds of commercial materials were used in this study that are dual phase 82%cBN/18%AlN with iron oxide as the impurity and 55%cBN/45%TiN. The average hardness of 82%cBN/18%AlN and 55%cBN/45%TiN composites was 46 GPa and 34 GPa respectively.

Table 4.2. *LWH treatment parameters*

Material	Laser power (W)	Scanning speed (inch/min)	Waterjet pressure	Gas
82%cBN/18%AlN	220	140	400 KPa	Compressed air
55%cBN/45%TiN	400	100	400 KPa	Compressed air
82%cBN/18%AlN	220	140	No WJ	Compressed air
55%cBN/45%TiN	400	100	No WJ	Compressed air

Similar with our previous experiments, the experiment consists of 3 steps. First, the heat treatment experiment was conducted by using a continuous wave CO2 laser beam of 1 mm spot size with a speed of 140 inch/min and 100 inch/min (table 4.2). A low laser power was used to prevent melting, scribing or cutting of boron nitride. The laser beam was immediately followed by a waterjet stream, shown in Figure 4.1. In order to investigate the waterjet effect on BN material hardness improvement, a series control experiments has been designed. Compare with LWH treatment experiments, the control experiments conducted without waterjet.

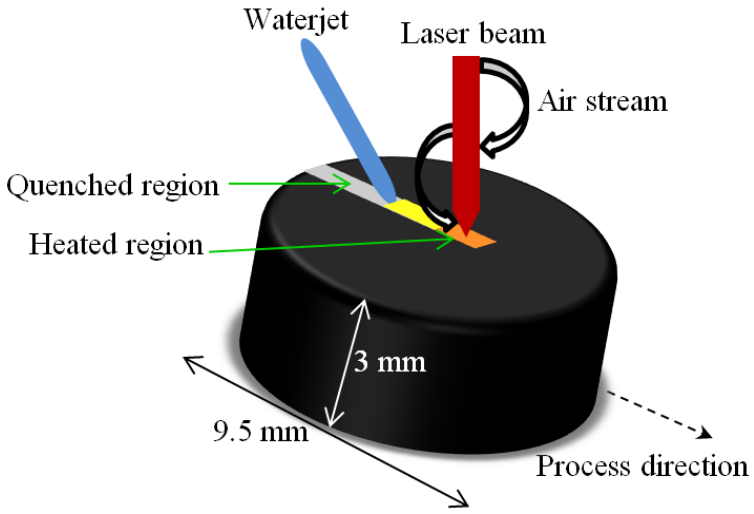

Figure 4.1 *Schematic of LWJ heat treatment process*

Second, in order to identify the change of the sample's hardness and toughness, Knoop microhardness tests and Vicker's fracture toughness tests were taken before and after LWH treatment. Indentation hardness tests were performed using a Tukon microhardness tester with a Knoop diamond pyramid indenter. The load was set at 0.5 kgf (4.9 N), and the test duration was set at 30 seconds. Length measurements were made along the long axis of the indentations using a high resolution (± 0.4 µm) optical microscope and optical profilometer to ensure that

no fracture had occurred in the indentation zone. Knoop hardness was then calculated using the relationship (Knoop et al., 1939):

$$HK = \frac{P}{C_p L^2} \tag{4.2}$$

where P is the load (kgf), C_p is the correction factor related to the shape of the indenter (0.070279 in this case) and L is the length of indentation along its long axis. The Vicker's indentation method for fracture toughness measurement is performed by making an impression on the ceramic surface at reasonably higher loads (Roy, 2015). This process generates cracks, mainly at the corners of the indentation mark. The toughness is guided by the crack length generated along with the hardness value of the sample. Toughness tests were performed used the Tukon microhardness tester with a Vicker's diamond pyramid indenter at a load of 2 kgf (19.6 N). According to Antis et al. (Anstis, Chantikul, Lawn, & Marshall, 1981), the fracture toughness of a material will be governed by the following equation for radial median type of crack geometry:

$$K_c = 0.016 \left(\frac{E}{H_v}\right)^{0.5} (P/C^{1.5}) \tag{4.3}$$

where, $\frac{E}{H_v}$ is the Young's modulus to apparent hardness ratio and $P/C^{1.5}$ is the ratio of change in the crack length with load. The Young's modulus in this study was set as 766 MPa (Roy, 2015).

In order to maintain precision while measuring the length of indentations, the indentation optical images were taken by optical microscope. The length of indentations were measured on optical images by a Java-based image processing program known as ImageJ.

Third, a detailed microstructure analysis of both untreated and LWH treated samples were done using a FEI Quanta 250 FE-SEM. The SEM was opereated in high vacuum mode which provides better resolution than low vacuum. The 82%cBN/18%wBN sample was coated

with 2 nm-thick conductive iridium layer to reduce sample charging in the SEM. Secondary electron (SE) and backscattered electron (BSE) imaging were used to obtain images of different areas on the sample surface. The BSE images provides compositional contrast if the specimen has features with different composition (Angseryd, Elfwing, Olsson, & Andrén, 2009). Thus, this paper used BSE images to analyze the microstructural change before and after the LWH treatment of boron nitride samples. EDS was used to identify the specific elements on certain areas by using dot mapping, point analysis, and line analysis.

4.3 Results

Visual examination of a sample that was laser heat treated revealed a color change from light-absorbing black/gray to transparent white on the center of the laser beam track (about 200 micron width). Figure 4.2 shows the color change of the LWH treated area on SEM. Compared with visual examination, the color change observed on SEM is different. The dark area on the right side of the figure is the center of the laser beam track which is transparent white in the optic picture. Such an effect is ascribed to a change in crystal morphology following S. Veprek's classification of the crystalline morphology of cBN according to color, size and transparency (S. Veprek et al., 2010). A transparent color of white to amber in cBN implies tetrahedral crystal morphology (as opposed to octahedral) with small grain size and loss of boron. It can also be noted that the color may also be caused by inclusions, dopants or defects. The formation of transparent white color of the cBN provides some clues on the possible phase, stoichiometry and grain size changes in laser waterjet heat treatment.

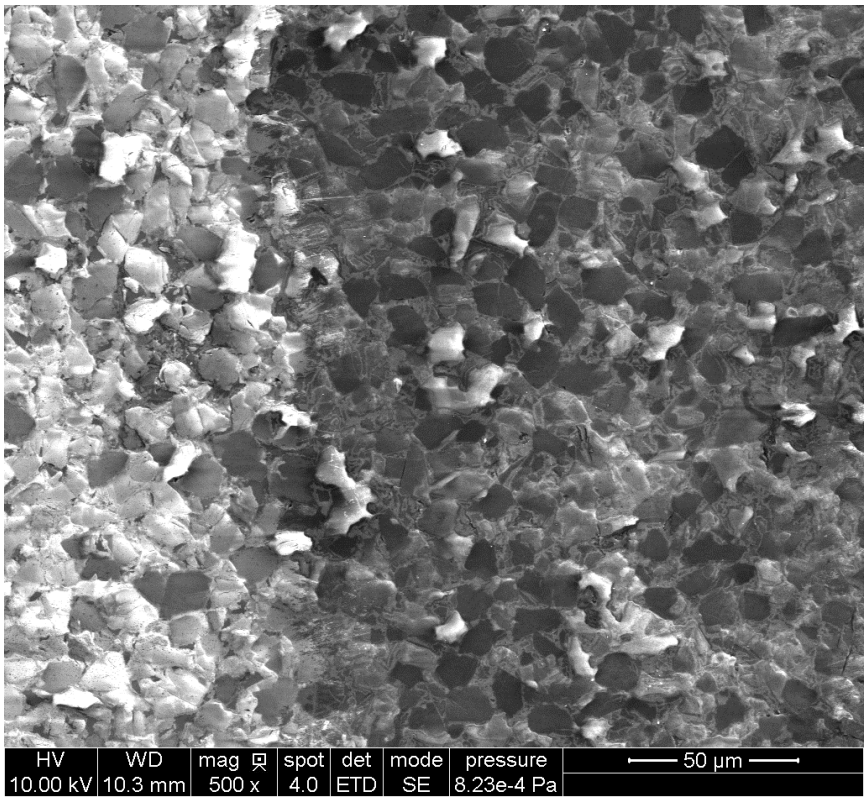

Figure 4.2 *SEM micrograph of cBN showing color change in LWH-treated area*

It was noted that the color change only occurred in the center of the laser track. The width of the laser beam track was 1 mm, but the width of color change area was 0.2 mm. This result is attributed to the Gaussian beam laser intensity distribution not being uniform across the laser track. According to equation 4.1, laser beam intensity is higher in the center of the laser beam track than other areas. Therefore, color, hardness, and toughness changes were more intense in the center of the laser beam track.

The hardness was measured from the edge to the center of the laser beam track for different numbers of laser passes. Figure 4.3 shows the SEM images of the indentations taken from the edge of the laser beam track to the center of laser beam track. The 5 laser beam pass areas in one laser beam track were divided by 5 different lines with different distances from the area edge (50, 150, 250, 350, and 450 micrometer from the center of the beam track). There are 5 indentations on each line to minimize the inclination.

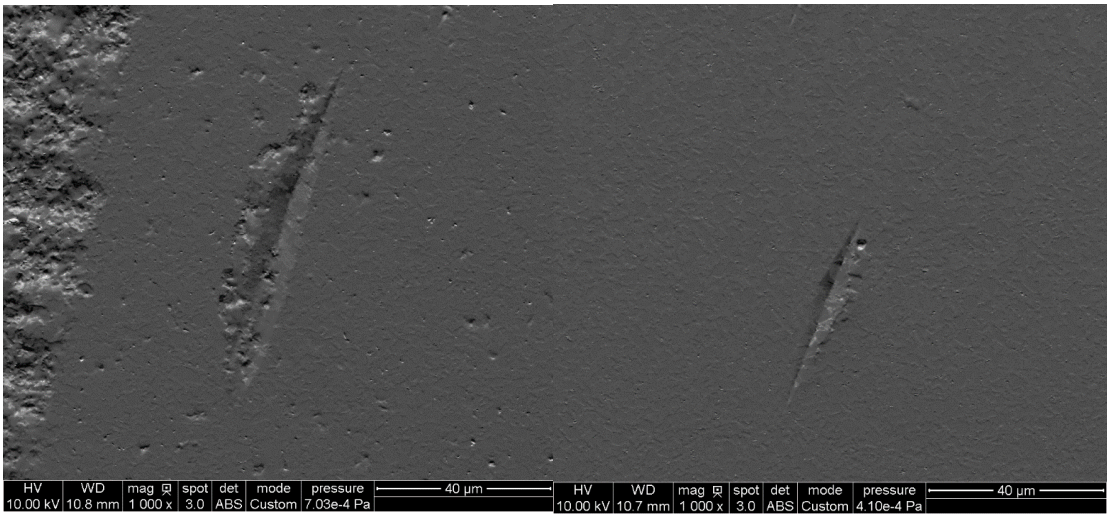

a *b*

Figure 4.3 *SEM images of the indentations: (a) untreated and (b) LWH treated dual phase cBN/TiN*

Figure 4.4 shows the hardness change ratio results of Knoop hardness tests for binderless 55%cBN/45%TiN as a function of the distance from the laser beam center. The different colors represent the number of laser beam passes. As shown in Figure 4.4, the hardness of LWH-treated sample increased by approximately 22% for the indentation placed 150 microns from the center of the beam track for 2, 8, and 30 laser beam passes. With the laser beam pass number increasing, the hardness change ratio of 50 micrometer area increase at beginning and then decrease to about 1 on 30 passes, which because material surface close to beam center has more defects than beam edge. With the distance from beam center increasing from 50 micron to 450 micron, less damage observed on whole laser track and the hardness improve ratio observed a trend, which increasing the laser beam pass, increase the hardness change ratio as well.

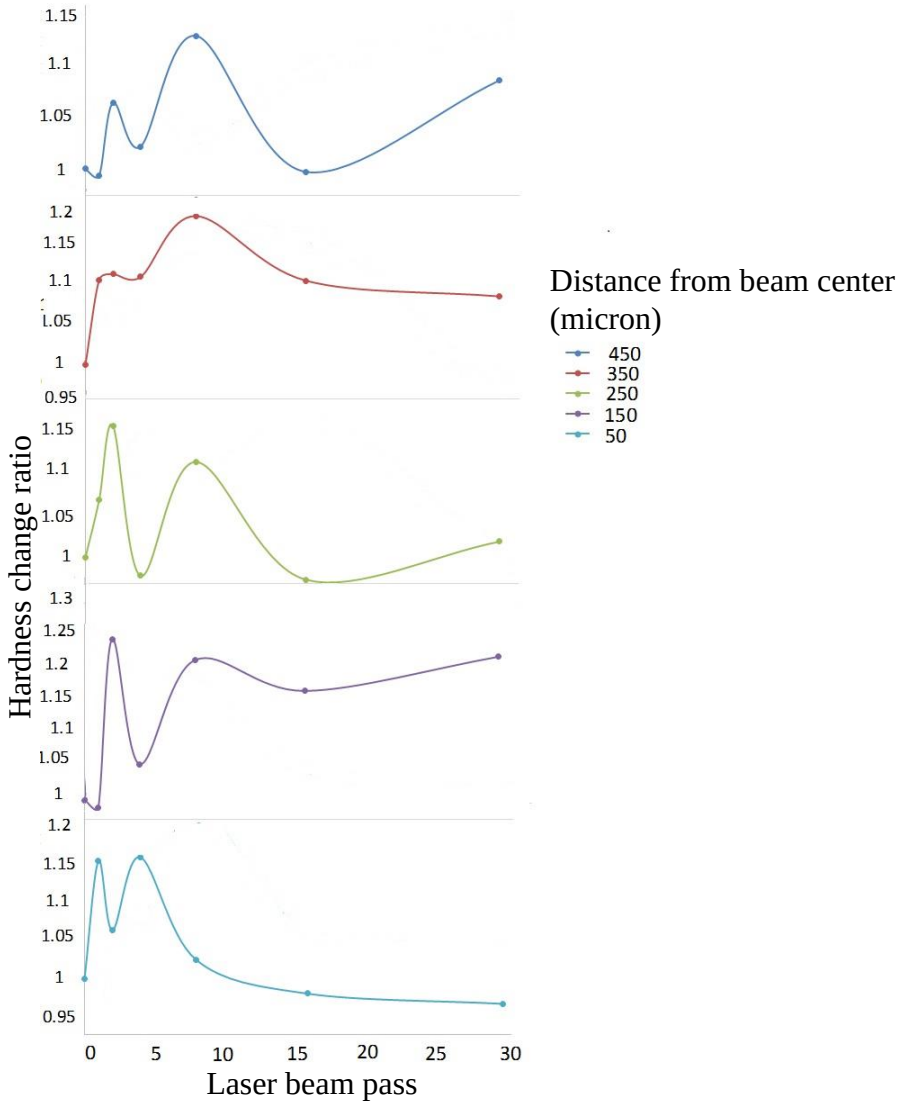

Figure 4.4 *LWH treated 55%cBN/45%TiN material hardness change ratio*

Figure 4.5 shows the hardness change ratio comparison results of Knoop hardness tests for binderless 82%cBN/18%AlN as a function of the distance from laser beam center. As shown in Figure 4.5, the hardness of the LWH-treated sample increased by up to 30% for the indentation placed 50 microns from the center of the beam track for 8 passes. Similar with 55%cBN/45%TiN, the LWH treated 82%cBN/18%AlN material surface observed some defects on the areas close to center beam of 30 passes beam track. The hardness ratios on those areas are observed around 1 which is relatively lower than other areas. However, there is a

trend could be concluded that with the laser beam pass increasing, the hardness change ratio increase as well if there is no any damage on the material surface.

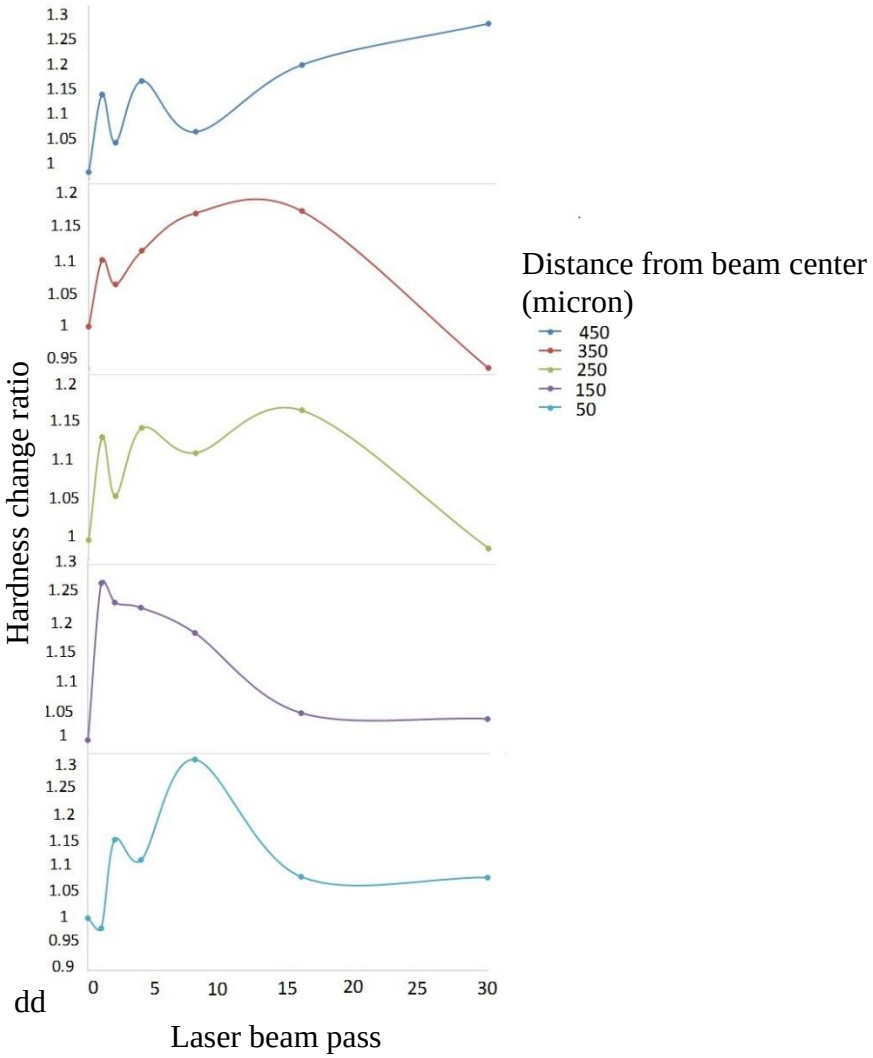

Figure 4.5 *LWH treated 82%cBN/18%TiN material hardness change ratio*

Compare with LWH treated materials, the laser only treated materials also have hardness improvement. The maximum hardness improve ratio for 55%cBN/45%AlN without waterjet is 1.14 that observed on 16 passes 450 micrometer from laser beam center. In Figure 4.6, we observed most data points values plotted between 0.9 and 1.05, which is not a significant hardness change ratio. Although, the maximum hardness improve ratio close to the value that observed on LWH treated material, it is only one spot and still well below LWH one.

In addition, the visual observation of laser only treated 55%cBN/45%AlN has a spalled region on 16 and 30 passes area. Similar with the spalled region we observed on laser fluence study, it only on laser beam center where has highest laser intensity (A. A. Melaibari et al., 2016). However, the spalled region was not observed on any area of LWH treated materials.

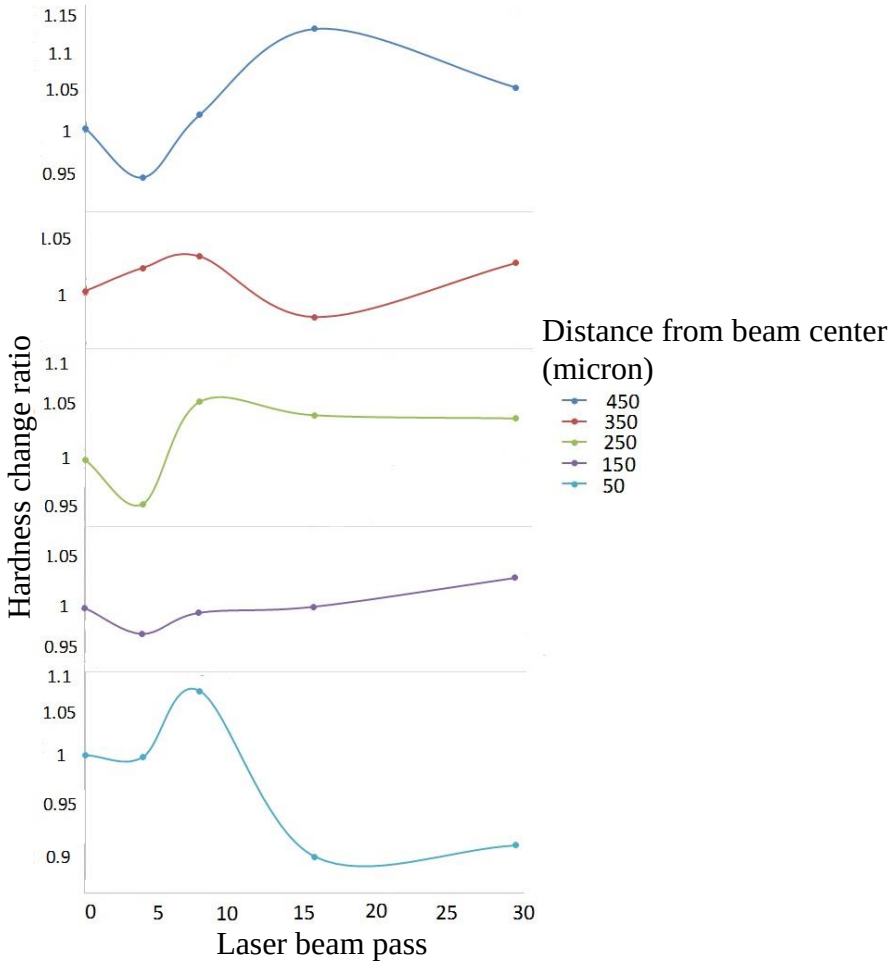

Figure 4.6 *Laser only treated 55%cBN/45%AlN material hardness change ratio*

Similar with 55%cBN/45%AlN material, most of laser only treated 82%cBN/18%TiN hardness change ratio between 0.9 and 1.1, which shown in Figure 4.7. The maximum hardness change ratio is 1.12, which observed on 30 passes 450 micrometer from laser beam. The spalled region also observed on beam center areas of 16 and 30 passes.

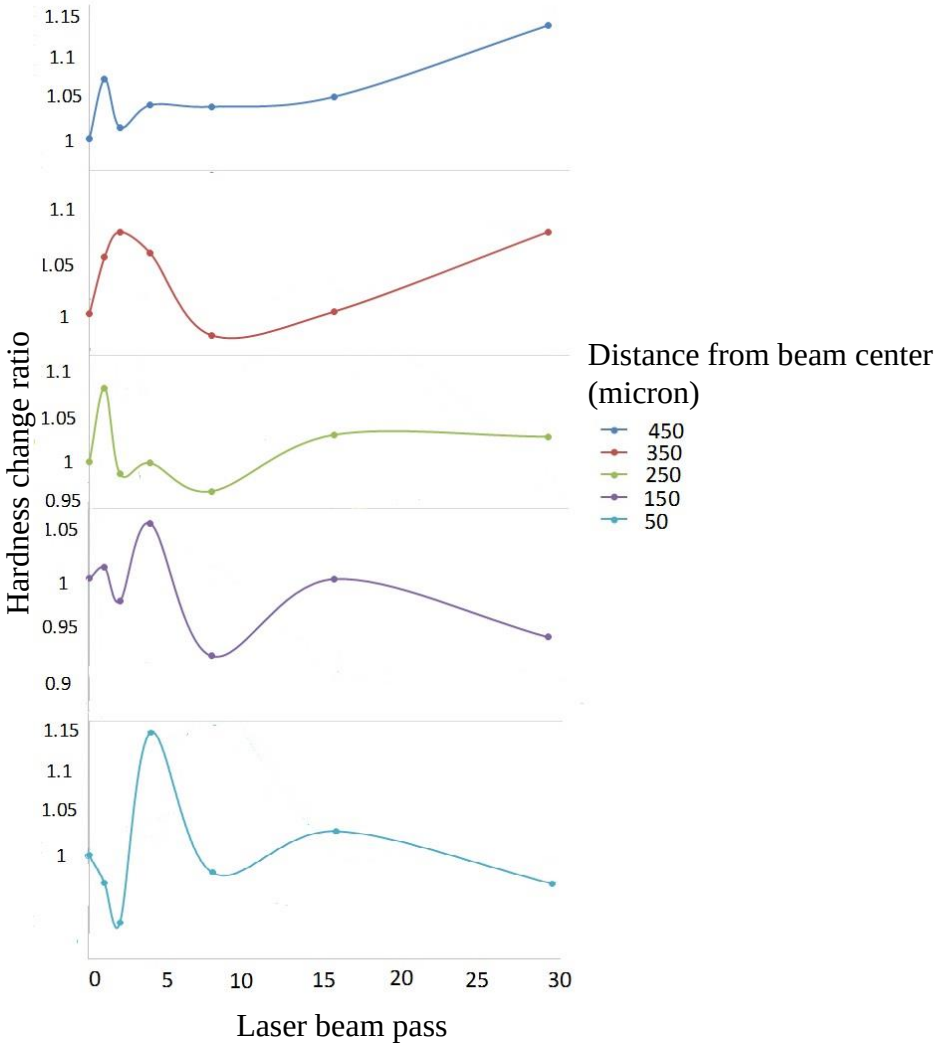

Figure 4.7 *Laser only treated 82%cBN/18%TiN material hardness change ratio*

In this study, 400X optical images of Vicker's indentations were captured on BN samples before and after LWH treatment. Two such images taken on 82%cBN/18%TiN sample are shown in Figure 4.8. The magnified images show that the cracks connect with the corners of the indentation which are characteristic features of radial median cracks.

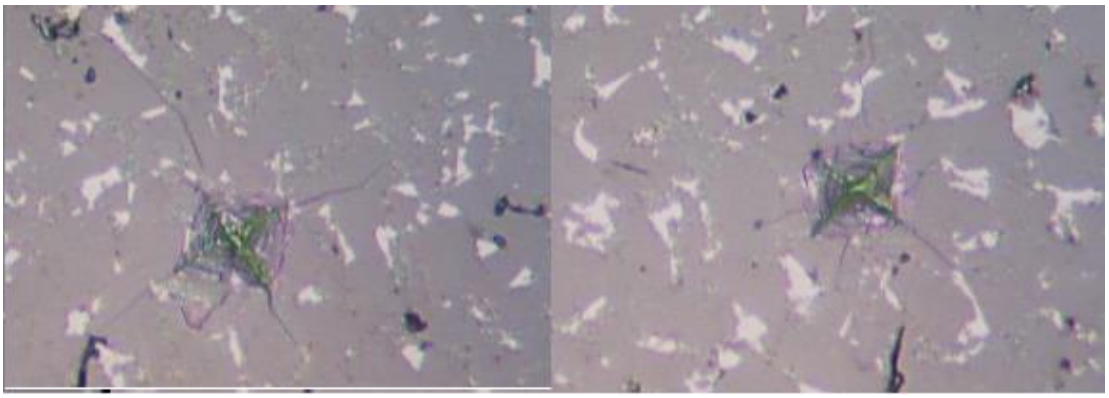

A *B*

Figure 4.8 *Indentation marks taken on untreated (A) and LWH treated (B) 82%cBN/18%TiN sample*

The fracture toughness of the samples was calculated by measuring the diagonals of the indentations and the crack lengths using Equation 4.3. A comparison of fracture toughness data for treated and untreated samples is shown in Figure 4.9. The error bars show the deviation of the hardness test data. It can be noted that the facture toughness of the treated 55%cBN/45%TiN sample decreased from 3.29 ± 0.77 MPa · $m^{1/2}$ to 2.4 ± 0.457 MPa · $m^{1/2}$ which was 27% less than the untreated sample. The facture toughness of the treated 82%cBN/18%AlN sample, conversely, increased from 2.4 ± 0.59 MPa · $m^{1/2}$ to 3.1 ± 0.84 MPa · $m^{1/2}$ which was 19% more than the untreated sample.

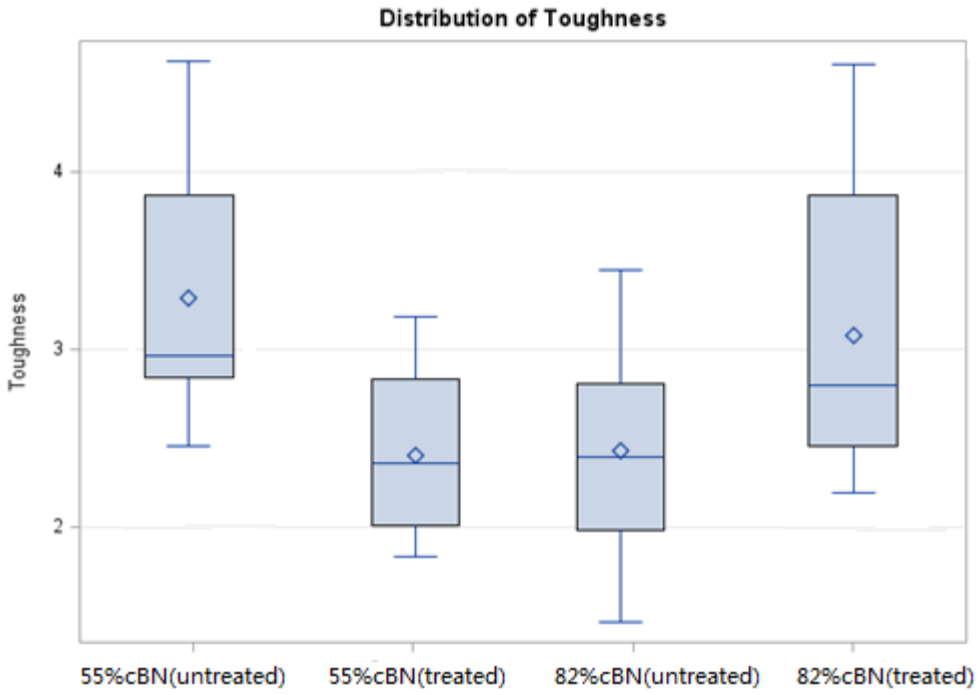

Figure 4.9 *Comparison of fracture toughness data on BN samples*

4.4 Discussion and conclusion

Results showed a direct correlation between the number of laser passes and the hardness for BN composites. It was noticed that the hardness change ratio was more pronounced in the center of the laser beam track as opposed to the edges of the track in most cases. The radial distance, r, of Equation 4.1 increases as it moves from the center and towards the edges. Thus, the laser energy in the center of the beam track is more than that of the track edges resulting in higher temperatures in the center of the laser beam track. The waterjet following the laser beam rapidly quenched the material to room temperature which created high compressive stresses. The combined action of high temperatures and compressive stresses may have led to microstructure refinement that resulted in the hardness enhancement observed in this study. We believe that as the number of laser passes increased, microstructure

refinement generated during the LWH process resulted in improved hardness for BN composites. Thus, two points of interest can be taken from this study:

1. The LWH-treated BN composite hardness improved with more laser beam passes;

2. The LWH-treated BN composite hardness increased with decreasing distance from the laser beam center.

However, these points are not necessarily always valid. According to experimental results, the maximum hardness improvement for the 55%cBN/45%TiN composite occurred after 2 passes in an area located 150 microns from the center of the beam track. For the 82%cBN/18%AlN composite, the maximum hardness improvement occurred in the center of the beam track after 8 passes; not the maximum number of passes in this study which is 30. As the number of passes increases, higher temperature changes can result in higher compressive stresses created by LWH treatment which may lead to surface damage. Previous studies have reported the presence of spalled regions on LWH-treated cBN/wBN composites (A. A. Melaibari et al., 2016). In this study, surface damage was noticed in the center of the beam track for 16 and 30 passes on the LWH-treated 82%cBN/18%AlN composite shown in Figure 4.10. As with the spalled regions identified in our previous experiments, the damaged surface displayed a lower average surface roughness compared to the surrounding areas that did not appear to be damaged. Surface damage can be avoided in future experiments by careful control of the number of laser beam passes admitted on the sample surface.

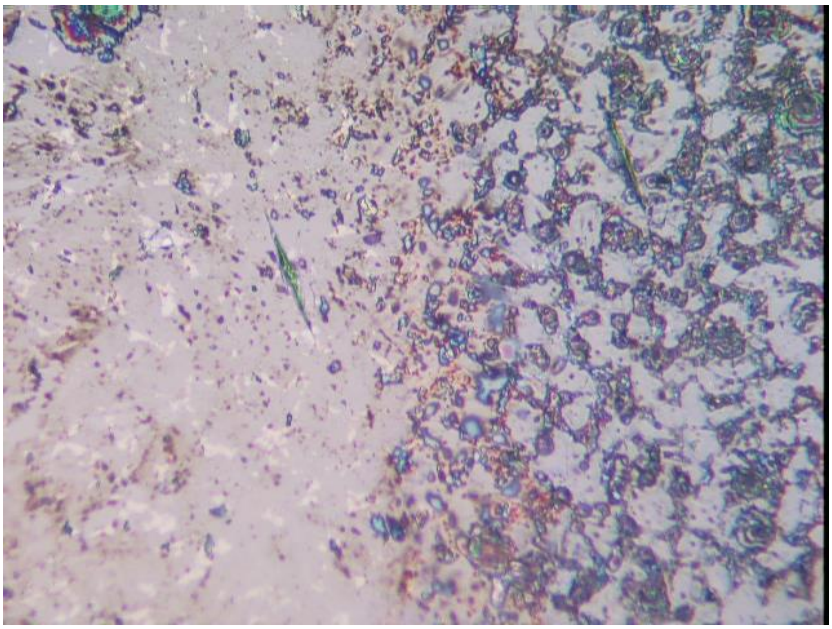

Figure 4.10 *Surface condition of LWH treated 30 passes area of 82%cBN/18%AlN composite*

4.4.1 Microstructure of the sample before LWH treatment

Since the increase in hardness for the dual phase cBN/TiN and cBN/AlN composites was significant, the reasons for the hardness change was further studied using SEM/EDS to analyze the microstructure and elemental information of the samples. The SEM study revealed images that indicate the formation of significant cracking and fracturing of cBN particles during the LWH treatment. The microstructure of the untreated 82%cBN/18%AlN sample consisted of two types of structures with different size and morphology. The first type of structural formation was identified as polyhedral faceting with facets of 1-10 μm in length with dark color shown in Figure 4.11. The second type of structure observed was identified as irregularly-shaped particles (unable to observe the grain boundary) with bright color shown in Figure 4.14. Polyhedron/polyhedron interfaces have straight-line boundaries with bright material filled in. The polyhedral grains are originally the cubic boron nitride grains, and the bright grains are alumina nitride according to EDS results in Figure 4.14.

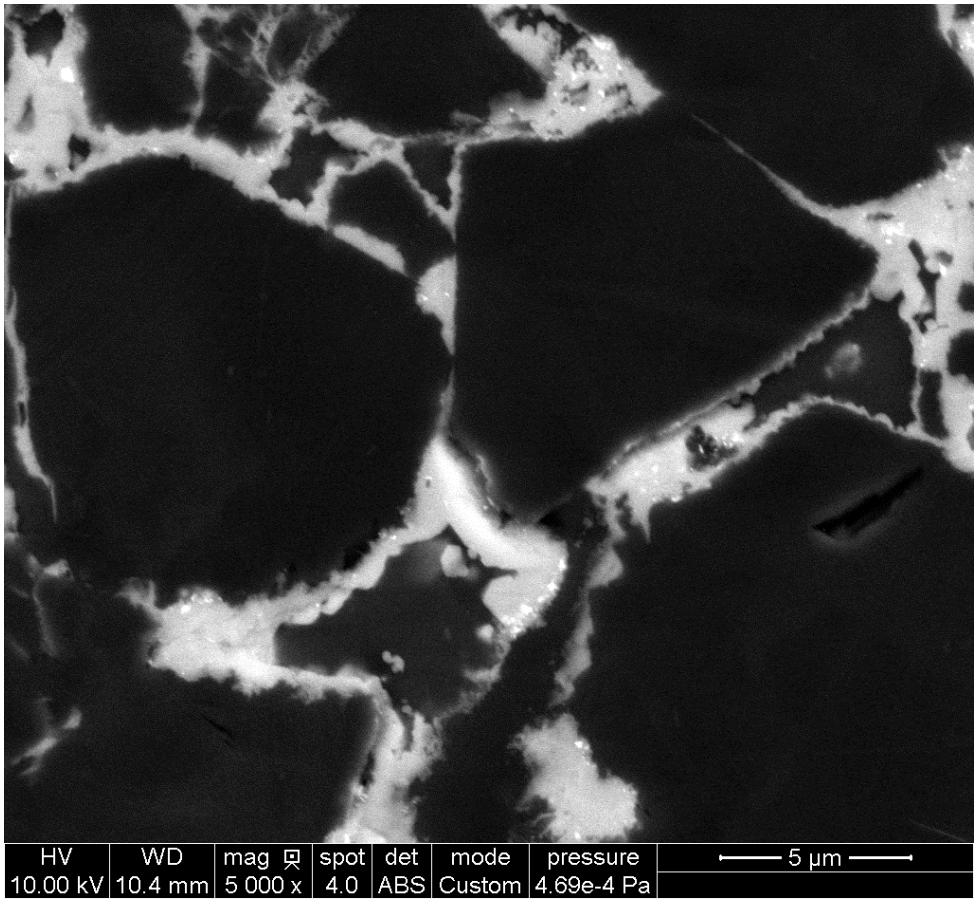

Figure 4*.11 SEM micrograph showing microstructure of untreated 82%cBN/18%AlN sample*

Similar to the untreated 82%cBN/18%TiN sample, the dual phase 55%cBN/45%TiN sample consisted of 3 types of particles which are shown in Figure 4.12. The first type was identified as trapezoidal particles with dark black color. The second type was identified as grayish particles without a visible grain boundary. The third type of particle was identified as nano-scale irregularly-shaped particles with bright color. EDS results shown in Figure 4.14 identify the trapezoidal particles as CBN, the gray particles as TiN particles, and the bright particles as a mixture of tungsten, alumina, and nitrogen composite.

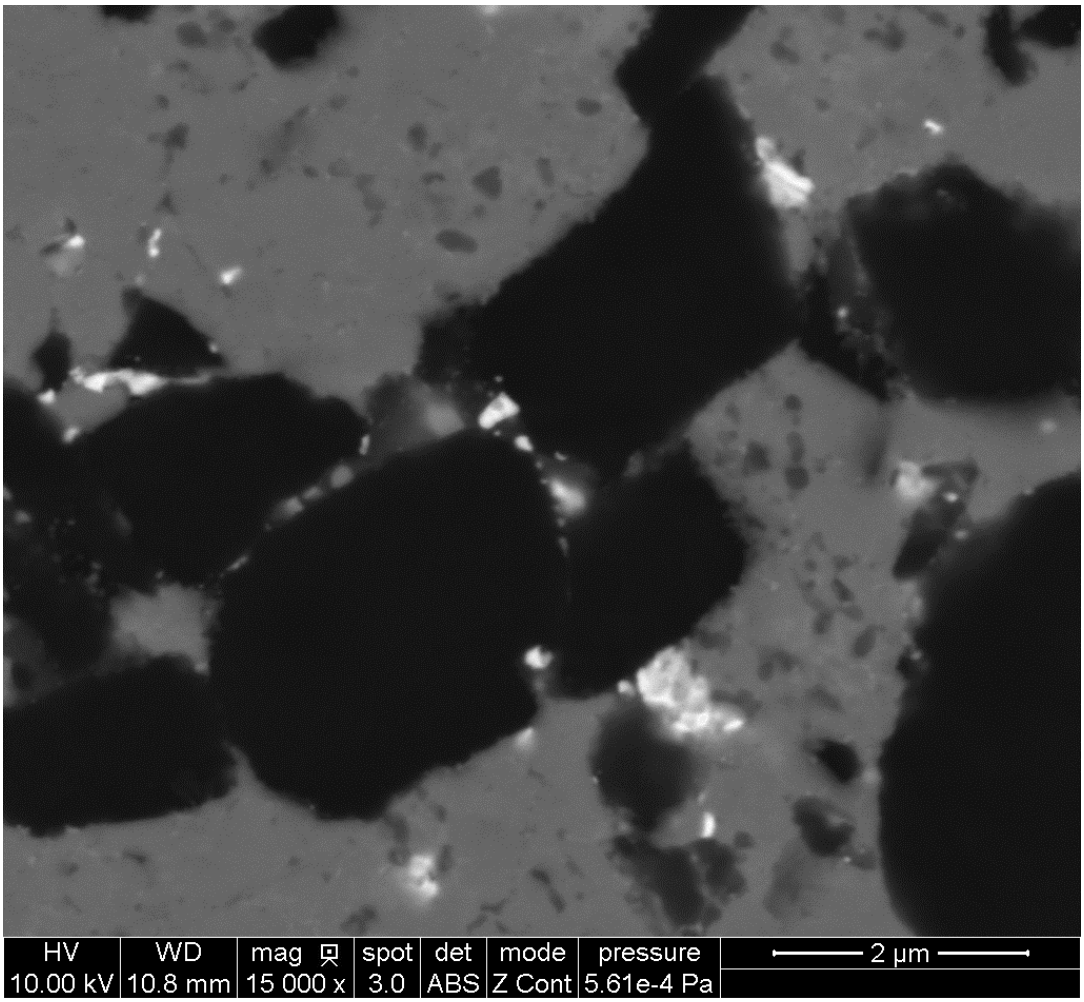

Figure 4.12 *SEM micrograph showing microstructure of untreated 55%cBN/45%TiN sample.*

4.4.2 Microstructure of the sample after LWH treatment

The microstructure of the cBN/AlN composite after LWH treatment consisted of the same two kinds of grain: the irregular shapes (AlN particles) and the polyhedrons (cBN particles). However, there were two main differences in the observed microstructure for the LWH-treated samples.

There was no dramatic change in the microstructure of the AlN particles because their grain boundary was not visible in the SEM images. However, the first main difference was that the polyhedron particles appeared to be cracked and broken into several smaller particles as

shown in Figure 4.13. According to the EDS point analysis results shown in Figure 4.14, the gap created by the crack was filled by AlN particles.

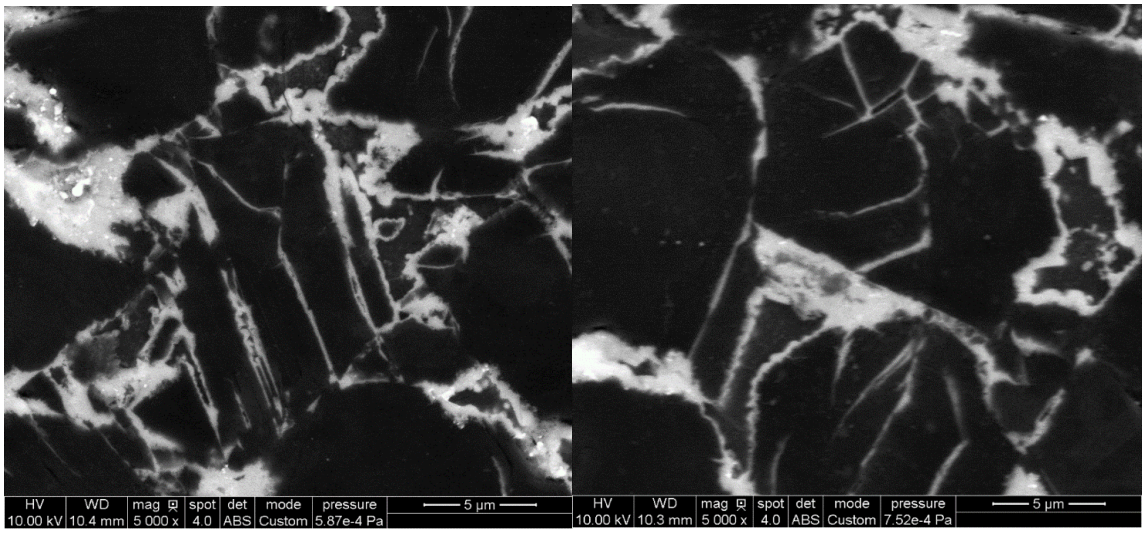

Figure 4.13 *SEM micrograph showing the LWH-treated microstructure of cBN/AlN composite*

Since single CBN particles appear to be broken and cracked into several smaller particles, the average particle size in LWH-treated samples was changed. In this paper, the grain size of the samples was calculated by using the standard formula of linear intercepts method:

$$G = 1.56L/MN \tag{4.4}$$

where G is the grain size, L is the random line length on the micrograph, M is the magnification of the micrograph, and N is the number of the grain boundaries intercepted by the lines (Roy, 2015). The average grain size of each sample was estimated from two images. For each image, four random lines were drawn to calculate the grain size.

It is commonly accepted that material hardness increases when grain size decreases which means that the material follows the Hall-Petch effects (Hansen, 2004; Hou, Bushby, &

Jennett, 2008). However, the grain size of a material is not the only factor that impacts material hardness. Crystallinity, precipitation along the grain boundary, porosity, and slip planes also influence increases and decreases in material hardness (Roy, 2015). The calculated average grain sizes for this study are listed in Table 4.2. Results show in increase in hardness with decreasing grain size among the different samples. The average grain size of LWH-treated cBN/AlN composite decreased from 5.644 μm to 3.026 μm which was 46.4% less than the untreated sample. The hardness of LWH-treated cBN/AlN composite increased from 46 GPa to 60 GPa; a 30% increase compared to untreated cBN/AlN composite. This hardness and grain size change is consistent with Hall-Petch effects.

Table 4.2 *Calculated grain size of BN composites*

Material	55%cBN/45%TiN		82%cBN/18%AlN	
	untreated	LWH treated	untreated	LWH treated
Average grain size (μm)	0.553	0.237	5.644	3.026
Change ratio	0.428		0.536	

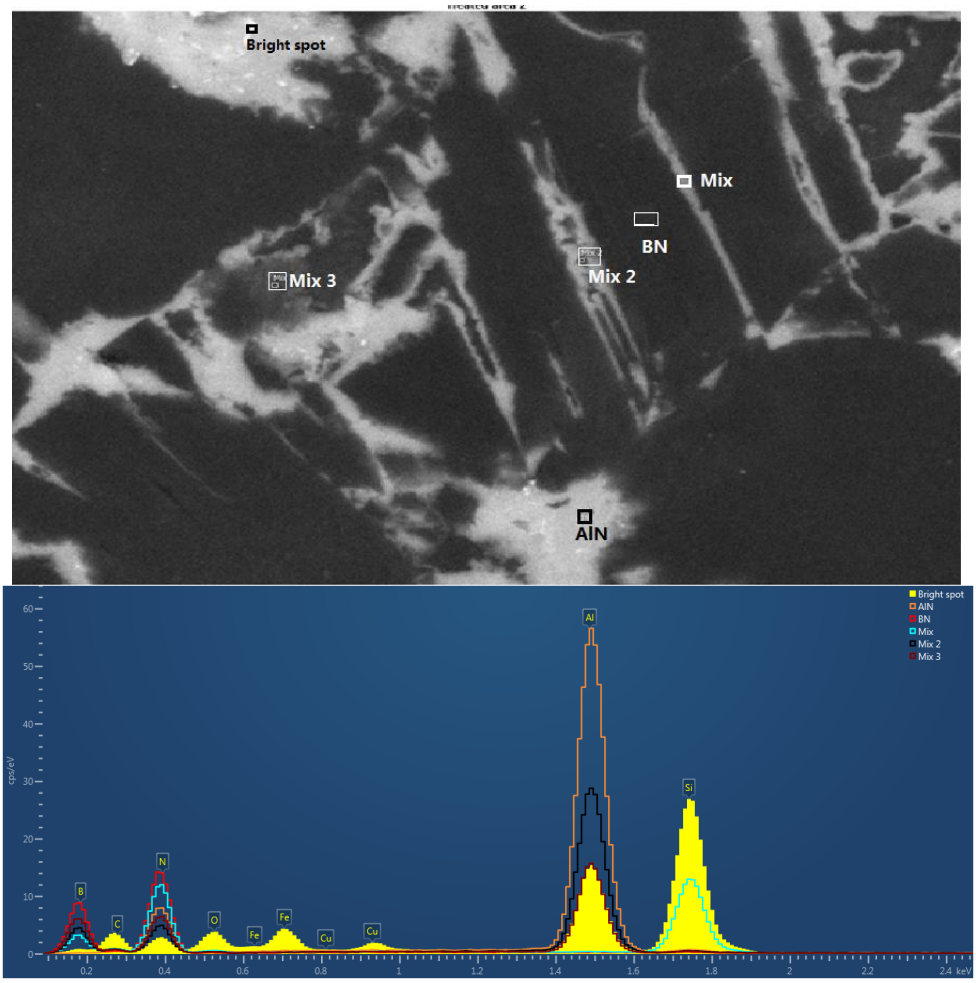

Figure 4.14 *SEM point analysis of LWH treated cBN/AlN composite*

Several mechanisms were attributed to the observed increase in hardness of cBN/TiN composite. First, the formation of nano-scale CBN grains not detected in untreated cBN/TiN composite can be seen in LWH-treated cBN/TiN composite shown in Figure 4.15. The nano-scale structure of the CBN grains is expected to introduce a grain-boundary strengthening mechanism which inhibits ease of dislocation movement across the boundary (He et al., 2008). The second observed mechanism attributed to increased hardness of cBN/TiN composite was the change in grain size of the composite after LWH treatment. Similar to LWH-treated cBN/AlN composite, the average grain size of cBN/TiN composite was decreased from 0.553 µm to 0.237 µm which is 57.2% less than the average grain size of the untreated sample. This

kind of structure change is expected to increase the energy needed to allow for dislocations among grains.

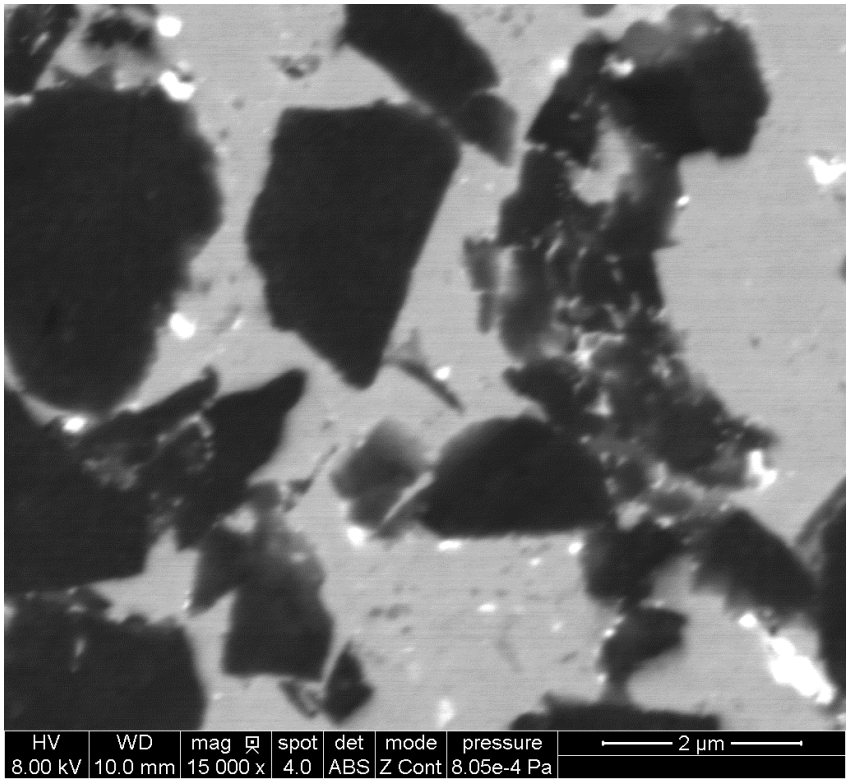

Figure 4.15 *SEM image of LWH treated cBN/TiN composite*

It is interesting to note the breaking of CBN particles to several smaller particles and the transition of filler materials to close the gaps between the newly developed smaller CBN particles. According to EDS results, the filler materials were identified as tungsten, alumina, and titanium. Tungsten and alumina were impurities while titanium nitride was a main particle in the composite.

It can be concluded that grain-boundary strengthening due to formation of cracks of large CBN particles and significant reduction in grain-size of the material are the dominant mechanisms of hardness improvement for BN composites.

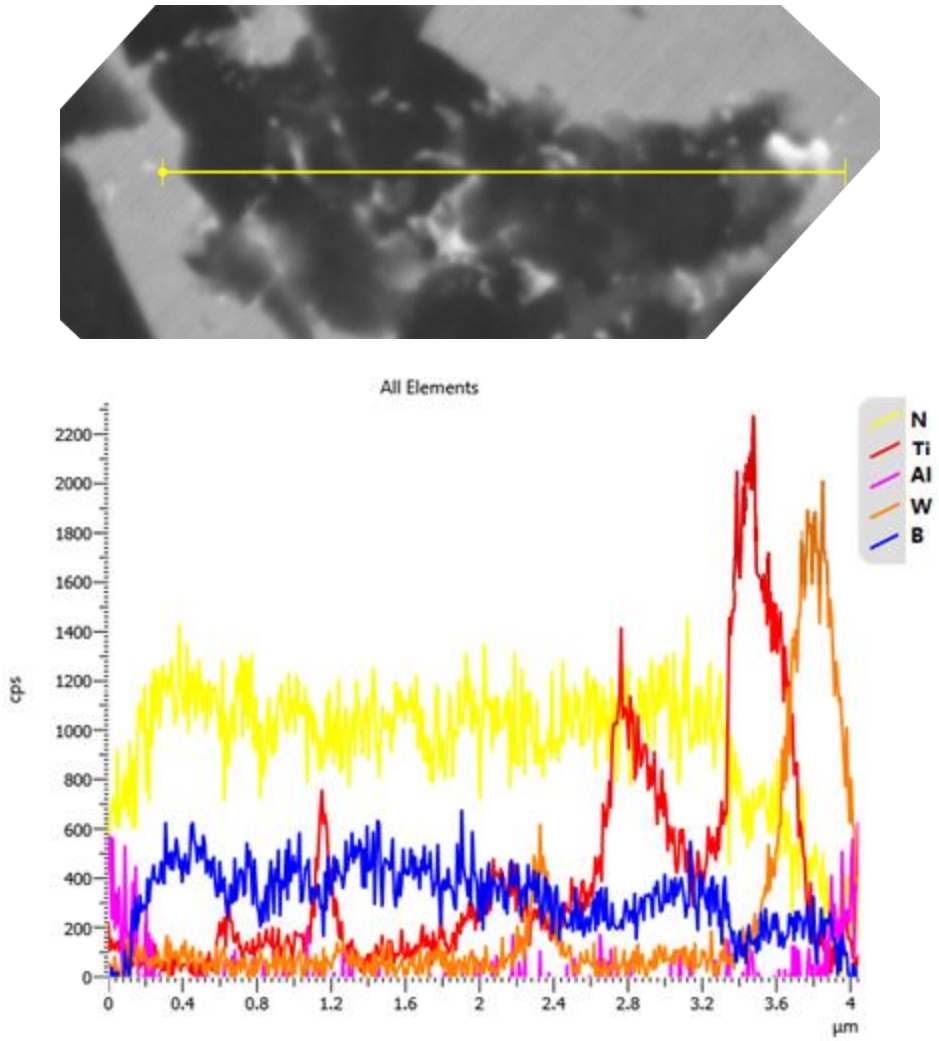

Figure 4.16 *EDS line analysis of LWH treated cBN/TiN composite*

4.4.3 Hall-Petch effect verification

According the Hall-Petch effect, a decrease in grain size leads to an increase in hardness. The grain size measured in this study revealed a decrease which might be the reason of the hardness improvement. In order to verify if the Hall-Petch effect is the reason of the hardness change, this paper calculated the hardness based on Hall-Petch equation (eq. 4.5).

$$H = H_0 + \frac{K}{\sqrt{d}} \tag{4.5}$$

where, K is the strengthening coefficient (a constant specific to each material), and H_0 is the constant. The H_0 value and K value in this study were set as 39 GPa and 126 GPa·nm$^{1/2}$ (Dubrovinskaia et al., 2007).

As shown in table 4.3, with the grain size of 55%cBN/45%TiN decrease from 552.9 nm to 236.9 nm, the Hall-Petch equation calculated hardness increased 6.4% which is very close to the experiment hardness change ratio of average hardness before and after LWH treatment. However, the 82%cBN/18%AlN Hall-Petch equation calculated hardness only increased 2%, which is 11% lower than experiment results. Thus, the Hall-Petch effect is one of the hardness improve mechanism but not the only one mechanism to explain the hardness improvement in this study. There are might be some other reasons for hardness improvement. For example, the microstructure change was observed on LWH treated area on SEM, which has been discussed above.

Table 4.3 *Comparison of wear coefficient*

Material	Grain size (nm)	Calculated hardness change ratio	Measured hardness change ratio (average LWH treated BN hardness/average untreated BN hardness)	Calculated/Measured hardness change ratio
55%cBN/45%TiN (Untreated)	552.9	1.064	1.059	0.995
55%cBN/45%TiN (treated)	236.9			
82%cBN/18%AlN (Untreated)	5644	1.02	1.13	1.11
82%cBN/18%AlN (treated)	3026			

4.4.4 Wear resistance study

Hardness and fracture toughness are two critical properties of tool materials. Both of them contribute to the tool wear resistance, which is the main eligibility criteria of tool material. In this study, the wear coefficient (W_H), which characterizes the wear resistance of a material, of original materials and LWH treated materials were calculated by using below formula

(Dubrovinskaia, Dub, & Dubrovinsky, 2006). Typically, the higher of wear coefficient and the higher of wear resistance.

$$W_H = K_C^{0.5} \cdot E^{-0.8} \cdot H_K^{1.43} \tag{4.5}$$

where, K_C is fracture toughness, E is Young's Modulus (766 GPa in this case), and H_K is Knoop hardness (Roy, 2015).

As shown in table 4.4, although fracture toughness of LWH treated 55%cBN/45%TiN composite dropped from 3.29 MPa to 2.4 MPa, the wear coefficient increased from 1.38 to 1.54 which indicated the better wear resistance. Because the wear resistance is the combine result of both hardness and fracture toughness. On the other hand, LWH treated 82%cBN/18%AlN composite increased both hardness and fracture toughness. Thus, it has higher wear coefficient value. This suggested that the LWH treated BN materials are more effective on mechanical machining in theory.

Table 4.4 *Comparison of wear coefficient*

Material	K_C (MPa)	H_K (GPa)	E (GPa)	W_H
55%cBN/45%TiN (Untreated)	3.29	34	766	1.38
55%cBN/45%TiN (treated)	2.4	41	766	1.54
82%cBN/18%AlN (Untreated)	2.4	46	766	1.82
82%cBN/18%AlN (treated)	2.86	60	766	2.90

To check the performance of LWH treated BN composites as a tool material, the mechanical tests will be done in the future.

4.5 Conclusion

Laser waterjet heat treatment experiments showed that the hardness of commercial BN composites (82%cBN/18%AlN) with high contents of cBN increased up to 21%, and the hardness of 55%cBN/45%TiN composites increased up to 30%. Commercial BN composite, though less pronounced on the effect of heat treatment, displayed similar hardness change mechanisms that helped in understanding why hardness improved after LWH treatment. In addition, the LWH treated BN composites hardness improve more pronounce than laser only treated BN composite, which confirmed the effect of new hybrid LWH treatment technique on hardness improvement.

The composite microstructures examined by SEM indicated that the formation of zones with nano-sized grains lead to the grain-boundary strengthening mechanism. A significant grain size change after LWH treatment was also detected in this study. These kinds of microstructure and grain size changes are expected to increase the energy needed to move dislocations that increase the hardness of the composites. In addition, the LWH treated BN composites have better wear resistance which indicated the better performance on mechanical machining. Future hardness improvement studies of cBN/wBN composites could include the development of a mathematic model that can be used to optimize the combined effects of cBN and wBN with respects to composition, microstructure, grain size, and the binder phase of cBN/wBN composites.

References

Angseryd, J., Elfwing, M., Olsson, E., & Andrén, H. O. (2009). Detailed microstructure of a cBN based cutting tool material. *International Journal of Refractory Metals and Hard Materials*, *27*(2), 249–255.

Anstis, G. ., Chantikul, P., Lawn, B. ., & Marshall, D. . (1981). A critical evaluation of indentation techniques for measuring fracture toughness: I Direct crack measurements. *Journal of the American Ceramic Society*, *46*(September), 533–538.

Aouici, H., Yallese, M. A., Chaoui, K., Mabrouki, T., & Rigal, J. F. (2012). Analysis of surface roughness and cutting force components in hard turning with CBN tool: Prediction model and cutting conditions optimization. *Measurement: Journal of the International Measurement Confederation*, *45*(3), 344–353.

Basu, B., Raju, G. B., & Suri, A. K. (2006). Processing and properties of monolithic TiB 2 based materials. *International Materials Reviews*, *51*(6), 352–374.

Brazhkin, V. V., Lyapin, A. G., & Hemley, R. J. (2002). Harder than diamond: Dreams and reality. *Philosophical Magazine A*, *82*(2), 231–253.

Callister, W., & Rethwisch, D. (2007). *Materials science and engineering: an introduction*. *Materials Science and Engineering* (Vol. 94).

Demazeau, G., Biardeau, G., & Vel, L. (1990). Synthesis of cubic boron nitride using magnesium or magnesium-based fluoronitrides. *Materials Letters*, *10*(3), 139–144.

Dubrovinskaia, N., Solozhenko, V. L., Miyajima, N., Dmitriev, V., Kurakevych, O. O., & Dubrovinsky, L. (2007). Superhard nanocomposite of dense polymorphs of boron nitride: Noncarbon material has reached diamond hardness. *Applied Physics Letters*, *90*(10).

Fischer-Cripps, A. C. (2011). *Nanoindentation*. *Springer*.

Gou, H., Wang, Z., Zhang, J., Yan, S., & Gao, F. (2009). Structural stability and elastic and electronic properties of rhenium borides: first principle investigations. *Inorganic Chemistry*, *48*(2), 581–7.

Haines, J., L, J. M., & Bocquillon, G. (2001). M Aterials. *Recherche*, *1955*(1), 1–23.

Hansen, N. (2004). Hall-petch relation and boundary strengthening. *Scripta Materialia*, *51*(8 SPEC. ISS.), 801–806.

He, W., Bhole, S. D., & Chen, D. (2008). Modeling the dependence of strength on grain sizes in nanocrystalline materials. *Science and Technology of Advanced Materials*, *9*(1), 1–7.

Hou, X. D., Bushby, a J., & Jennett, N. M. (2008). Study of the interaction between the indentation size effect and Hall–Petch effect with spherical indenters on annealed polycrystalline copper. *Journal of Physics D: Applied Physics*, *41*(7), 074006.

Huang, Q., Yu, D., Xu, B., Hu, W., Ma, Y., Wang, Y., … Tian, Y. (2014). Nanotwinned diamond with unprecedented hardness and stability. *Nature*, *510*(7504), 250–3.

Irifune, T., Kurio, A., Sakamoto, S., Inoue, T., & Sumiya, H. (2003). Materials: Ultrahard polycrystalline diamond from graphite. *Nature*, *421*(6923), 599–600.

Jiménez, I., Sutherland, D., van Buuren, T., Carlisle, J., Terminello, L., & Himpsel, F. (1998). Photoemission and x-ray-absorption study of boron carbide and its surface thermal stability. *Physical Review B*, *57*(20), 13167–13174.

John, P., Polwart, N., Troupe, C. E., & Wilson, J. I. B. (2002). The oxidation of \lattplane{100} textured diamond. *Diamond and Related Materials*, *11*, 861–866.

Knoop, F., Peters, C. G., & Emerson, W. B. (1939). A sensitive pyramidal-diamond tool for indentation measurements. *Journal of Research of the National Bureau of Standards*,

23(1), 39.

Levine, J. B., Betts, J. B., Garrett, J. D., Guo, S. Q., Eng, J. T., Migliori, A., & Kaner, R. B. (2010). Full elastic tensor of a crystal of the superhard compound ReB2. *Acta Materialia*, *58*(5), 1530–1535.

Levine, J. B., Tolbert, S. H., & Kaner, R. B. (2009). Advancements in the search for superhard ultra-incompressible metal borides. *Advanced Functional Materials*, *19*(22), 3519–3533.

Li, B., Sun, H., & Chen, C. (1996). Large indentation strain stiffening in nanotwinned cubic boron nitride. *Nature Communications*, *94*(May), 90.

Li, B., Sun, H., & Chen, C. (2014). Large indentation strain-stiffening in nanotwinned cubic boron nitride. *Nature Communications*, *5*(May), 4965.

Liu, K., & Li, X. P. (2001). Ductile cutting of tungsten carbide. *Journal of Materials Processing Technology*, *113*(1-3), 348–354.

Melaibari, A. A., Zhao, J., Molian, P., Bushlya, V., Zhou, J., Ståhl, J.-E., … Shrotriya, P. (2016). Ultrahard boron nitride material through a hybrid laser/waterjet based surface treatment. *Acta Materialia*, *102*, 315–322.

Melaibari, A., Molian, P., & Shrotriya, P. (2012). Laser/waterjet heat treatment of polycrystalline cubic/wurtzite boron nitride composite for reaching hardness of polycrystalline diamond. *Materials Letters*, *89*, 123–125.

Meng, Y., Mao, H., Eng, P., Trainor, T., Newville, M., Hu, M., … Hemley, R. (2004). The formation of sp3 bonding in compressed BN. *Nature Materials*, *3*(2), 111–114.

Dinesh Kalyanasundaram. (2009). Mechanics guided design of hybrid laser / waterjet system for machining hard and brittle materials. A dissertation for the degree of DOCTOR OF

PHILOSOPHY. Iowa State University, Ames , Iowa.

Riedel, R. (1994). Novel Ultrahard Materials. *Advanced Materials*, *6*(7-8), 549–560.

Roy, T. K. (2015). Assessing hardness and fracture toughness in sintered zinc oxide ceramics through indentation technique. *Materials Science and Engineering: A*, *640*, 267–274.

Zhuoru Wu. (2015). The mechanism governing cutting of hard materials with hybrid Laser / Waterjet system through controlled fracture. A dissertation for the degree of DOCTOR OF PHILOSOPHY. Iowa State University, Ames , Iowa.

Smith, R. L. et al. (1922). an Accurate Method of Determining the Hardness of Metals, With Particular Refernce To Those of a High Degree of Hardness. *proc.Inst.Mech.Eng.*, *1*(May), 623–641.

Solozhenko, V. L., Kurakevych, O. O., & Le Godec, Y. (2012). Creation of nanostuctures by extreme conditions: High-pressure synthesis of ultrahard nanocrystalline cubic boron nitride. *Advanced Materials*, *24*(12), 1540–1544.

Superhard, U. (2007). Comment on " Synthesis of, *318*(December), 1–2.

Taniguchi, T., Akaishi, M., & Yamaoka, S. (1996). Mechanical Properties of Polycrystalline Translucent Cubic Boron Nitride as Characterized by the Vickers Indentation Method. *Journal of the American Ceramic Society*.

Thévenot, F. (1990). Boron carbide—A comprehensive review. *Journal of the European Ceramic Society*, *6*(4), 205–225.

Tyne, U. (1965). METAL BORIDES By N. *Quarterly Reviews*.

Ulrich, S., Ehrhardt, H., Schwan, J., Samlenski, R., & Brenn, R. (1998). Subplantation effect in magnetron sputtered superhard boron carbide thin films. *Diamond and Related Materials*, *7*, 835–838.

Vepřek, S. (1997). Conventional and new approaches towards the design of novel superhard materials. *Surface and Coatings Technology*, *97*(1-3), 15–22.

Vepřek, S. (1999). The search for novel, superhard materials. *Journal of Vacuum Science & Technology A: Vacuum, Surfaces, and Films*, *17*(5), 2401.

Veprek, S., & Argon, A. S. (2002). Towards the understanding of mechanical properties of super- and ultrahard nanocomposites. *Journal of Vacuum Science & Technology B: Microelectronics and Nanometer Structures*, *20*(2), 650.

Veprek, S., Argon, A. S., & Zhang, R. F. (2010). Design of ultrahard materials: Go nano! *Philosophical Magazine*, *90*(31-32), 4101–4115.

Wentorf, R. H. (1961). Synthesis of the Cubic Form of Boron Nitride. *The Journal of Chemical Physics*, *34*(3), 809.

Yin, L., Vancoille, E. Y. J., Lee, L. C., Huang, H., Ramesh, K., & Liu, X. D. (2004). High-quality grinding of polycrystalline silicon carbide spherical surfaces. *Wear*, *256*(1-2), 197–207.

Dubrovinskaia, N., Dub, S., & Dubrovinsky, L. (2006). Superior wear resistance of aggregated diamond nanorods. Nano Letters, 6(4), 824–826.

CHAPTER V

HYBRID CO2 LASER WATERJET HEAT (LWH) TREATMENT OF BINDERLESS BORON NITRIDE COMPOSITES WITH HARDNESS IMPROVEMENT

Abstract

The material, boron nitride (BN), is chemically and thermally stable which is desirable for high-speed machining in demanding chemical and thermal environments. Although BN's hardness is lower than that of single polycrystalline diamond, the laser waterjet heat (LWH) treatment process provides a new approach to increase the hardness of boron nitride materials close to or as high as diamond's hardness. This study investigated the hardness change of LWH-treated commercial cBN/TiN and cBN/AlN materials. Results indicated that the measured hardness increase was dependent on the number of laser beam passes and the hardness measurement's distance from the beam center.

KEYWORDS: Laser waterjet heat treatment, binderless BN, hardness, fracture toughness

5.1 Introduction

Carbon is the 15th most abundant element in the Earth's crust and it is usually found in the form of graphite which can be synthesized into diamond under high pressure (5.5-6 GPa) and high temperature (1500-1900 K) (Haines, L, & Bocquillon, 2001). It is well known that diamond is the hardest material on the earth with a hardness varying between 70 and 100 GPa depending on the quality and purity of the crystal. In industry, diamond's ultra-hardness makes it unique for drilling, grinding, cutting, polishing, and machining. However, diamond also has limitations in the tooling industry. Diamond is not logical tool for cutting ferrous materials

because its chemical instabilities cause it to produce iron carbide when in contact with the ferrous materials. Also, diamond is not effective at high temperatures because of its thermal instability. These limitations of using diamond in the tooling industry have motivated researchers to develop other super-hard materials with improved chemical and thermal properties to replace diamond.

Boron nitride (BN) is a chemically inert and thermally stable compound of boron and nitrogen. It exists in five major crystalline forms: cubic boron nitride (cBN), hexagonal boron nitride (hBN), rhombohedral boron nitride (rBN), wurtzitic boron nitride (wBN), and explosive boron nitride (eBN) (Wentorf, 1961). Cubic boron nitride (cBN) is the second known hardest substance on the earth (40–50 GPa) whose crystal structure is similar to that of diamond (Haines et al., 2001). Unlike diamond, cBN does not react with iron which makes it a more efficient tooling material for fabricating steel. Additionally, cBN has a higher oxidation temperature (1300 °C) than diamond (700 °C) which is a critical property for high speed manufacturing. Similar to cBN, wBN is a chemically inert and thermally stable compound with a lower hardness (20-30 GPa) than diamond and cBN. The hexagonal form of boron nitride (hBN) which is graphite crystal structure is the normal phase stable at room temperature and pressure. However, the hardness of hBN is much lower than cBN and wBN because of the graphite structure. Thus, only cBN and wBN are considered as super-hard materials. Although cBN, wBN, and other forms of BN materials have good mechanical properties, chemical inertness and thermal stability, they cannot replace diamond as their hardness characteristics are well below those of diamond. Thus, the search for new super-hard materials is not only of great scientific interest, but also of great practical value.

Pal. Molian and his group developed a hybrid laser waterjet (LW) technique to process BN materials (A. A. Melaibari et al., 2016; A. Melaibari, Molian, & Shrotriya, 2012; Philosophy, 2009). They found that the hardness of laser waterjet heat (LWH) treated 50%cubic/50%wurtzitic boron nitride (cBN/wBN) increased by almost 100%, reaching the hardness of diamond (A. A. Melaibari et al., 2016). The novel hybrid LWH technique provides an efficient process for producing BN materials with hardness characteristics in the vicinity of or equal to those of diamond.

The hybrid LWH process allows the elements of laser and water-jet treatment to be synergistically combined such that material processing is accomplished by thermal shock-assisted fracturing of particles into micro structured refinements rather than the melting and solidification of surface materials. The LWH process consists of a low-power laser (160W – 400W) for precise heating of a small processing zone (1 mm width) on the work-piece. The laser heating creates a temperature gradient in the treated zone, and rapid waterjet quenching of the zone creates thermal stresses that fracture the large particles and create smaller particles within the zone (Dinesh Kalyanasundaram, 2009).

The new discovery of rapidly quenched cBN/wBN composites whose hardness matches the hardness of diamond can have vast implications in the tooling industry. Hence, in this paper, a series of experiments on laser heat-treated dual-phase cBN/wBN tools was designed in order to identify the fundamental phase transition and microstructure refinement features that contribute to hardness improvements.

In previous studies (A. A. Melaibari et al., 2016; A. Melaibari et al., 2012), the relationship between laser fluence, laser beam overlap percentage and the hardness improvement was evaluated. The test results show that a low laser fluence could improve the

hardness of cBN/wBN composite without damaging the sample, and a laser beam overlap of approximately 50% will lead to higher hardness improvement. However, the hardness improvement mechanism is still not clear since the hardness change ratio is not uniform across the laser beam track. Thus, a new experiment was designed in order to find the effect of the number of laser beam passes and laser power distribution on hardness improvement for a LWH-treated cBN/wBN composite.

The search for materials with hardness characteristics comparable to diamond is a fascinating challenge for researchers. In this paper, a novel hybrid laser waterjet heat treatment process is described in detail. Next, an experimental design for optimizing LWH treatment parameter settings is discussed. The LWH process parameters include the proportion of cBN and wBN in the material, number of laser beam passes, and the Gaussian laser beam profile effect. At last, the hardness change mechanism on BN materials is discussed.

5.2 Method

A continuous wave CO2 (Laser Spectra Physics 820) of 10.6 micron wavelength and 1.5KW rated power was employed to conduct the experiments with the laser parameters shown in Table 5.1. The LWH treatment process consists of laser heating and waterjet quenching in tandem. Following our previous study (A. A. Melaibari et al., 2016), heat treatment was performed using a low laser fluence with 1 mm beam spot size at low power to avoid scribing or melting the materials.

Three factors were studied in this paper. The first factor was the laser pass number on boron nitride materials. In previous studies, a set of experiments were designed to find the relationship between boron nitride’s material hardness change and the laser beam overlap. It

was reported that boron nitride's material hardness change ratio varied with different laser beam overlaps. This leads to the thinking that multiple laser beam hits at the same location on the BN material may enhance the surface hardness. Six levels of laser beam pass were used in this study and are identified as 1 pass, 2 passes, 4 passes, 8 passes, 16 passes, and 30 passes.

The second factor was the laser energy effect on hardness change ratio. Laser energy was measured with respect to the distance of the measurement from the center of the laser beam track. The five distances considered for this study were 50, 150, 250, 350, and 450 microns. Because the laser beam used in this study was a Gaussian beam, the power density was not uniform along the entire beam path. Therefore, the laser beam energy irradiated on the cBN/wBN composite was not uniform along the width of the laser beam. The Gaussian profile of the laser beam was approximated as a surface heat source whose intensity at radial distance r from the center is given in Eq. (5.1):

$$\mathrm{I(z)} = a_s I_0 \exp\left(\frac{-2r^2}{w^2}\right) \tag{5.1}$$

where I_0 is the intensity at the center of the beam, a_s is the absorption coefficient, and w is the diameter of the laser beam spot. The absorption coefficient was chosen to be 0.75 (A. A. Melaibari et al., 2016).

The third factor was the composition of the boron nitride material. The workpiece materials used in this study were binderless dual phase 94%cBN/6%wBN, 79%cBN/21%wBN, 45%cBN/55%wBN, 33%cBN/67%wBN, and 18%cBN/82%wBN with iron oxide as the impurity. All materials were round disks with a diameter of 8 mm and thickness of 3 mm. The initial hardness of the workpiece materials used in this study is listed in Table 5.1.

Table 5.1 *LWJ treatment parameters*

Material	Initial hardness (GPa)	Laser power (W)	Scanning speed (inch/min)	Waterjet pressure	Gas
94%cBN/6%wBN	36	220	140	400 KPa	Compressed air
79%cBN/21%wBN	42	210	180	400 KPa	Compressed air
45%cBN/55%wBN	44	160	240	400 KPa	Compressed air
33%cBN/67%wBN	37	180	160	400 KPa	Compressed air
18%cBN/82%wBN	31	170	350	400 KPa	Compressed air

Similar to our previous experiments, the laser waterjet process used a continuous wave CO2 laser beam. A low-laser power (160 W-220 W) was used to prevent melting, scribing or cutting of boron nitride. The laser beam was immediately followed by a waterjet stream as shown in Figure 5.1.

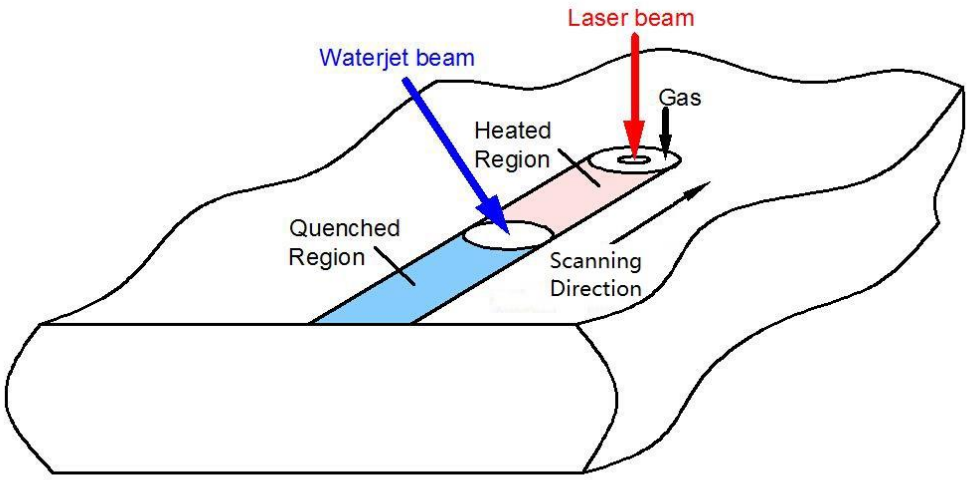

Figure 5.1 *Schematic representation of LWH treatment process*

Figure 5.2 shows the LWH treatment system. The laser head was designed to accommodate the low-pressure waterjet (< 1000psi or < 8MPa) for realizing the LWH treatment. A CNC table with freedom in the horizontal plane was implemented to control the movement of sample mounted on it. The beam from the laser was sent through a focusing lens (127 mm focal length) and irradiated on the sample surface. The laser beam has a focal spot diameter of 0.2 mm upon passing through the focusing lens. When varying the distance between the laser head and sample surface, a defocused laser beam spot size with a diameter larger than 0.2 mm could be achieved. The distance between the waterjet and laser beam could also be varied by changing the location of the spray hole on the laser nozzles. Three nozzles were manufactured with a spacing of 2 mm, 4 mm and 6 mm between the laser outlets. In order to guarantee the waterjet quenched the sample surface immediately after the laser beam pass, the 6 mm nozzle was employed for this study. A compressed air stream with a designed pressure was employed around the laser beam in order to prevent direct interaction of the laser and water jet.

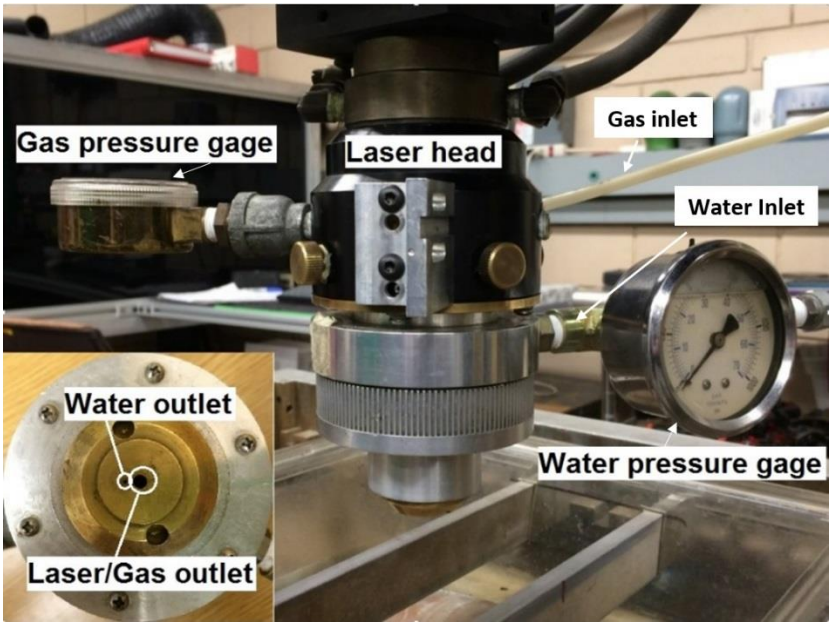

Figure 5.2 *LWH treatment system*

In order to identify the change of the samples' hardness and toughness, Knoop microhardness tests and Vicker's fracture toughness tests were performed before and after LWH treatment.

Indentation hardness tests were performed using a Tukon microhardness tester with a Knoop diamond pyramid indenter. The load was set at 0.5 kgf (4.9 N), and the test duration was set at 30 seconds. Length measurements were made along the long axis of the indentations using a high resolution (± 0.4 μm) optical microscope and optical profilometer to ensure that no fracture had occurred in the indentation zone. Knoop hardness was then calculated using the relationship:

$$HK = \frac{P}{C_p L^2} \tag{5.2}$$

where P is the load (kgf), C_p is the correction factor related to the shape of the indenter (0.070279 in this case) and L is the length of indentation along its long axis.

The Vicker's indentation method for fracture toughness measurement was performed by making an impression on the ceramic surface at reasonably higher loads (Roy, 2015). This process generates cracks, mainly at the corners of the indentation mark. The toughness is guided by the crack length generated along with the hardness value of the sample. Toughness tests were performed using a Tukon microhardness tester with a Vicker's diamond pyramid indenter at a load of 2 kgf (19.6 N). According to Antis et al. (Anstis, Chantikul, Lawn, & Marshall, 1981; Knoop, Peters, & Emerson, 1939), the fracture toughness of a material will be governed by the following equation for a radial median type of crack geometry:

$$K_c = 0.016 \left(\frac{E}{H_v}\right)^{0.5} (P/C^{1.5}) \tag{5.3}$$

where, $\frac{E}{H_v}$ is the Young's modulus to apparent hardness ratio and $P/C^{1.5}$ is the ratio of change in the crack length with load. The Young's modulus in this study was set as 766 GPa (Roy, 2015).

In order to maintain precision while measuring the length of indentations, images were captured by optical microscope. Afterwards, the length of the indentations were measured using a Java-based image processing program known as ImageJ.

A detailed microstructure analysis of both untreated and LWH-treated samples was to be performed using scanning electron microscopy (SEM) or transmission electron microscopy (TEM). EDS and Raman spectroscopy were also to be used to identify the specific elements or chemical bonding of materials for the treated samples in this study. Due to a lack of resources, these studies will be done at Lund University in Sweden in the future.

5.3 Results and discussion

5.3.1 LWH treated materials hardness measurements

The average measured and calculated Knoop hardness before and after LWH treatment of surfaces composed of varied cBN compositions are shown in Table 5.2. The maximum hardness change ratio was achieved on 45%cBN/55%wBN sample at 8 passes 150 micron from center area, where closes the edge of spalled region developed by laser works.

Optical images examination of the LWH-treated surfaces with 79%cBN/21%wBN and 18%cBN/82%wBN indicates a color change from black to white on each beam center. LWH-treated 33%cBN/67%wBN showed no signs of spalling within the treated zone, but more micron-scaled defects were observed in areas exposed to 16 and 30 passes in the beam center.

On LWH-treated 94%cBN/6%wBN and 45%cBN/55%wBN, the 100 – 400 micrometer width spalled region on each beam center were observed starts on 16 passes and 4 passes respectively.

Table 5.2 *Experiment results*

BN composition	Initial Hardness (GPa)	std	Maximum hardness change ratio	Maximum hardness value (GPa)	Observed on where	Spall region?	Observed on where
94%cbn	36	2.21	1.148	41	30 passes 250 micron from center	Yes	Starts on 16 passes
79%cbn	41	4	1.34	55	30 passes beam center	No	--
45%cbn	36	2.21	1.418	41	8 passes 150 micron from center	Yes	Starts on 4 passes
33%cbn	36	2.4	1.277	47	8 passes 450 micron from center	No, but more defects observed on beam center.	--
18%cbn	30	2.0	1.23	38	30 passes beam center	No	--

The Figure 5.3 shown the hardness change ratio comparison among all 5 uncommercial samples. It was hypothesized that the hardness change ratio would keep increasing as the composition of wBN increased. However, the results show that the hardness change ratio increased at a low rate until the composition 45%cBN/55%wBN. When wBN portion keep increasing, the material hardness change starts decrease but still above 1.2. The maximum

hardness change ratio measured in this study is 1.418, which observed on 45%cBN/55%wBN material 8 passes laser beam area at 150 micron from beam center.

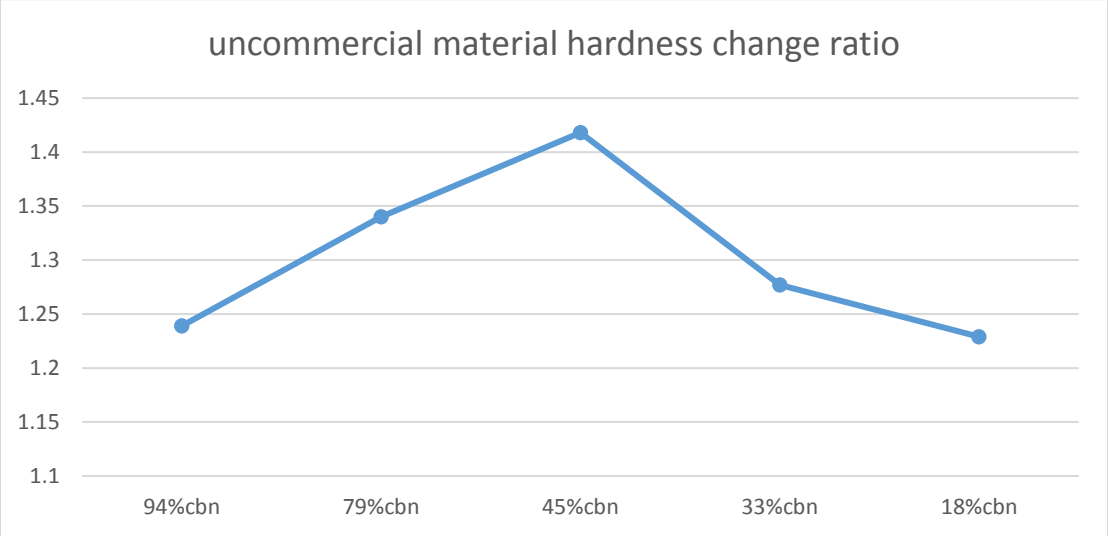

Figure 5.3 *Hardness change ratio comparison based on cBN compositions*

5.3.2 LWH treated materials toughness measurements

The fracture toughness measurements were conducted on 94%cBN/6%wBN, 79%cBN/21%wBN, and 33%cBN/67%wBN samples and calculated by measuring the diagonals of the indentations and the crack lengths using equation 5.3. A comparison of fracture toughness data for treated and untreated samples is shown in Figure 5.4. The error bars show the deviation of the hardness test data. The average toughness of LWH treated 33%cBN/67%wBN was increased from 2.09 MPa · $m^{1/2}$ to 2.41 MPa · $m^{1/2}$ which was 15% more than the untreated material. On LWH treated 79%cBN/21%wBN, the average toughness calculated in this study was decreased from 2.72 MPa · $m^{1/2}$ to 2.62 MPa · $m^{1/2}$ which was 4% less than untreated sample. Different with other materials, LWH treated 94% cBN/6%wBN material was observed a large toughness drop from 2.88 MPa · $m^{1/2}$ to 2.38 MPa · $m^{1/2}$ which was 18% less than untreated sample.

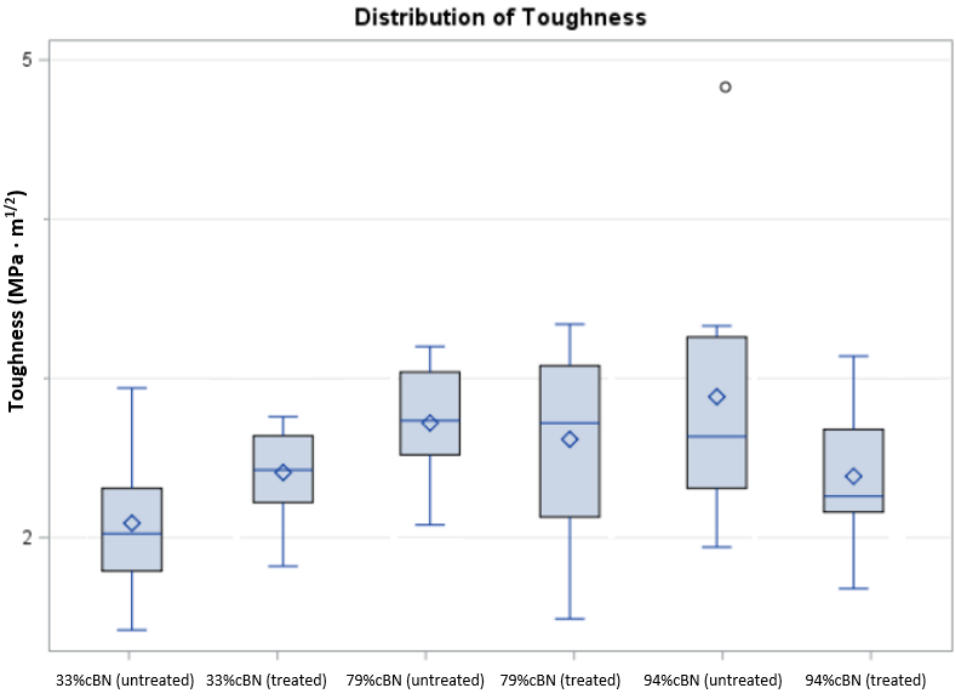

Figure 5.4 *Comparison of fracture toughness data on BN samples*

5.3.3 Wear resistance study

Hardness and fracture toughness are two critical properties of tool materials. Both of them contribute to the tool wear resistance, which is the main eligibility criteria of tool material. In this study, the wear coefficient (W_H), which characterizes the wear resistance of a material, of original materials and LWH treated materials were calculated by using below formula (Dubrovinskaia, Dub, & Dubrovinsky, 2006). Typically, the higher of wear coefficient and the higher of wear resistance.

$$W_H = K_C^{0.5} \cdot E^{-0.8} \cdot H_K^{1.43} \tag{5.4}$$

where, K_C is fracture toughness, E is Young's Modulus (766 GPa in this case), and H_K is Knoop hardness (Roy, 2015).

As shown in table 5.3, although fracture toughness of LWH treated 94%cBN/6%wBN and 79%cBN/21%wBN composites dropped, the wear coefficient increased 9% and 48% respectively. Because the wear resistance is the combined result of both hardness and fracture

toughness. On the other hand, LWH treated 33%cBN/67%wBN composite increased both hardness and fracture toughness. Thus, it has higher wear coefficient value. This suggested that the LWH treated BN materials are more effective on mechanical machining in theory.

Table 5.3 *Comparison of wear coefficient*

Material	K_C (MPa)	H_K (GPa)	E (GPa)	W_H
94%cBN/6%wBN (Untreated)	2.88	36	766	1.41
94%cBN/6%wBN (treated)	2.38	41	766	1.54
79%cBN/21%wBN (Untreated)	2.72	42	766	1.70
79%cBN/21%wBN (treated)	2.62	56	766	2.52
33%cBN/67%wBN (Untreated)	2.1	37	766	1.25
33%cBN/67%wBN (treated)	2.4	45	766	1.77

To check the performance of LWH treated BN composites as a tool material, the mechanical tests will be done in the future.

5.4 Conclusion

Novel hybrid laser-waterjet treatment technique was used in this study was developed for ceramic machining. However, the utility of this approach on uncommercial boron nitride

composites achieved an increase of the hardness of dual phase BN based material. The maximum hardness change ratio measured in this study is 1.418, which observed on 45%cBN/55%wBN material 8 passes laser beam area at 150 micron from beam center. This result matched the commercial BN material study on chapter 4. In addition, the LWH treated BN composites have better wear resistance which indicated the better performance on mechanical machining. Although, this study lack of the microstructure study of pre and post LWH materials because the limitation of SEM equipment. The measured hardness and toughness values were confirmed by optical images and Java-based image processing program known as ImageJ with minimum error controlled within 0.5 micrometer, which is 2.7 GPa and 0.55 GPa. Future LWH treatment studies of BN composites could be conducted on hardness improved material cutting test to verify if the new materials better than untreated materials on tooling industry.

5.5 Reference

Anstis, G. ., Chantikul, P., Lawn, B. ., & Marshall, D. . (1981). A critical evaluation of indentation techniques for measuring fracture toughness: I Direct crack measurements. Journal of the American Ceramic Society, 46(September), 533–538.

Haines, J., L, J. M., & Bocquillon, G. (2001). M Aterials. Recherche, 1955(1), 1–23.

Knoop, F., Peters, C. G., & Emerson, W. B. (1939). A sensitive pyramidal-diamond tool for indentation measurements. Journal of Research of the National Bureau of Standards, 23(1), 39.

Melaibari, A. A., Zhao, J., Molian, P., Bushlya, V., Zhou, J., Ståhl, J.-E., … Shrotriya, P. (2016). Ultrahard boron nitride material through a hybrid laser/waterjet based surface treatment. Acta Materialia, 102, 315–322.

Melaibari, A., Molian, P., & Shrotriya, P. (2012). Laser/waterjet heat treatment of polycrystalline cubic/wurtzite boron nitride composite for reaching hardness of polycrystalline diamond. Materials Letters, 89, 123–125.

Dinesh Kalyanasundaram. (2009). Mechanics guided design of hybrid laser / waterjet system for machining hard and brittle materials. A dissertation for the degree of DOCTOR OF PHILOSOPHY. Iowa State University, Ames , Iowa.

Roy, T. K. (2015). Assessing hardness and fracture toughness in sintered zinc oxide ceramics through indentation technique. Materials Science and Engineering: A, 640, 267–274.

Wentorf, R. H. (1961). Synthesis of the Cubic Form of Boron Nitride. The Journal of Chemical Physics, 34(3), 809.

Dubrovinskaia, N., Dub, S., & Dubrovinsky, L. (2006). Superior wear resistance of aggregated diamond nanorods. Nano Letters, 6(4), 824–826.

CHAPTER VI

CONCLUSIONS AND FUTURE WORKS

6.1 Conclusions

The research studies presented in this thesis explore the use of a hybrid laser waterjet heat (LWH) treatment process to fabricate super-hard tooling materials. The candidate materials of the research studies include dual phase 50%cBN/50%wBN, commercial 55%cBN/45%TiN, commercial 82%cBN/18%AlN, and 5 different cBN composition of un-commercial cBN/wBN composites. Specific accomplishments of these research studies include the following:

1. Addressed the hardness improvement mechanism and the effect of laser fluence on hardness change for LWH-treated dual phase BN

2. Investigated the laser beam overlap percentage effect on the hardness improvement of dual phase BN materials and determined the ideal laser beam overlap percentage value for achieving maximum BN hardness.

3. Compared the effects of different laser waterjet parameters (laser pass number, laser energy) on LWH-treated commercial cBN/AlN and cBN/TiN composites and investigated the hardness improvement mechanism of BN composites.

4. Compared the effects of different laser waterjet parameters (laser pass number, laser energy) on LWH-treated un-commercial cBN/wBN composites with different cBN compositions.

6.2 Future works

Even though the new developments in laser waterjet heat treatment have been discussed in with great details, it is still in the early stage and can be extended to different directions:

Machining test comparison on LWH treated BN and other tooling materials

The work done on LWH treated BN composites can be further tested in machining application. BN is commonly used as tool insert for turning and milling applications. Therefore, testing the effect of the LWH treatment on the efficiency and performance of these tools is the logical next step.

LWH treatment tests of BN composites on other Laser parameters

The work done on LWH treatment of BN composites may be affected by environmental gas as well. This study only employed the compressed air as environmental gas. Further tests could be designed to test of other environmental gas effect on BN composite hardness improvement, such as nitrogen, argon, oxygen, and helium.

LWH treatment tests of BN composite in other working environments

The work done on LWH treatment of BN composites was simulated by FEM on temperature and compressive stress. The reason for BN material refinement maybe is the huge temperature change within 1 second which created at least 1.5 MPa compressive stress. Thus, further tests could be studied only on temperature change without laser waterjet to verify this assumption. For example, the new test could be design with laser beam (not CO2 laser) on BN material in water or other liquid, or design a special oven to heat the BN sample to a certain temperature and then quench the BN sample very quickly to room temperature.

Modeling of LWH treatment of BN composites

The work done on LWH treatment of BN composites can be modeled by FEM to verify how much contribution from each of the proposed mechanisms lead to the hardness improvement. This is important to optimize the microstructure and LWH treatment parameters to find the maximum hardness improvement for this material as well as other materials in the future.